AN ANALYSIS OF MULTI-YEAR ICE

DISTRIBUTIONS OCCURRING IN THE SAGLEK

BANK REGION OF THE LABRADOR SEA

DURING 1979

EUGENE VICTOR GUY

AN ANALYSIS OF MULTI-YEAR ICE

DISTRIBUTIONS OCCURRING IN THE SAGLEK BANK

REGION OF THE LABRADOR SEA DURING 1979

BY

© Eugene Victor Guy, B.Sc., B.Ed.

A thesis submitted to the School of Graduate

Studies in partial fulfillment of the

requirements for the degree of

Master of Science

Department of Geography

Memorial University of Newfoundland

February 1985

St. John's   Newfoundland

ABSTRACT

Air photographs taken during six overflights of the Labrador marginal ice zone over Saglek Bank, during the 1979 ice season, have been visually examined to isolate the occurrence of multi-year floes. Along the flight lines, which extended seaward from the coast, the floes were significantly grouped into zones of high concentration with areas of few or zero occurrences lying between. Correlation between floe frequency and sum of diameters indicated that greater amounts of multi-year ice did exist in these groups and that a higher frequency was not due to an occurrence of smaller pieces.

For flights of April 25, May 01, and May 12 most floes were observed in bands which crossed the flight line from top to bottom and which were deflected progressively shoreward through time. By May 26 individual bands had disappeared and the floes were found to occur in two main groups, while the center of the distribution had attained its farthest measured shoreward advance. On May 31 and June 07 the distribution was mainly scattered, however a return to the banded effect was observed near the ice edge.

The banding phenomenon observed in the distribution of multi-year floes is thought to be a product of differential shear across a horizontal velocity gradient, occuring in a current regime dominated by laminar flow. Under these conditions, individual constituent floes of a hypothetically uniform floe field, which are located at opposite ends of an axis orthogonal to the direction of current flow, are moving in a common direction at unequal velocities. This creates differential rates of shear across the initially uniform field and causes it to elongate into a band. During this process, the originally orthogonal axis is progressively re-oriented until it is parallel to the direction of laminar flow. The subsequent attenuation of this banding phenomenon is probably due to a temporary transition from the laminar to a turbulent mode of flow within which random cross-flow components disperse the bands.

The landward deflection of the centers of the multi-year floe distribution was probably due to a meandering of the thermal front which separates the cold water of the Labrador Current core from the warmer water offshore. The most severe disruption of banding, on May 26, was probably due to the passage of a cyclonic eddy along the frontal zone. A re-emergence of bands which occurred near the seaward ends of the May 31 and June 07 flight lines is considered normal because current velocities are greatest near the seaward edge of the bank, and the effects of turbulent events would be expected to disappear most quickly in this region.

Seasonal trends in floe size occurrence suggest that larger floes deteriorate into smaller pieces by fracturing, which increases as the floes become weaker due to higher temperatures. Beyond a lower size limit fracture ceases and melt processes are dominant.

ACKNOWLEDGEMENTS

In addition, the guidance provided by the following people was of paramount importance in leading to the completion of this project:

Mr. Alastair Allan (C-CORE) provided valuable consultation needed for familiarization with the highly diversified nature of the sea ice milieu. Mr. Allan maintained close contact and gave valuable guidance throughout the program. It was his suggestion which provided the initial impetus for a study of multi-year ice distributions.

Dr. Colin Banfield (Department of Geography, M.U.N.) provided direction as supervising professor during the program. His guidance and comments were crucial to collating various aspects of the research into a completed thesis.

Mr. Alvin Simms (C-CORE) provided consultation on statistical and quantitative methodology applied during this project. He also gave pertinent advice on computer programming and data base management techniques.

Mr. William Winsor (C-CORE) also provided useful comments and was especially helpful in arranging opportunities for field experience.

Other people who deserve acknowledgement regarding this project are as follows:

TABLE OF CONTENTS

LIST OF FIGURES

x

LIST OF TABLES

CHAPTER 1

ICE REGIME OF THE LABRADOR SEA

1.1 Introduction

The marginal ice zone (MIZ) of the Labrador Sea represents
an open system ice regime. Input occurs from Arctic regions as
well as locally along the coast, resulting in ice of varying age
and type flowing south in an ice belt bordered to the west by
land and to the east by open water. Influenced by changes in
synoptic weather conditions and the Labrador Current, the system
is in a continuous state of internal flux, producing forces which
constantly deform, reshape and sometimes destroy ice floes
during their meandering southward drift. The resulting varia-
tions lead to a myriad of sea ice distribution patterns which
makes the Labrador pack a distinctive east coast component of
the boreal region of the earth's cryosphere.

1.2 Freeze up: pack ice occurrence in the Labrador Sea

Ice formation usually begins in November with freezing in
inner channels along the northern Labrador coast and sea ice
formation north of Cape Harrison (refer to Figures 1 and 2).
First-year ice from Davis Strait, measuring approximately 1.2 to
1.5 m thick (Skidmore 1979, Dinsmore 1972) will reach Cape Chid-
ley at about the same time; fast-ice formation at this time
occurs in sheltered regions north of Nain usually on an average
of once in every five years. Early into December, the ice
extends as far south as Cape Harrison and will reach the Belle
Isle area by the end of the month. By early January, Hamilton

1
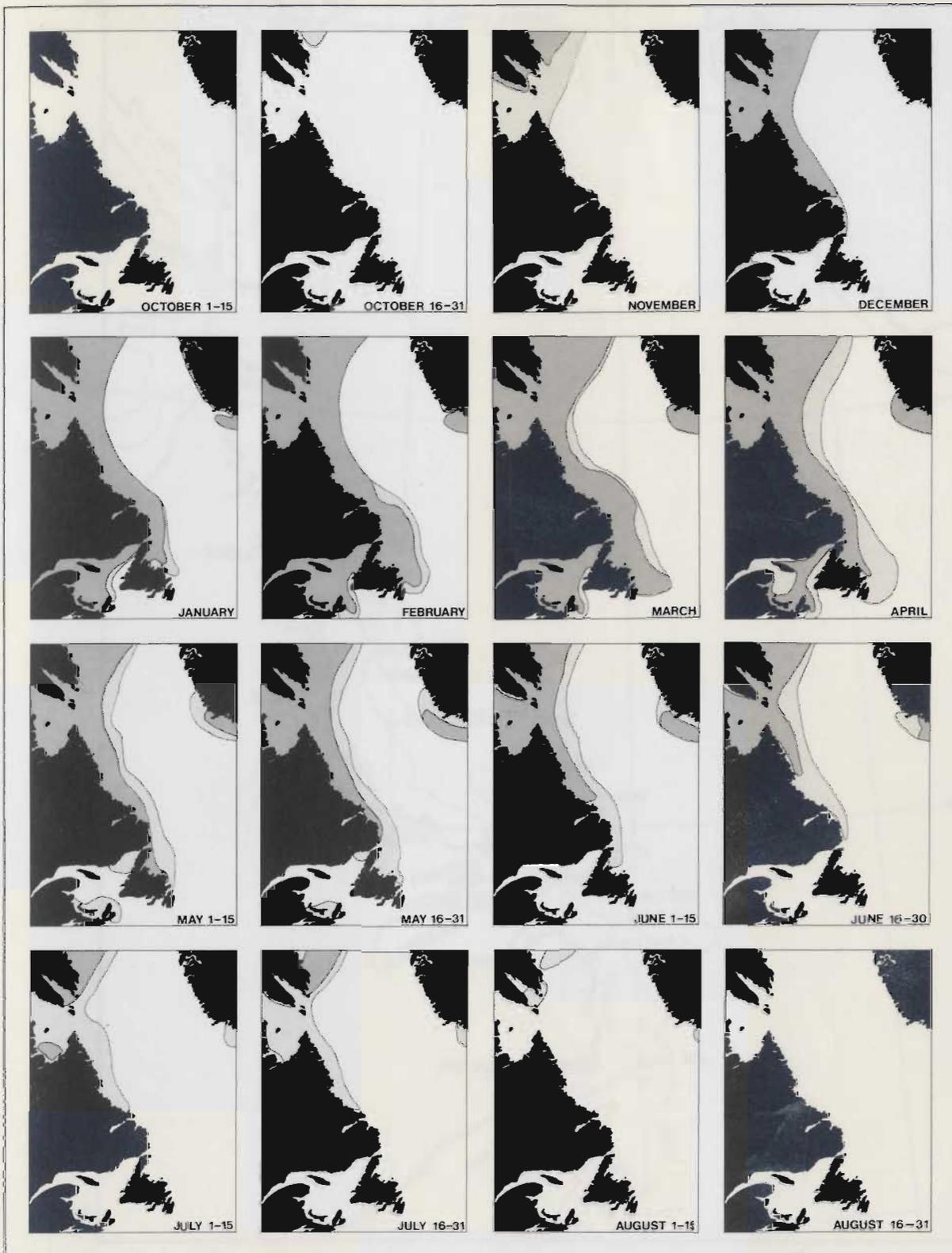
Figure 1 - Median ice coverage conditions for the Labrador Sea (source: Oceanographic Atlas of the North Atlantic Ocean, 1968).

FOUR TENTHS OR LESS

FIVE TENTHS OR GREATER
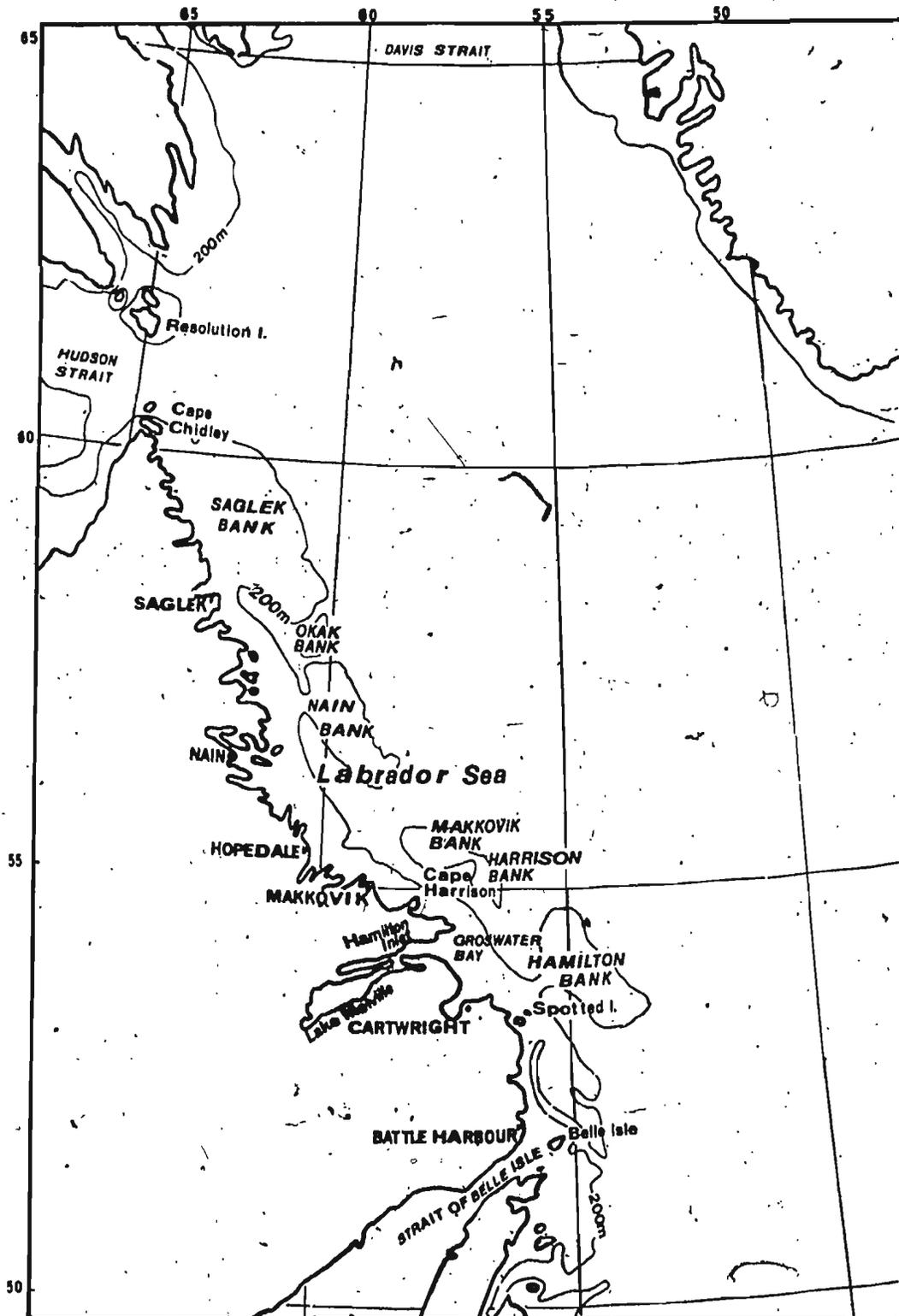
Figure 2 — Place names and geographic features of coastal Labrador as referred to in text.

3

Inlet and other similarly sheltered regions usually have ten tenths coverage of grey-white ice and offshore areas south to Spotted Islands will have six tenths coverage. In mid-January up to eight tenths young or first-year ice exists north of Cartwright with four to six tenths farther south. At this time, the pack usually extends to between 160 and 240 km offshore; occurrence of thick first-year ice will have begun and by the end of the month the pack will reach as far south as the northeast coast of Newfoundland, or maybe even St. John's depending upon the rates of freezing in these regions and their resulting degree of input into the pack. Continuing ice growth through February results in an increased concentration of thick first-year ice, with the pack reaching its maximum extent in March, at which time it can extend an average of 9/10 coverage up to 400 km offshore (Bradford 1973, Culshaw, 1977, Markham 1980a). Although this is representative of the general pattern, the southward advance of the pack in any one year might be accelerated under conditions of extreme cold and calm seas, or retarded by periods of heavy wind and wave action (Wright and Berenger, 1980).

By April, ice conditions usually begin to ease along the southeast Labrador coast as the southwest extremes of the pack begin to retreat, allowing shore leads to open north of the Strait of Belle Isle. Pack deterioration is accelerated when ice melt and dispersal at the seaward margin exceeds the southward delivery of ice, so that by late May or early June naviga-

tion is usually possible to Lake Melville, although heavy first-

year and multi-year ice still lies about 40 km offshore. Before

mid-June most ice disappears below 55°N and by mid-July the

entire Labrador Sea is clear, except for occurrence of icebergs

(Masterson & Wright, 1982; Bradford, 1973; Culshaw, 1977).

1.3 Sea Ice Formation in the Labrador MIZ:

Ice crystal formation generally begins at a water surface

temperature near -1.67°C; however freezing temperatures vary geo-

graphically depending upon water salinity, which can be altered

by evaporation rates or local fresh water discharge. These crys-

tals, collectively known as frazil ice, represent the first

stage of sea ice formation and occur as individual platlets of

ice measuring 1-3 mm in diameter and 1-10 μm thick. During

agitated sea surface conditions these platelets increase in con-

centration to form a thick soupy layer known as grease ice which

is composed of 20-40% ice by volume (Martin and Kauffman, 1981).

Grease ice gives the sea surface a matte appearance; as it

thickens it dampens wave action, hence facilitating faster con-

solidation. Before solidifying it can reach thicknesses in

excess of 1 m and under quiescent conditions consolidation can

pass through the grey (10-15 cm) and grey-white (15-30 cm)

stages to become first-year ice over 30 cm thick (Skidmore,

1979).

If surface agitation continues, progressively greater num-

bers of frazil platelets will sinter (Martin, 1981) into little

lumps to form shuga ice; because freezing only occurs (at first)

5

SEA WATER

calm conditions ← cooling → SNOW

agitated water

FRAZIL ICE

FRAZIL ICE   SLUSH

GREASE ICE   → SHUGA ←   NEW ICE
                                        (developmental)
                    SNOW ICE

NILAS
[dark nilas 0-5 cm]   wind and   PANCAKE
[light nilas 5-10 cm]   wave action →   ICE

YOUNG ICE ← refreezing ←
10-30 cm
grey ice 10-15 cm
grey-white ice 15-30 cm

heavy snow
high temperatures

FLOODED ICE

refreezing

SNOW ICE
forms on top of
an existing ice sheet

further   ← refreezing
ice growth

FIRST-YEAR ICE
30 cm to ≥2 m
thin, 30-70 cm
medium, 70-120 cm
thick, >120 cm

protected near-shore   wind and wave action
conditions

turbulent   turbulent
mixing   mixing

FAST ICE   ICE FLOES

                              refreezing

summer conditions   PACK ICE   ICE FIELDS →   summer conditions

ROTTEN FAST ICE   deformation   ROTTEN PACK ICE

Arctic regions   Labrador Sea   DEFORMED ICE   Arctic   Labrador
                                                regions   Sea

complete   fall   complete   fall freeze-up ← "fresh" melt water   complete
melting   freeze-up   melting   melting

OLD FAST ICE   OLD PACK ICE ← percolation beneath rotten
                                          ice and subsequent refreezing

Figure 3 — Stages of sea ice formation as displayed by Weeks
(1976); with modifications for relevance to Labrador.

6

near the upper 10 cm of the water column and because the sur-
faces of shuga balls protrude slightly from the water, fur-
ther sintering will concentrate along the horizontal axis of the
lump, between the water surface and the lower limit of freezing;
this causes the lumps to grow laterally, evolving into small
pans of ice known as pancake ice which have diameters of 3-20m.
Constant collision between adjacent pancakes will cause unconsol-
idated grease ice to be pumped up onto the periphery of the pan-
cake and deformation of the edges will also occur; this combina-
tion produces the raised edge rims characteristic of pancake
ice. Pancakes might also form when a larger floe or a semi-
consolidated surface layer of slush is broken into smaller
pieces by wave action.   In this case, the angular corners will
be rapidly rounded by repeated floe collisions and abrasion
which will also produce raised rims.   During quiescent condi-
tions, pancakes will become consolidated by the freezing of the
interstitial grease ice matrix; this produces large agglomerate
or brecciated floes comprised of ice of varying ages including
first-year (Weeks and Lee, 1958; WMO, 1970; Skidmore, 1979).

In sheltered areas such as small bays or the open leads in
pack ice, the formation of pancakes does not always occur.
Under these calm conditions, sintering frazil platelets will
first form dark nilas, a thin elastic crust of about 5 cm thick
which evolves into light nilas of 5-10cm; if undisturbed, the
ice sheet will grow into grey and grey-white or first-year ice.
Thin ice sheets growing in leads are often destroyed by pack con-

7

vergence before reaching these stages however, so this process
is most prevalent in the formation of fast ice in bays and in-
lets of coastal Labrador. The shore-fast ice usually forms best
in the characteristically lower temperatures and low salinity of
shallow water and where offshore islands are present to protect
it from destructive wave action during early stages of growth
(Weeks and Lee, 1958).

First-year floes whether formed from freezing together of
pancakes and other floes, or from growing as a single floe
from the grey-white stage, usually reach undeformed thicknesses
of 0.5 to 1.5m in the Labrador Sea (Masterson & Wright, 1982;
Nordco, 1980).

1.4 Marginal ice zone dynamics

Movement of ice cover in the Labrador Sea is influenced by
winds and ocean currents. Wind speeds in the winter months
average about 20 knots, prevailing from the north or northwest,
and current velocities are near 0.15-0.30 ms^{-1} (Masterson &
Wright, 1982). It is in response to these influences that most
pack-ice movements occur, during which floes can be moved
several miles and undergo extensive deformation. Mean veloc-
ities for first-year floes approach an average of 0.15-0.25
ms^{-1} with expected maximums near 0.80 ms^{-1} during storm condi-
tions (Petro-Canada, 1982).

Due to interaction with winds and swell, the pack ice in a
typical marginal ice zone divides into three regions (Bauer and
Martin, 1980). Next to the open water, and the outermost, is

8

the edge zone which, depending upon prevailing conditions, will vary in width between 1 and 15 km; landward from this is the transition zone nearing 5 km in width, and inside of this is the interior zone which borders the land. In the Labrador MIZ, these zones are comprised of pack ice which is formed locally, as well as pack ice which is advected southward from the more northerly latitudes.

It is in the low-concentration dynamic edge zone that floes are most affected by wind and propagating waves. Pancake ice forms almost continuously at the ice edge during winter, along with ice pulp from their constant interactive grinding, in addition to the naturally forming grease ice. As the accumulation of pancakes advances the ice edge seaward, those contained within the pack have an attenuating effect upon the swell (Wadhams, 1973, 1978) so that, in combination with low temperatures, these pancakes will eventually consolidate into a series of large floes. During subsequent periods of prolonged wave and swell propagation these floes, and any flat undeformed floes from inner regions of the pack, will be fractured at right angles to the direction of the wave movement (Squire and Allan, 1977). The cracks usually form between 10 and 40 m apart to produce strips of ice which might measure hundreds of metres long; however, upon rotation of their long axis parallel to the wave path they are broken into smaller floes and eventually form small pieces of 5 to 15 metres across. With continued agitation by waves, floe grinding again produces ice pulp which, if temperatures are below freezing, will be complemented by grease ice formation. When the pack becomes compressed by onshore winds,

9

the converging floes will push this mixture beneath them as they meet to form a compact ice cover of individual floes (Winsor and LeDrew, 1979).

During these pressure conditions, edges of the floes will fail in response to lateral pressure loading, leading to pressure ridge formation during which fragmented portions of floes are pushed upward and downward to form linear piles of rubble. Smaller shear ridges will also be formed when adjacent floes grind against each other while rotating or moving in opposite, paralleling directions (Parmeter and Coon, 1972). Additionally, when floes are in collision, rafting occurs during which one floe slides up over another; this process might produce multiple-rafted floes which are stacked several layers deep beneath the surface. Rafting and ridging can produce composite thicknesses between 3 and 5 m; ridges average 3 m thick up to a maximum near 7.5 m, with a length of 9 to 15 m and a width of 3 to 4.5 m (Nolte and Trethart, 1971; Bursey, 1977; Nordco, 1979; Fenco, 1975; Fenco, 1976).

When pressure is released, the floes diverge allowing the submerged ice pulp and grease ice to resurface where it then freezes under calm conditions to consolidate the floes into a continuous cover of ice breccia once more (Winsor and LeDrew, 1979). When propagating swells again infiltrate the edge zone, the entire process is repeated; each repetition produces a new generation of brecciated floes which themselves are frozen agglomerations of floes formed over several previous generations. Winsor and LeDrew (1979) estimate the cycle for these events to be between 5 and 10 days, coinciding with the mean frequency of passage of winter low pressure systems over the region.

In the transition zone the wave amplitude is sufficiently reduced so that the ice breaks into rectangular floes which experience little or no subsequent deformation or rounding abrasion. In contrast to the thick, small floes of the edge zone, these floes are typically 20-40 m in diameter and have thicknesses characteristic of undeformed first—year ice.

The interior zone is typically much wider than the others; swells are sufficiently attenuated before reaching this area such that they propagate without breaking the ice. This results in floe sizes much larger than in either of the two seaward zones (Bauer and Martin, 1980).

Interchange between the edge and transition zones is occurring constantly and often leads to an alternate banding of large and small floes in these regions (Wadhams, 1980). This process occurs when large floes from the inner zones are advected to the edge zone due to the continuous motion of the pack in response to wind and waves. As a result, some of the floes found in the edge zone are not the result of locally intrinsic formation processes, rather they are due to the destruction of larger floes originating from deeper within the pack (Wadhams, 1980). Reciprocally, pancake ice and agglomerate floes formed in the edge zone are also advected landward into the pack; conceivably, a large floe could be carried to the edge zone and pulverized by the local wave action, with some of its smaller pieces eventually returning to the inner zones frozen within a brecciated floe. In other cases, the ice from the edge zone

11

might be advected, perhaps under the influence of a local off-

shore wind, out into the open ocean where it eventually melts.

Such seaward advection of ice usually occurs in the form of

strips or streamers extending sinuously outward from the ice

edge (Wadhams, 1980; LeBlond, 1982).

1.5 Exotic ice types in the Labrador MIZ

1.5.1 Icebergs

Icebergs entering the Labrador Sea originate mainly from

the calving margins of tidewater glaciers in the fiords of West

Greenland north of Disko Bay. These account for 85% of the

total input with remaining contributions coming from the Devon,

Bylot, western Ellesmere and Baffin Islands, as well as some from

east Greenland (Petro-Canada, 1982). Over a period of several

years, these bergs first drift north along the west Greenland

coast and then south along eastern Baffin Island to enter the

Labrador Sea in two main streams. The one closest to shore

occurs in the Baffin Current segment of the Labrador Current,

flowing along the marginal trough between the coast and offshore

banks. Another main zone of transport is along the outer edge

of the continental margin which is dominated by the West Green-

land Current segment (Petro-Canada, 1982; Dinsmore, 1972).

Iceberg distributions in the Labrador Sea are described by

Gustajtis and Buckley (1977). In winter the berg frequency is

low and occurrences extend south to about 56°N latitude. In

spring, the frequency increases rapidly to establish a central

12

zone of high concentration, extending north and south parallel to the coast, near the edge of the continental margin; berg frequencies decrease both landward and seaward of this zone, but characteristically occur throughout the pack. Within the pack, the icebergs are protected from deterioration by the ice cover which itself perpetuates lower water temperatures and the absence of strong swell. From May however, water temperatures begin to increase as the pack retreats and this significantly reduces the number of bergs, which then begin to decay through ablation and calving. By August the berg densities are light and confined to the cold Baffin Current segment of the Labrador Current. This decrease continues into fall by which time water temperatures are highest and bergs are fewest, being confined to sporadic individual occurrences (Gustajtis and Buckley, 1977).

Reported iceberg masses in the Labrador offshore range between 100,000 and 20,000,000 tons; bergs drift at about 30° to the right of the mean wind direction at about 2.5% of the wind velocity (Gustajtis, 1979). Observed average drift velocities are at 0.1-0.3 ms^{-1}, nearing maximums of 0.5-1.2 ms^{-1} (Wright and Berenger, 1980).

1.5.2 Multi-Year Ice

Much of the Labrador Sea multi-year ice originates in Nares Strait and Smith Sound. Markham (1981) indicates that an outflux occurs into Baffin Bay from these areas during autumn. Dunbar (1973a, 1978) also mentions the transport of old floes through Nares Strait during fall; as well, Kovacs and Sodhi

13

(1980) briefly describe two old floes occurring near Hans Island in Kennedy Channel, one of which had an area of 10 by 16 km. In some cases this autumn efflux will produce two or three tenths of old ice near the eastern tip of Devon Island and across the entrance to Lancaster Sound (Markham, 1981). Discharge rates are highest in fall and decrease in early winter, eventually terminating with the occurrence of an annual ice bridge which begins to form across Smith Sound during the early-December to late-February time period (Dunbar, 1973b; Markham, 1981). A secondary source of input to the Labrador Sea is from the east-ward drift of old floes through Jones Sound and Lancaster Sound into Baffin Bay; Milne, Herlinveaux, and Wilton (1977) describe their research on some of these floes which had drifted south through Barrow Strait, destined to eventually join with the east-ward drift in Lancaster Sound.

As new ice forms in Baffin Bay during fall, the old floes become embedded in the first-year coverage (Masterson and Wright, 1982), and drift southward at a rate of approximately 5 degress of latitude per month, passing through Davis Strait by spring (Markham, 1981). The actual time of multi-year ice arrival in the Labrador Sea and its magnitude of occurence is variable and dependent upon weather conditions in the Arctic. Crane (1978) reports that, during years of an early pack-ice advance in Davis Strait, the associated northerly or westerly winds will result in an increased delivery of multi-year ice from the Baffin Bay and Foxe Basin areas. In addition, these

14

winds produce lower air temperatures leading to reduced melt

rates. Years of late pack-ice advance however, are associated

with easterly or southerly winds which originate from over

warmer waters and produce higher temperatures. Southerly winds

also impede the delivery of multi-year ice from farther north

because they act against the southward drift of the ocean cur-

rents (Crane, 1978). Years of late pack-ice advance therefore

are associated with lower concentrations of multi-year ice off

Labrador.

Irrespective of annual variations in frequency however, the

concentrations of multi-year ice off Labrador does not increase

to significant amounts until late May when it usually comprises

less than 1/10 of the aggregate ice coverage in any region of

the pack (Markham, 1980b) - a value which is rarely exceeded.

Unfortunately, detailed information regarding multi-year ice in

the Labrador Sea is not widespread, being confined to only a few

reports which are based on measurements obtained from either

photographic reconnaissance or on-site study of floes-of-

opportunity encountered within the pack. It was this paucity of

information which prompted the undertaking of the study

described in the chapters which follow.

In 1979, multi-year floe thicknesses were reported at

between 4.3 m and 32.2 m with an average of 14.2 and a standard

deviation of 4.6 m (Fenco, 1979). Thicknesses in 1978 ranged

from 5.3 to 28.8 m with a mean of 15.1 m and a standard deviation

of 4.6 m (Fenco, 1978). The 1978 and 1979 measurements were con-

ducted from aerial photographs however, and used an assumed ice density. Thicknesses measured from drilling of individual floes by Fenco (1976) range from 1.5 to 15 m with a mean of 7.41 m and a standard deviation of 3.9 m. Butt, et al., (1979) reported a thickness of 14.6 m for a floe near Groswater Bay; Imperial Oil Ltd. (1977) reported thicknesses up to 16 m and diameters up to 100 m in Davis Strait.

Nolte and Trathart (1971) reported a floe measuring 9.14 m by 24.38 m (222.8 m^2) in the southern Labrador Sea (Skidmore, 1979). Fenco (1979) reported surface areas ranging from 540 m^2 to 24,522 m^2 with a mean and standard deviation of 4085 m^2 and 2221 m^2 respectively for 1979. For 1978, surface areas varied between 835 m^2 and 74,371 m^2 with a mean of 4187 m^2 and standard deviation of 3557 m^2 (Fenco, 1978). Fenco (1976) estimated floe areas ranging between 100 and 10,000 m^2 (Wright and Berenger, 1980).

Floe masses estimated by Fenco (1979a) for the 1979 ice sea-son ranged between 6050 and 379,710 metric tonnes with a respec-tive mean and standard deviation of 55,472 and 45,654 tonnes. For 1978, the range was between 8,327 and 1,076,770 tonnes with a mean of 98,313 tonnes and a standard deviation of 150,725 tonnes (Fenco, 1978).

Floe drift velocities during 1976 (Fenco, 1976), near Hope-dale and Cartwright, averaged 0.29 ms^{-1} with maximum speeds of 1.0 ms^{-1}. Masterson and Wright (1982) report speeds, measured over a few hours, averaging in range between 0.05 and 0.5 ms^{-1}

16

with maximums up to 1.5 ms^{-1}, for the 1976 and 1977 winter seasons. Over short time periods these drifts varied in direction, but the mean resultant was southeastward.

Internal temperatures in a multi-year floe range between -4°C and -17°C with an average of -5°C at the 2 m depth (Masterson and Wright, 1982). In comparison, first-year floe temperatures measured during freeze-up in 1979 ranged between -5°C at the surface and -1.9°C near the bottom (Fenco, 1979b); in 1976 first-year temperatures ranged between 0°C and -12° with a mean of -4.2°C in March and -2.6°C in April (Fenco, 1976). Because the initial brine content will drain out over several melt seasons (Bennington, 1967; Untersteiner, 1968) salinities for multi-year ice average near 1 °/oo (Petro-Canada, 1982). It is this combination of lower temperatures and lower salinity as well as a different crystal structure which makes multi-year ice much stronger than younger sea ice types (Masterson and Wright, 1982).

CHAPTER 2

STUDY OBJECTIVE AND METHODOLOGY

2.1 Study rationale

Previously completed studies concerning multi-year ice in the
Labrador Sea have ignored its spatial aspects, preferring to deal
mainly with its mechanical and physical properties in anticipation of
engineering problems related to loading on offshore structures, or pos-
sible damage to vessels traversing the pack. While these studies have
produced valuable results, there is still very much to be done in the
interests of assimilating an informative data base describing this type
of ice. Although the collection of data regarding the intrinsic proper-
ties of multi-year ice falls outside the realm of the geographer, it
does seem sensible that the gathering of such data could be better
facilitated if information was available to give the field scientist a
more accurate description of its patterns of occurrence. It might then
be possible to anticipate multi-year ice distribution contingencies to
be encountered in the Labrador offshore. Clearly, this void could be
at least partially filled by a detailed spatial analysis of multi-year
ice occurrence within the Labrador MIZ.

At least two of the previous studies had indicated that multi-year
ice might not be homogeneously distributed within the MIZ. Fenco
(1976) observed a highly concentrated strip of multi-year ice between
90 and 120 km offshore near Hopedale, and a few years later gave
another limited description (Fenco, 1979a) indicating that multi-year
floes had been seen to occur both as a single floe surrounded by
younger ice types as well as within fields of other multi-year floes.
In neither case were descriptive spatial statistics provided, but the
suggestion was that multi-year ice might occur as groups of relatively

high floe frequency with adjacent regions having very low occurrences.

To investigate the hypothesis that multi-year floes might in fact occur as groups, the study detailed herein was undertaken to produce the necessary spatial statistics from a large sample of multi-year ice. Although the study, having been based on analysis of one year's photography, might not be representative of any long-term trend, it does give factual data regarding the distribution for the 1979 season. It is hoped therefore that the information presented will provide some insight into how multi-year ice has occurred spatially in the Labrador offshore and that it will serve both to stimulate and aid further studies.

2.2 Data base characteristics

Data to be used were extracted from a portion of a set of aerial photographs on loan from Petro-Canada Exploration Inc. and the Labrador Group of Companies. This set contained information collected along four different flight lines across the Labrador pack, with origins at Saglek, Cape Kiglapait, Kikkertavak Island and Fish Cove Point (Figure 4).

The Saglek line, being the northernmost, was chosen for this study because of its geographic ability to portray the characteristics of multi-year ice upon its entering the Labrador MIZ on its journey south. This set of photographs, from eight flight missions, contained data collected along a flight line bearing 097° Mag. from Saglek, Labrador, crossing over the Gilbert wellsite. Photography was begun near the inshore edge of the Eastcan offshore lease holdings and, with one exception, continued offshore until the ice edge was encountered; due

19
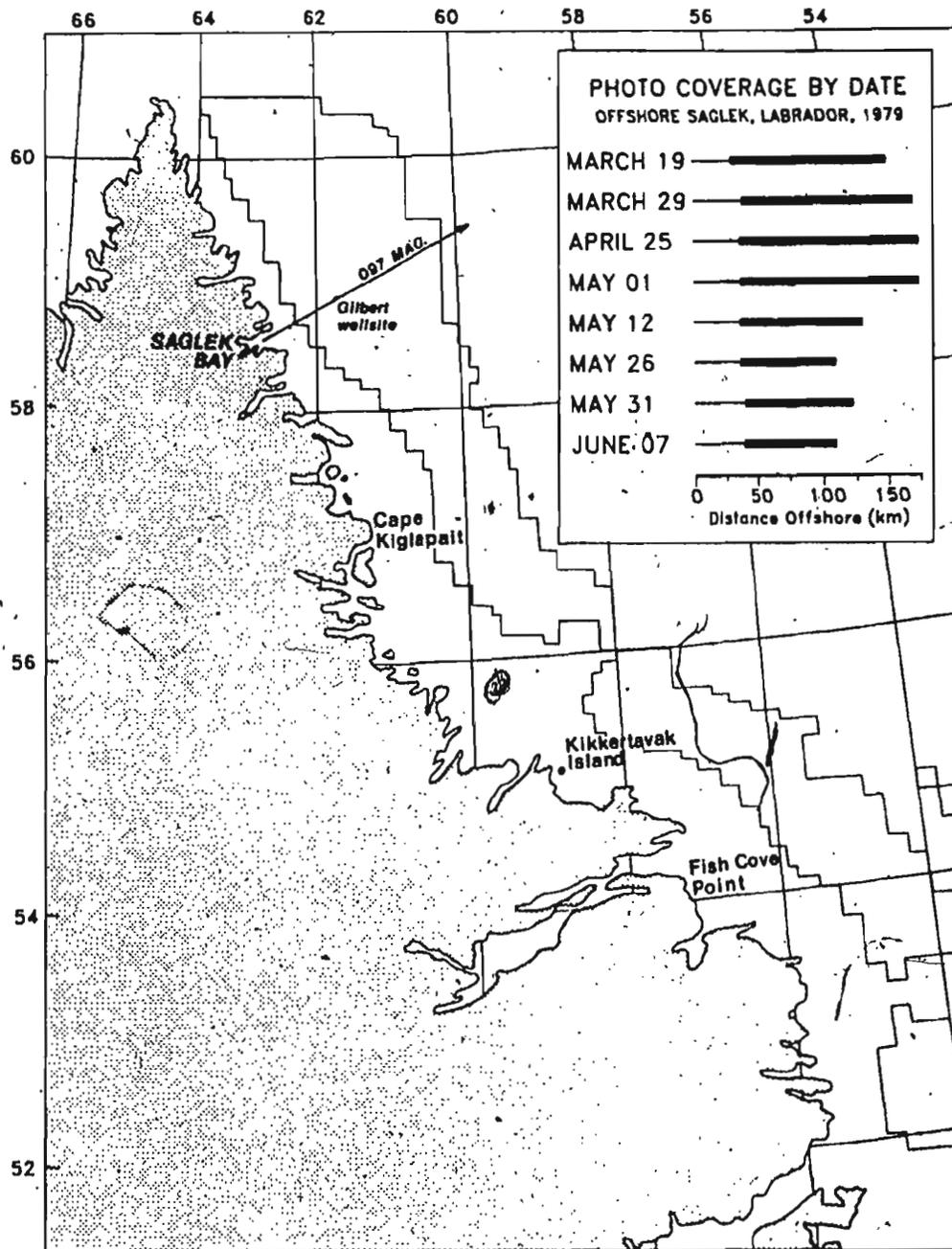
Figure 4 – Study region and photographic coverage by
date. Solid bars in inset indicate the extent of
photographic coverage with reference to the bar
scale; thin lines indicate that portion of the
distance along 097° Mag. for which no photos were
taken.

20

to ice-fog off Labrador on May 12, one flight was aborted at 130 km and did not reach the ice edge at 148 km. The nominal photographic scale was 1:6000; refer to Figure 4 for flight dates and extent of coverage.

2.3 Data collection

The collection of multi-year ice data from air photographs is dependent upon visual identification which may sometimes be a diffi- cult procedure. Therefore, a detailed two-stage process of data recognition and recording, described below, was carried out over a ten-month period to ensure achievement of optimum accuracy for the information extracted.

2.3.1 Establishment of identification criteria

Since no comprehensive list of criteria for identifying MIZ multi- year ice was available, the initial priority was given to establishing the identification characteristics by which it could be recognized and isolated from other ice types.

During 1981, preliminary observations were conducted from CCGS Sir John Franklin between February 21 and March 6 while enroute to and from Lake Melville, Labrador, and from an Atmospheric Environment Service (AES) ice reconnaissance aircraft on May 6; although no multi-year ice was encountered, valuable knowledge and experience was gained in the identification of younger ice types as well as in general familiariza- tion with the ice regime of the Labrador Sea. In early January 1982, with the arrival of photographs from Petro-Canada Inc., a tentative list of criteria was established through visual analysis of the photos,

coupled with information from available literature and previous discussion with AES ice observers. Between March 20 and 27, 1982, field observation of ice types was again conducted from the Sir John Franklin, mainly in a region north of Groswater Bay; on this occasion use of the ship's helicopter facilitated both aerial and on-surface photographic studies of two multi-year floes. The observed morphological characteristics of these floes, along with further study of the Petro-Canada photos, a review of appropriate slides from the C-CORE Data Bank, and discussions with Mr. A. Allan of C-CORE, led to the establishment of the final list of criteria. In June 1982, two supplementary overflights were carried out aboard an AES aircraft on the 5th and 21st; visual observations at these times substantiated the contents of the existing list and did not suggest any further revisions.

2.3.2 Analysis of photography

Having established the criteria, identification of floes from the 1979 photography was commenced in early April 1982 and continued until November. In each case, during the first examination of a series of photos, a floe was isolated by circling it with a grease pencil in a color appropriate to its identification status -- definite multi-year or possible multi-year. After the photo sets had been examined in this manner, each photo in each set was examined a second time, during which the status of individual floes was again evaluated based on the surface criteria they exhibited; this time particular attention was paid to either deleting or positively identifying those floes previously marked as possible. In a third and final scrutinization, each photo was again studied to ascertain the status of all previously isolated floes.

22

The photographs were studied in the region to the right of the principal point, containing the 40% of forward overlap coverage not common with the preceeding photo in the series; this area was considered to be a cell. Since the actual size of this region would vary slightly, depending on aircraft altitude and speed, special care was taken to ensure that each successive cell was begun at exactly the same point, with reference to the ice surface, where coverage from the previous photo had ended. In this manner, the researcher would avoid counting the same floe twice in a situation where a cell might contain coverage common to the previous cell, or missing a floe where a gap existed between the end of the previous cell and the beginning of the next.

All photos were viewed as a stereopair under eighth power magnification using a WILD mirror stereoscope. The stereopair was affixed to a metal plate which could be shifted sideways while the stereoscope was placed on a specially constructed frame which allowed it to be moved backwards and forwards relative to the user. In a cartesian sense, the movement of the stereopair was along a X-axis while the movement of the stereoscope was along a Y-axis. This setup allowed the user to focus on a small portion of the photo cell while moving the stereoscope along the Y-axis to scan the photo from bottom to top; at the top, the photos were shifted left along the X-axis so that the stereoscope was now positioned slightly to the right of the area covered in the upward scan. The scope was then moved back down the Y-axis to the bottom of the photo, in a track paralleling and immediately adjacent to the upward track; at the bottom, the photos were again shifted

and another track begun upwards. This structured approach allowed each photo to be examined in minute detail; use of a cartesian coordinate system of X and Y movements ensured that all regions of a photo cell could be examined sequentially in this manner without fear of omitting any portion or of losing track of what regions had been studied.

2.4 Data assimilation

2.4.1 Recording data

As each cell was scanned, an identified floe was measured along its axis of maximum diameter, with the size being recorded along with the serial number of the photo cell in which it was found. In addition, from the margin of each photo, an altitude reading was taken for calculating the actual size of the multi-year floes it contained.

2.4.2 Data transformation

Recorded data were entered and stored on a Digital VAX/VMS computing hardware/software system and processed using algorithms written in the 1977 FORTRAN standard.

In the first stage, diameter measurements taken from photos were transformed from raw to actual surface values by calculating a specific scale for each photo, using a formula from Avery (1977). This incorporated the mathematical relationship between flight altitude for each photo and the camera focal length:

$$\text{Scale} = \frac{\text{Camera Focal Length (m)}}{\text{Altitude Above Surface (m)}}$$

Calculating specific scales allowed floe sizes to be determined as accurately as possible and eliminated the error which might have been introduced by altitude fluctuations if a mean flight level had been

24

calculated for the entire line.

Following this, a program was written which positioned the cells
sequentially along the flight line, giving their positions in terms of
calculated distances from the ice edge and from the shoreline. For
this procedure a mean cell size was assumed for the entire photo set
and was determined from a sample of photos randomly chosen with no dis-
cernment made towards the ice type they contained. While several
methods of cell positioning were considered, the one deemed most satis-
factory was to position the cells with reference to the ice edge. This
was accomplished by obtaining the serial number of the photo at the ice
edge as well as the distance offshore at which the edge was located on
the given flight date. Actual positioning was achieved through an
algorithm which determined the number of intervening cells between a
given cell and the final one in the series and then multiplied by the
average cell size. This program also read the data previously calcu-
lated on floe sizes and produced summary information detailing the floe
frequency, sum of floe diameters, as well as average, maximum, minimum
and ranges of floe sizes for each cell.

Implementation of this two-phase programming approach to data
transformation allowed for a subsequent diversity of analysis since two
distinct, numerical data bases were produced for each flight date. One
contained individual floe sizes useful for production of descriptive
floe size statistics, while the other contained a summary of multi-year
ice data by cell position within the pack and was useful for spatial
and temporal analysis.

25

2.5 Data analysis

When analyzing data for a given flight date, spatial analysis
primarily involved data at the cell level. An exception occurred in
the case of the chi-square analysis where the cell categories were too
small to satisfy test requirements; in this case data were grouped into
distance categories of five kilometres, a satisfactory interval width
which was still small enough to avoid obscuring the true shape of the
distribution. For the chapter on temporal analysis (Chap. 6), the
data were grouped into categories of ten kilometres width; since the
objective here was to provide a synoptic overview of multi-year ice
occurrence and associated trends through the season, rather than a
detailed description, this category was chosen because it avoided the
awkwardness and confusion of comparing the numerous graphs which would
have resulted from the use of cell data.

Statistical analysis utilized mainly the Statistical Package for
the Social Sciences (SPSS) which was supported on the university VAX.
An exception was the calculation of floe size statistics which were pro-
duced using the Statistical Analysis System (SAS) supported by a New-
foundland and Labrador Computing Services (NLCS) computer.

Graphical analysis utilized the SPSS Graphics package, the Geo-
graphical Information Management and Mapping System (GIMMS), the Zeta
Plotting Subroutines package, and Surface II which is capable of produc-
ing three-dimensional mathematical surfaces representing numerical
trends. All of these were supported on VAX, with processed plot files
being spooled to a four-pen Nicolet-Zeta plotter for hard-copy pro-
duction.

2.6 Evaluation of method

While great care was taken to achieve optimum quality in data control, especially in the verification of programming logic, there remained some aspects which were beyond the control of this research project and which therefore represent certain margins of error.

2.6.1 Ice edge positioning

An operational report supplied with the photographs gave the ice edge position for each flight date and, except for May 12, stated that photography was terminated at this point. However, for some photo dates, even though the condition of the pack ice indicated the edge to have been very close, it was not contained in the last serial photograph; in these cases the only solution was to positon the last photo at the offshore distance given for the ice edge. This would have introduced a small error in cell positioning so that while many distances are later given to one decimal place, this is merely for the purpose of spatially distinguishing between individual cells and no attempt should be made to apply these calculated positions in a site-specific manner without consideration of this error margin.

2.6.2 Incomplete data

Occasionally an identified multi-year floe was located at the upper or lower margin of a photo such that a portion of its surface fell outside the coverage region and was lost. Since it was not possible to ascertain its maximum diameter in this case, the floe was deleted from the final count because entry of a partial diameter reading would produce spurious results in calculation of average size

27

and other statistics. Due to this, the total count given of identified multi-year floes for each date is slightly less than actually observed; Table 1 lists the number of omitted floes by date.

For the March 19 and March 29 flight lines, even though there was photo coverage to the ice edge, only five multi-year floes were found for each date, presumably because these lines had been flown early in the season, before the major influx of multi-year ice had occurred. Owing to such a small count, these data sets were deemed incomplete for production of any representative statistics and therefore no analysis was performed upon them.

2.6.3 Missing data

The most severe case of missing data concerned the photos for May 12, when photography was aborted at a position 19 km from the ice edge. As a result, the analysis for this date deals only with the spatial distribution along the line to this position and is not based upon total coverage to the ice edge.

Other, more minor, instances occurred when it was decided, for the purpose of this study, to truncate all flight line coverage to a common origin of reference beginning at 37 km offshore. This was the innermost point at which multi-year ice had been photographed on any of the flight missions between April 25 and June 07. Some of the flights had originated shoreward of this point and posed no problems, however others had begun slightly seaward from this point so that these flight lines are displayed as having missing data between the common origin of reference and the seaward point at which photography was actually started.

28

Table 1 - Deleted data by flight date

DATE	NO. OF FLOES
April 25	10
May 01	13
May 12	34
May 26	24
May 31	21
June 07	39

2.7. Summary

While problems are usually not uncommon in research, the underlying causes of such margins of error in this study arose partially from having to plan the research around an already collected photo series, within which any intrinsic variations or omissions could not be corrected for, as well as the absence of any analogous study which could have been used as a reference model. In the overall context of the study however, it is felt that these problems are minor and do not alter the ability of this project to provide hitherto unavailable information regarding the 1979 multi-year ice distribution in the region near Saglek.

CHAPTER 3

IDENTIFYING MULTI-YEAR ICE IN THE LABRADOR MIZ

3.1 Official Terminology

Sea ice older than first-year is described generally by the
World Meteorological Organization as old ice and is subdivided
into two official categories, being first described as second-
year ice after surviving one summer's melt and multi-year ice
upon surviving any subsequent summer. The official birthday of
old ice is October 1, when any ice existing in the Arctic from
the last winter or several previous winters is assumed to have
survived the current melt season and is classified accordingly
(Markham, 1981). By official definition both classes have a
higher freeboard than younger ice types. Second-year ice has
a greenish-blue melt pattern of many small isolated puddles
interspersed with bare hummocks. Multi-year ice, being almost
totally void of brine, exhibits a blue melt pattern of more
fully developed puddles, with interconnecting channels located
between hummocks much smoother than those of the second-year
type (WMO, 1970; SPRI 1973; MANICE, 1980).

Although these descriptions are generically correct within
the age-hierarchical structure of sea ice nomenclature, they are
of only peripheral use in identifying individual multi-year floes
within the physical setting of a marginal ice zone. Mainly
because of the wide range of dynamic conditions existing in this
region and also due to the melt conditions previously occurring
in the Arctic source region, many old floes exhibit differing

31

combinations of distinguishing and/or camouflaging character-
istics which often make them appear distinctly different from
one another.

Because of fracturing during transport from the Arctic
source regions, floes arriving in the MIZ are actually fragments
of larger parent floes (Fenco, 1979) which existed in the
Arctic. On a macro-scale, a large parent floe would exhibit an
overall melt pattern similar to generic description. However,
on a meso or micro-scale some of its regions which contained,
for example, prominent hummocks would be distinctly different
from other areas of the same floe containing mainly melt ponds.
Given that MIZ multi-year floes are the fractured remanents of
larger floes then correspondingly, their melt patterns are also
meso or micro-scale portions of the original macro-scale melt
patterns. As such, their individual characteristics will be
determined by which portion of the original floe surface they
initially comprised. Consequently, while these floes collec-
tively represent a typical multi-year melt surface, as individ-
ual floes they appear unrelated.

The descriptions contained herein are based on conclusions
drawn from study of the 1979 data base and observations made
during field-related experiences in the Labrador MIZ. They sum-
marize nomenclature descriptive of multi-year ice in a marginal
ice zone and serve to expand upon official descriptions. While
there are situations where it is practical to distinguish between
second and multi-year ice (Markham, 1981) such differences are

not emphasized here; rather, descriptions are confined to two main categories dealing with the identifying and disguising surface characteristics exhibited by old ice.

3.2 Identifying surface features

3.2.1. Hummocks, ponds, and channels

The first stage in the formation of these features probably begins with the presence of an undulating snow cover on a first-year floe. With increasing solar radiation, melt-water forming on the crests of snowdrifts will run off to collect in the intervening troughs, where it will darken the surface of the snow, turning it to slush (Lister, 1962). The resulting decrease in albedo causes accelerated melt in this depression which leads to formation of a small pool between the drifts. As the season progresses, melt will continue to widen and deepen the pond, but the surrounding snowdrifts, with their higher albedo, will protect the surface underneath them from experiencing an equivalent degree of melt. By the time the snow has completely disappeared, the result will be a series of entrenched melt depressions scattered amongst the raised hummocks which themselves mark the location of the last remnants of protective snow cover. In another scenario, hummock formation can be initiated by the bending and fracturing of thick first-year floes during collision or shearing in response to in-plane compressive forces (Kovacs and Sodhi, 1980). This leads to floe fragmentation and produces piles of rubble in first-year ice; after a few summers of ablation and subsequent refreezing, these piles will

33

consolidate into a solid hummocky mass known as a multi-year hummock field (Metge, et al, 1982).

Of course, this is only a schematic description of a formation process which apparently has a number of variations in reality, depending upon the condition of the original floe surface. No matter what the formation process though, hummocks are rarely of uniform height and can have a range of relief. Clearly, the resulting pattern of weathered surface is related to the condition of the original surface which is determined by ice dynamics and weather conditions occurring in the source region. Therefore, the relative proportions of coverage by melt-ponds and hummocks will be intrinsically variable, however the final outcome is always some variation on this pattern.

Once a melt-pond has been formed, its lower albedo, in relation to the surrounding ice surface, will result in ablation rates of two to three times higher than for the bare ice (Hanson, 1961). In addition to deepening, it will continue to widen by melting the ice along its peripheral region; this is accomplished through a process of convective overturning of water under the influence of wind (Crarey, 1960). If the floe remains stationary, either through grounding or because it is landfast, and if the winds blow from a prevailing direction, the meltwater will be forced towards a region of concentrated melt in the downwind portion of the pond causing its outline to become progressively elongated. However, elongation processes might be

34

short-lived if the floe rotates, or the wind changes, causing the melt-water to concentrate at a different point, thus equalizing the outward rate of melt. The net result is often more of an oval-shaped depression, rather than one which is long and narrow.

Continuing melt pattern evolution will see the ponds connected by a growing network of drainage channels. Since many of these channels sometimes change direction in a sharp and angular fashion, it would appear that they are formed by cracks which have propagated along the floe surface. Such cracks, which are the tensile product of thermally-induced stress, can initially be up to several centimetres wide (Evans and Untersteiner, 1971; Evans, 1971; Lazier and Métge, 1972); some other cracks might also be formed by surface flexing in response to wave action (Goodman, Wadhams and Squire, 1980). The warm melt-water from a pond seeps along a crack, melting its walls to widen and perhaps deepen it into a functional melt-water channel. As water flows along its course, any sharp bends in the channel will become rounded due to melt-water concentration at this point and the channel might take on a sinuous shape.

As this established melt pattern continues to develop over several melt seasons, the relatively rough hummocked surface of early age will give way to one of gentle undulations with numerous streams and ponds, which approximates the generic pattern by which multi-year ice is most frequently described.

35

.3.2.2 Embayments

The edges of a multi-year floe are sometimes cut by small
bays which enhance its weathered appearance. These features are
formed when a large floe breaks into two or more smaller ones,
at which time a crack propagating through the floe will dissect
the melt depressions along its path. When the piece of ice
breaks away, the melt depressions are fractured such that their
compatible portions are left suspended along the juxtaposing
edges of two newly-formed floes. Once formed, if a bay is at or
below sea level it will fill with sea water which will begin to
melt its periphery, causing it to migrate back across the sur-
face of the floe. This process is probably enhanced by tiny con-
vection currents near the margin of melt; these are induced by
variations in water density due to temperature change and dilu-
tion of seawater salinity by the melting ice (Marschall, 1977;
Zubov, 1943). Similtaneous with this, the bay might also widen
by melting laterally outwards along the edge of the floe, per-
haps joining eventually with an adjacent bay undergoing the same
process. As back-cutting and widening progresses, the bottom
surface of the bay might be relatively unaffected so that it is
left behind to project out from the waterline edge of the floe
as an underwater ram.

This process probably occurs in the Labrador offshore in
late spring and might occur earlier during periods of prolonged
pack compression and consolidation. In a compressed pack, sea-

36

water would not be constantly flushing into and out of the bays, so that with a restricted water-mixing process, solar radiation would increase local water temperature and accelerate the melt, especially when surface temperatures were above freezing. In spring, with an open pack, wind and wave turbulence around the edge of a floe (Wadhams, 1980) would also accelerate the melt rate.

3.2.3 Weathered Ridges

Multi-year ridges are the ablated remnants of younger ridges formed in the Arctic when thick first-year ice is deformed under compression. During the melt season, ablation will round the protruding blocks and produce melt-water which then seeps into the interblock voids where it freezes. Through a repeated series of freezings these voids eventually fill completely with ice which consolidates the blocks, making the ridge structurally massive (Kovacs et al., 1973). Over several melt seasons the sides of the ridge are progressively ablated so that as age increases, the slope angle becomes more gentle. Depending on its age and degree of melt, a ridge sail might have a serrated apex caused by the protruding remnants of individual blocks or it may exhibit several gentle undulations along a rounding top.

When a multi-year floe is studied from overhead, the ridges, if present, appear as linear features truncated at one or both ends. The sides are usually gently sloping; sometimes a melt pattern of rivulets runs down either side from the crest, termin-

37

ating in a marginal melt-water trough, or series of troughs run-
ning along the base of the ridge. A ridge will also have a much
larger keel extending downward from the bottom of the floe.

3.2.4 High freeboard and undeformed edges

In a pressured pack, where younger floes are undergoing
peripheral deformation, a multi-year floe is often clearly
visible because of its undeformed edges and its greater free-
board which gives it a higher relief relative to the surrounding
ice. High freeboard is due to the greater thickness of the
floe. Undeformed edges are due to a higher compressive strength
which enables the floe to withstand greater lateral loading with-
out experiencing failure; this is a product of brine loss during
previous melt seasons. As a result, the edges of a multi-year
floe, when they are visible, are undeformed and usually abrupt.
When viewed from above, the peripheral outline is often one of
rounded corners (produced by continuous pack-ice abrasion) and
gentle undulations along the sides. The presence of angular
corners and sharp angular serrations along one or more of its
sides indicates that a floe has recently separated from another
piece of multi-year ice; such a floe will usually have rounded
corners and sides along the remainder of its outline.

3.2.5 Color

Its salt-free condition also determines the manner in which
the internal structure of a multi-year floe affects the trans-
mission of light, causing the floe to exhibit a distinctive blue

color. Neither sunny nor overcast conditions seem to alter its tonal value when viewed from an airborne platform, but when viewed at an angle from the surface this color might be more apparent during overcast conditions. Color is a very useful criterion for multi-year ice identification; even under a cover of snow, a bluish tint can be observed from overhead, distinguishing this floe from the surrounding younger ice types which will remain white or grey.

3.3 Disguising features

3.3.1 Surface rubble

Surface rubble is produced through deformation and destruction of younger ice types in the surrounding pack region by dynamic processes which later deposit some of the resulting debris onto the surface of the older ice. The pattern of deposited rubble fragments will vary depending upon the mode of deposition.

One mode occurs most when the pack is in an open condition or when the floe lies very near the ice edge. In these situations ocean swells and surface waves will infiltrate the pack for some distance before being attenuated by the ice. Because of its greater mass, a multi-year floe will not respond vertically to the wave energy in the same manner as will the thinner and smaller floes of younger ice types. Consequently, a propagating wave will temporarily innundate a portion, or the total surface, of the floe, depositing younger forms of floating ice

onto its surface in the process. Rubble deposited in this manner is distinctive in its usually random pattern of dispersal which originates near the edge where the wave first made contact and extends across the floe surface.

A second process, known as ice pile-up, occurs when floes are confined within a pack under lateral compression. Pile-up has been observed in the Arctic where, in one instance, a grounded multi-year floe having vertical sides was almost completely covered with rubble through a process described by Kovacs and Sodhi (1980). This occurs when thinner sea ice is driven past a floe on either side; ice which cannot pass because of obstruction by the floe then piles on the up-pressure side. In the process, the ice becomes severely fragmented and piles up high enough to fall down onto the floe surface near the edge; during prolonged periods of this action most of the floe surface might eventually be covered. Although such pile-ups observed on multi-year ice in the Labrador MIZ might be the products of relict pressure conditions occurring in the Arctic, it is more likely that they are the product of MIZ dynamics since pile-up has been observed to occur on at least one tabular iceberg grounded in the near-shore region of the pack (Kovacs and Sodhi, 1980). While the multi-year floes would not be subjected to grounding in the Labrador Sea, a similar piling process might occur when, under the pressure of a converging pack, younger floes are compacted into collision with a multi-year floe.

40

Should the floe have sloping sides the younger ice will likely raft and ride up onto its surface. Alternatively, as floes rotate and shear against one another a vertical-sided old floe would cause the ice to be pulverized at the line of contact whereupon it would pile up in the manner described.

Whatever the cause, such pile-ups were observed to have occurred frequently in the Labrador MIZ during 1979. Usually confined to the peripheral region of the multi-year floe, many pile-ups encircled either all or a portion of the edge area, creating the illusion that the floe had undergone a process of pressure deformation indicative of first-year ice. Since the extremes of sea ice dynamics in the Labrador pack are relatively unknown, it seems possible that total surface obliteration of a multi-year floe could result from complete-overriding by younger ice forms.

While surface rubble solely will aggravate the identification of a multi-year floe, especially where the use of black and white photography negates the reliance upon floe color, a portion of the melt pattern is often visible between the scattered blocks or at the center where edge pile-ups do not usually reach. It is in conjunction with snow cover that surface rubble features become most problematic.

3.3.2 Snow cover

Snow can be a problem in the identification of a multi-year floe because of its ability to visually alter or totally cover surface melt features, hence requiring greater care in inter-

pretation. Often, deposition of edge rubble on a multi-year
floe serves as a wind break, allowing a snowdrift or series of
drifts to form on its lee side and extend across the surface of
the floe. Sometimes a portion of the melt surface is still
visible, but if the rubble extends around the entire edge then
as the wind shifts, the orientation and coverage of snowdrifts
will alter accordingly, producing a complete covering of snow
encircled by edge rubble. If, on the other hand, scattered rub-
ble exists it will facilitate the deposition of snow in the
areas between the blocks so that portions of them will protrude
from beneath the snow cover suggesting themselves to be pieces
of a deformed first-year surface. In either case, if a portion
of the melt pattern does not appear from beneath a thin region
of the snow cover, the floe is not very different in appearance
from the nearby first-year ice. Identification then becomes
difficult and freeboard does not help because thick first-year
floes having apparently similar surface features can occasion-
ally have freeboards equivalent to some multi-year floes.

In a region of the pack where deposited rubble is absent
however, careful study of the surface of a snow-covered multi-
year floe usually produces positive results. Hibler, et al (1972)
found that snow cover on a multi-year floe will reflect surface
undulations having a wavelength of 8 m or more, but will mask
those of less than 4 m by infilling of the depressions. This is
significant because in a snow-covered pack containing both first
and multi-year ice, young ridges and other features of recent

42

pressure deformation will protrude from the snow revealing the nature of the first-year surface beneath. Reciprocally, the multi-year floe, with its usually gentle surface undulations, will have an unbroken snow cover which is an approximate reflection of its surface contour. Positive identification though would still depend on correlation with other factors such as high freeboard and undeformed edges. Usually identification is aided by the presence of at least one multi-year floe which has a tiny portion of its melt pattern exposed, thereby confirming its identity. Study of the surface characteristics in the snow-covered region of this floe then serves as a key for comparison with the surface features of other suspected multi-year floes.

In the case of wind-swept surfaces, if a multi-year floe has pronounced surface hummocks then its chances for identification under snow-covered conditions are even better. If the snow fall occurs in conjunction with wind and the absence of sheltering edge rubble, then blowing snow will settle into the melt depressions, filling them approximately flush with the surface; however the hummocks, because of their exposed and rounding surface, will remain bare. Unlike rubble, which when protruding from a snow cover will also appear white, these hummocks exhibit the blue color of multi-year ice. The resulting pattern is one of a white snow cover interspersed with dark, bare hummocks. In some instances, after a strong wind has completely swept all exposed surfaces (except the lower regions of the melt depres-

sions) these snow-filled cavities are more visible than the hummocks, and appear as distinct white blotches against the darker, blue background of the floe surface.

3.4 Temporal aspects of floe surface characterization

Some aspects of multi-year floe characterization described are consistent in their frequency of occurrence while others exhibit a distinct temporal variation in association with long-term weather trends occurring in the Labrador offshore. Weathered ridges, surface rubble and, to an extent, melt hummocks, are visible throughout the period of multi-year occurrence in the marginal ice zone; however other features will increase or decrease in frequency over the same time span.

In April multi-year floes are predominantly either snow-covered with protruding hummocks as described, or bare and windswept with occasional patches of snow; melt depressions and connecting channels, where visible, are also snow-filled. Moving into early or mid-May the occurrence and extent of snow coverage lessens under the influence of increasing temperatures and solar radiation, so that the hummocks become more visible and many melt-ponds fill with water. By this time the spring melt pattern will have begun to re-emerge but generally does so as the winter snow cover disappears. As a result, many floes will have a par-

tial covering of snow (usually near the edge where snow is thickest in the lee of pile-ups) coinciding with water-filled meltponds in the bare regions where the snow has melted. By the end of May snow will have mostly disappeared (but might still recur), and the melt pattern of ponds and interconnecting channels firmly re-established. Also, the increasing absence of snow will allow more floes to clearly exhibit their blue color, making them distinctive from the surrounding pack. In June, with pack-ice deteoriation in reponse to increasing sea surface temperatures, lateral melt increases along the edges of multi-year floes, and jagged edges are observed more frequently as undercut fragments break away and floes slowly disintegrate.

While this represents the general chronology of multi-year melt pattern re-establishment in the Labrador offshore, the actual time frame for any given year is variable, being contingent upon prevailing weather conditions which might produce delays, accelerations, or a combination of both.

3.5 Illustrative examples

To illustrate the concepts of multi-year ice identification and characterization, Figures 5 to 9 have been included. These should not be considered as being representative of all multi-year floes occurring in the Labrador MIZ, but rather as discrete cases which depict only the characteristics of the floe being described. The varying combination of characteristics they each exhibit serve to indicate that, within the context of floe

45

identification, the concept of a "typical" multi-year floe is

unrealistic.
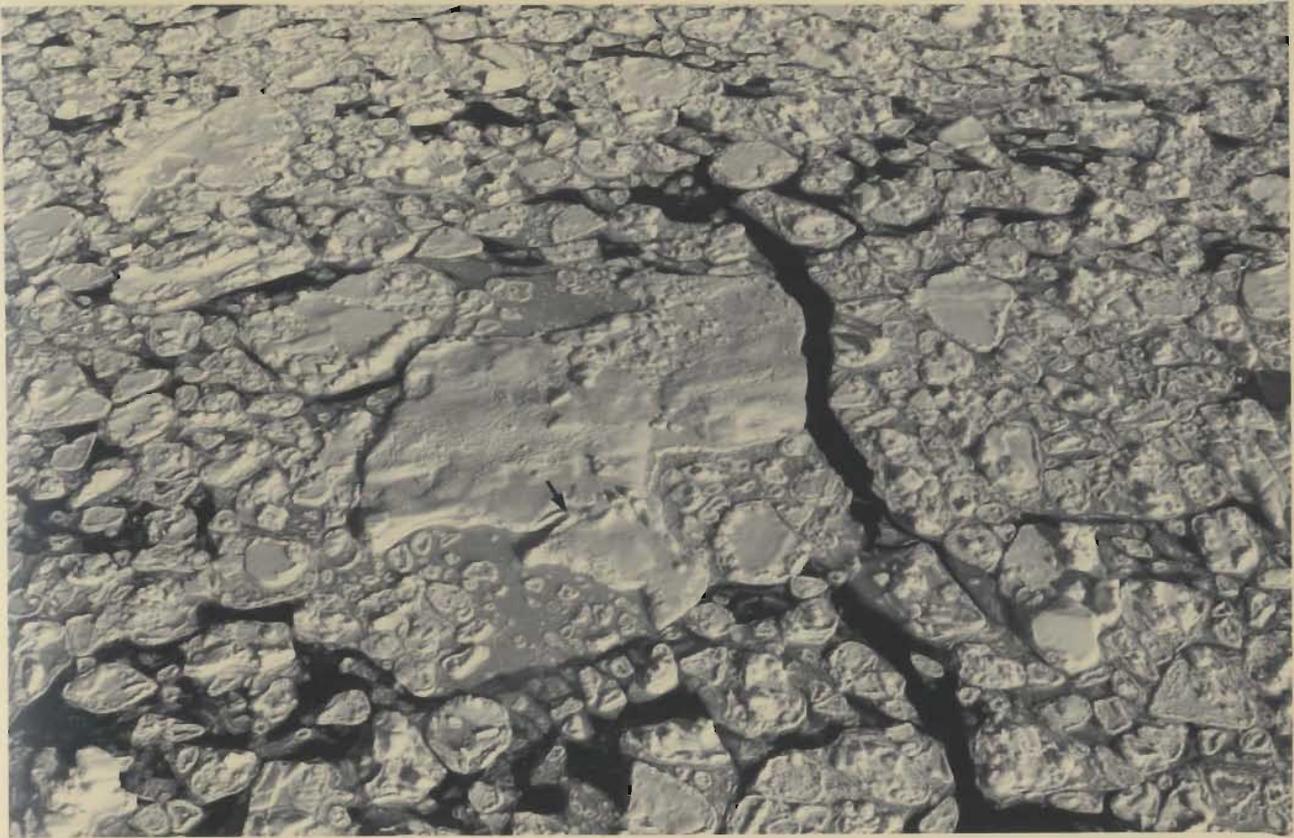
Figure 5: Multi-year floe photographed in the offshore region north of
Groswater Bay during late March, 1982. A light cover of
snow is present but is not sufficient to mask the surface
features which are a series of gently undulating hummocks.
No completely intact melt depressions are present but the
occurrence of two bays along the left margin of the floe
indicates that it has broken from a larger parent floe on
which there were melt-ponds; since the bays are above sea
level, no backcutting has occurred. The presence of large,
flooded and ice-filled bays on the near and far sides of the
floe is probably the result of a merging of two or more bays
which were backcutting at sea level. Since the larger of
the surrounding younger floes do not project into these bays
the suggestion is that there might be underwater rams which
have prevented larger floes from drifting into these areas
during the calm conditions just prior to freezing. The deep
notch indicated by the arrow is a zone where high concentra-
tions of wave energy will accelerate melt, eventually cut-
ting across the peninsula to separate it from the main por-
tion of the floe. Floe edges are clean and undeformed; the
sides and corners are rounded, indicating that separation
from other pieces of multi-year ice did not recently occur.
Presence of scattered rubble indicates that the floe sur-
face has, at sometime, been washed by a passing wave.

Figure 6: Multi-year floe embedded in large agglomeration of ice brec-
cia. The pile-up of ice fragments along the edge of the
multi-year floe is obvious and illustrates how pack compres-
sion leads to these deposits. Although compression might
not have been ongoing at the time of photography, evidence
that it has occurred can be found in the fragmented and
tilted nature of the surrounding younger ice floes. A small
snowdrift is also present, extending partially across the
floe surface from behind a portion of the pile-up. The blue
color of the multi-year floe causes it to visually stand out
from the younger ice types, even in this black and white
photo.
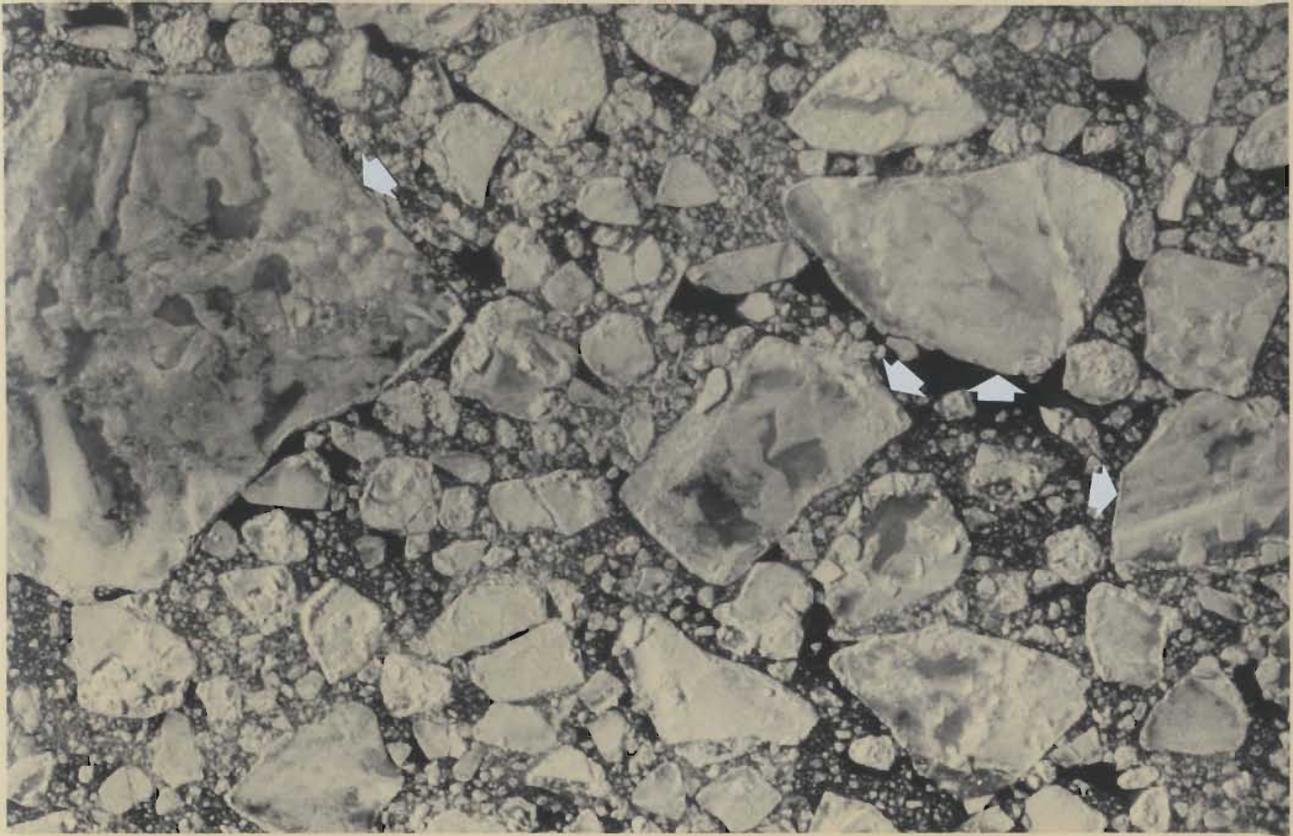
Figure 7: A group of four multi-year floes photographed in June, 1982
near Groswater Bay. Floes show varying degrees of melt pat-
tern emergence. The floe at the extreme right of the photo-
graph is barely recognizable due to lack of a well devel-
oped melt pattern and the presence of snow cover; a few
fragments of younger ice are also present on its surface.
The floe on the extreme left shows an almost fully emerged
melt pattern coinciding with remnants of snow cover.
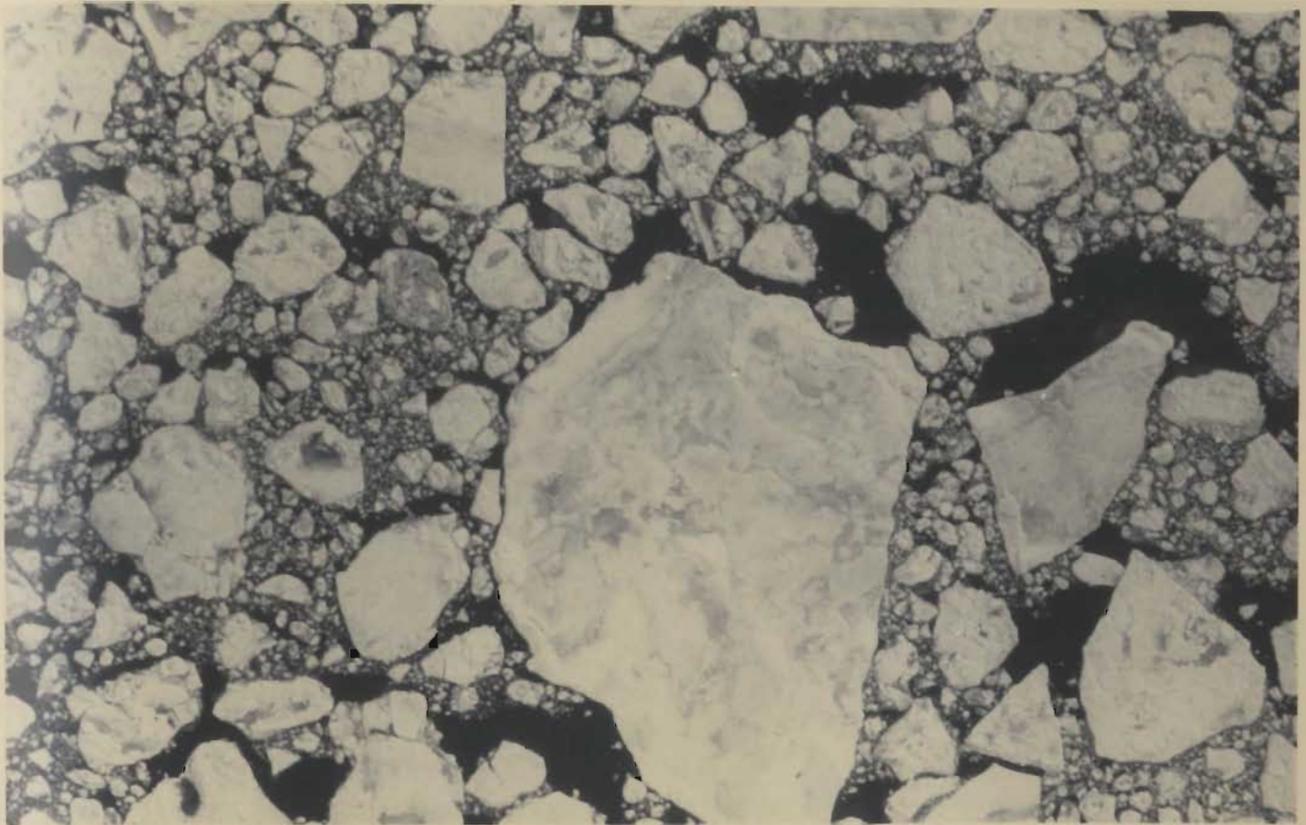
Figure 8 – Multi-year floe showing established melt pattern, partially
covered near the left edge by snow which has collected
behind the edge pile-up. The absence of a pile-up up on the
right edge indicates in this case, along with the truncated
melt depressions, that the floe is a portion of another one
which has recently broken up. A smaller floe is also locat-
ed to the right and, in contrast to the larger, it does not
have a well-developed melt pattern. Photograph was taken
during June, 1982.
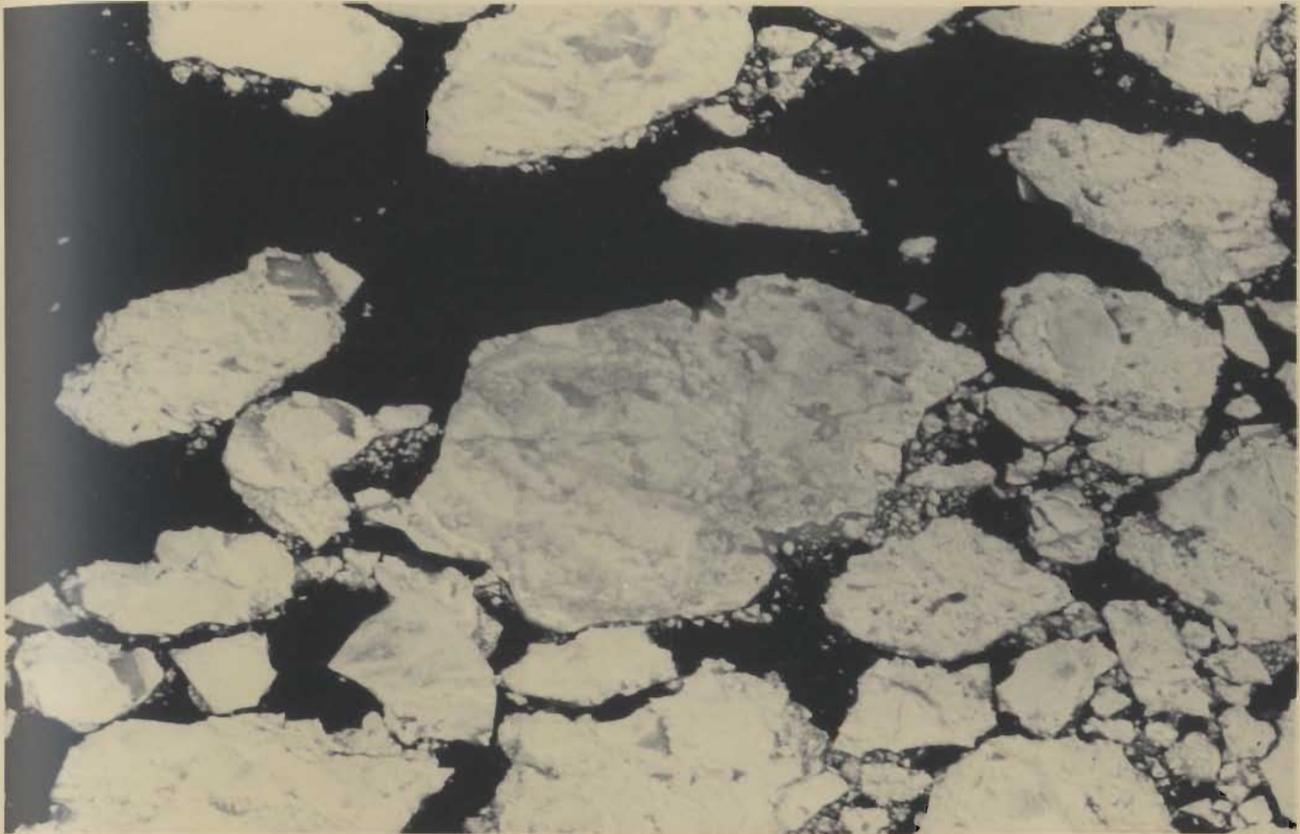
Figure 9 - Multi-year floe in relatively open pack, photographed
in June, 1982. In this example, all snow has disap-
peared and the melt-ponds and channels contain water;
bays are at sea level and are flooded. Once more the
color of the floe results in a darker tonal value in
relation to the surrounding ice.

CHAPTER 4

MULTI-YEAR ICE: FLOE SIZE CHARACTERIZATION

4.1 Overview

Analysis of the 1979 data base produced 7179 measured floe di-
ameters, the largest sample yet obtained for multi-year ice in the
Labrador Sea; 31 extra full diameters were also measured but later
ignored because of suspicion regarding their accuracy. As a prelude
to spatial analysis of occurrence it was first necessary to investigate
the statistical characteristics of the individual floes in order to
generate descriptive statistics of the floe size frequency distribution
within the sample. Knowledge of this was necessary in leading to a bet-
ter appreciation for the magnitude and proportions of sizes of multi-
year floes occurring as part of the spatial patterns later described.
Of particular interest was how the number of floes was related to the
actual amount of multi-year ice in a given spatial distribution. This
was important because all subsequent analysis would be based upon the
assumption that an increase in floe frequency actually represented a
proportional increase in the amount of ice and not simply the occur-
rence of smaller pieces. Finally, an examination of the distribution
of cell averages and ranges of floe size was applied to see if any
relationship could be found with variations in distance from the ice
edge.

4.2 Floe size statistics 1979

When data from the six flight lines were combined, the mean floe
diameter of the total sample of 7179 floes was 48.5 m with a standard
deviation of 17.4 m. The median was 46 m and the mode was 38 m; when

collapsed into categories of 10 m the modal class midpoint was 45 m.

The absolute size range was 137 m, extending from a minimum of 10 m

to a maximum size of 147 m; the interquartile range was 22 m, falling

between 58 m at the 75th percentile and 36 m at the 25th. The third

moment, skewness (π_3) (Norcliffe, 1977), of the frequency distribu-

tion curve (Figure 10a) reflected a positive skew with an index value

(β_1) of 0.895, responding to the position of the mode and median

which were located to the left of the mean; the fourth moment, kurtosis

(π_4) (Norcliffe, 1977), was platykurtic having an index value (β_2)

of 1.48. The skewness indicates that most of the floe sizes fell towards

the lower end of the distribution and to the left of the mean, near which

they were closely grouped as is indicated when the low interquartile

range (containing 50% of the distribution) is compared to the absolute

range between maximum and minimum. Over the entire sample, the upper

threshold of the floe size at the 95% probability level of occurrence was

80 m, with only 5% of the floes expected to be of a greater diameter.

Other levels of probability are detailed in Table 2 and illustrated in

Figure 10b, whilst summary statistics are listed in Table 3. By W.M.O.

classification standards, 87.5% of the total sample was composed of floes

in the small category (20-100m), with the remaining 2.5% made up by 0.9%

medium floes (100-500m) and 1.6% ice cakes (<20m).

On an individual basis, the general characteristics of the fre-

quency curves (Figure 11) were approximately the same, with each having

varying degrees of positively-skewed and platykurtic higher-order

moments; Figure 12 graphs the probability levels for floe size occur-

53
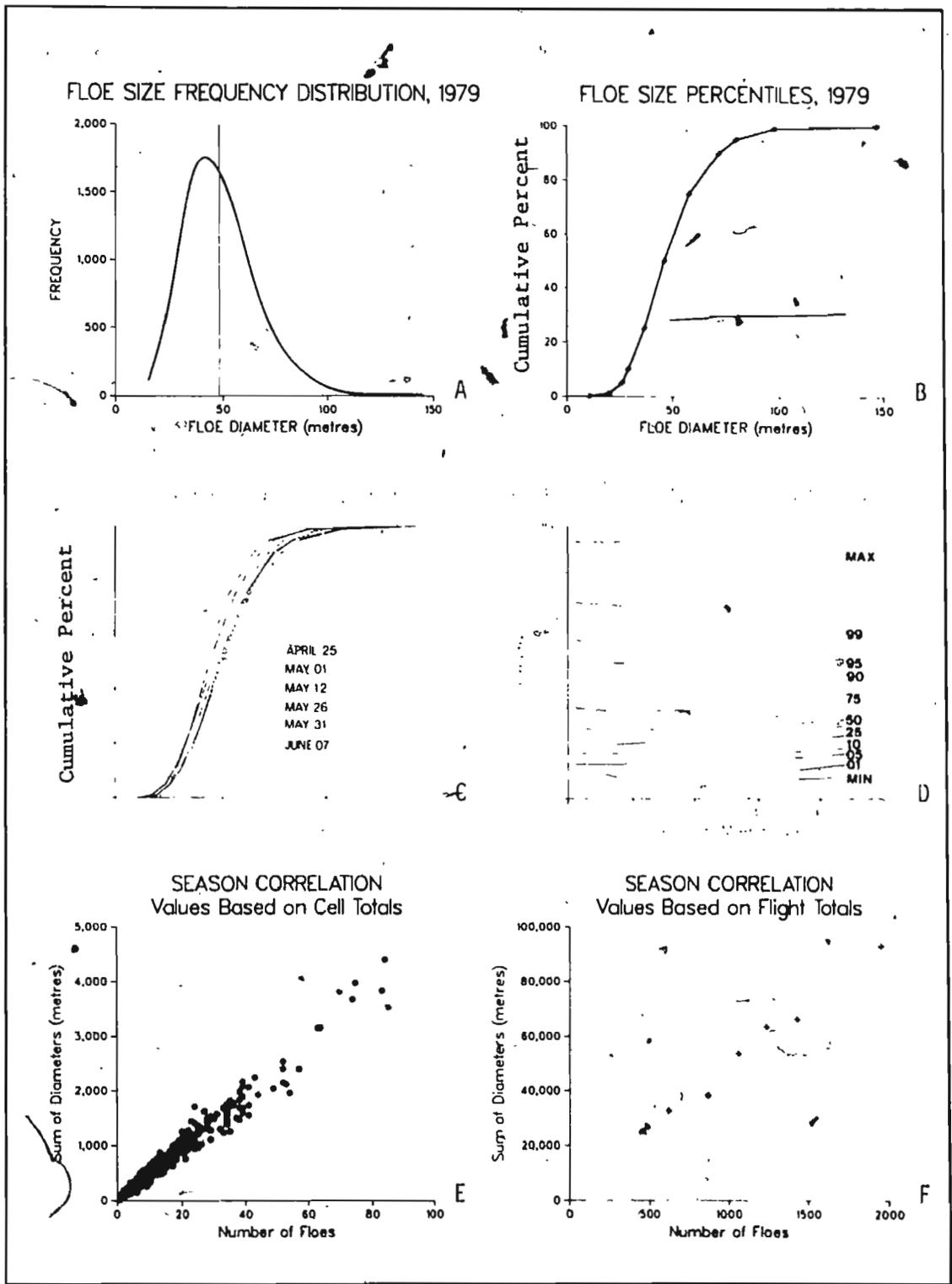
Figure 10 – Summary of descriptive statistics for total of 1979
multi-year ice sample. Significance of 10e and
10f is explained on p.64.

TABLE 2 - Percentile probability levels for
floe size (m) occurrence by date
and for 1979 season.

PROB%	APR 25	MAY 01	MAY 12	MAY 26	MAY 31	JUNE 07	SAMPLE TOTAL
MIN	17	12	11	10	11	12	10
1	19	19	22	17	16	19	19
5	25	25	28	23	23	25	25
10	30	30	32	27	26	28	28
25	39	37	39	35	33	35	36
50	50	48	49	46	42	44	46
75	63	61	62	58	53	56	58
90	78	75	74	72	65	68	72
95	88	84	84	80	73	75	80
99	108	107	99	97	92	91	98
MAX	142	142	147	132	129	134	147

TABLE 3 — Floe size statistics by date

	APR. 25	MAY 01	MAY 12	MAY 26	MAY 31	JUNE 07	Total Sample
FREQ.	624	1061	1235	1957	872	1430	7179
MEAN (m)	52.4	50.6	51.4	47.7	44.0	46.4	48.5
ST.DEV. (m)	19.22	18.54	16.86	17.51	15.67	15.71	17.4
RANGE (m)	125	130	136	122	118	122	137
MODE (m)	44	43	50	40	38	38	38
MODAL CLASS MIDPOINT (m)	45	45	45	45	35	35	45
MEDIAN (m)	50	48	49	46	42	44	46
INTERQUARTILE RANGE (m)	24	24	23	23	20	21	22
MINIMUM (m)	17	12	11	10	11	12	10
MAXIMUM (m)	142	142	147	132	129	102	147
SKEWNESS	0.849	1.021	0.852	0.764	0.882	0.885	0.886
KURTOSIS	1.247	1.909	1.307	0.942	1.409	1.745	1.475
Floe Size Category (% content):							
MEDIUM	2.2	1.6	0.9	0.8	0.3	0.3	0.9
SMALL	96.5	97.1	98.7	97.2	97.3	98.0	97.5
ICE CAKE	1.3	1.3	0.4	2.0	2.4	1.7	1.6
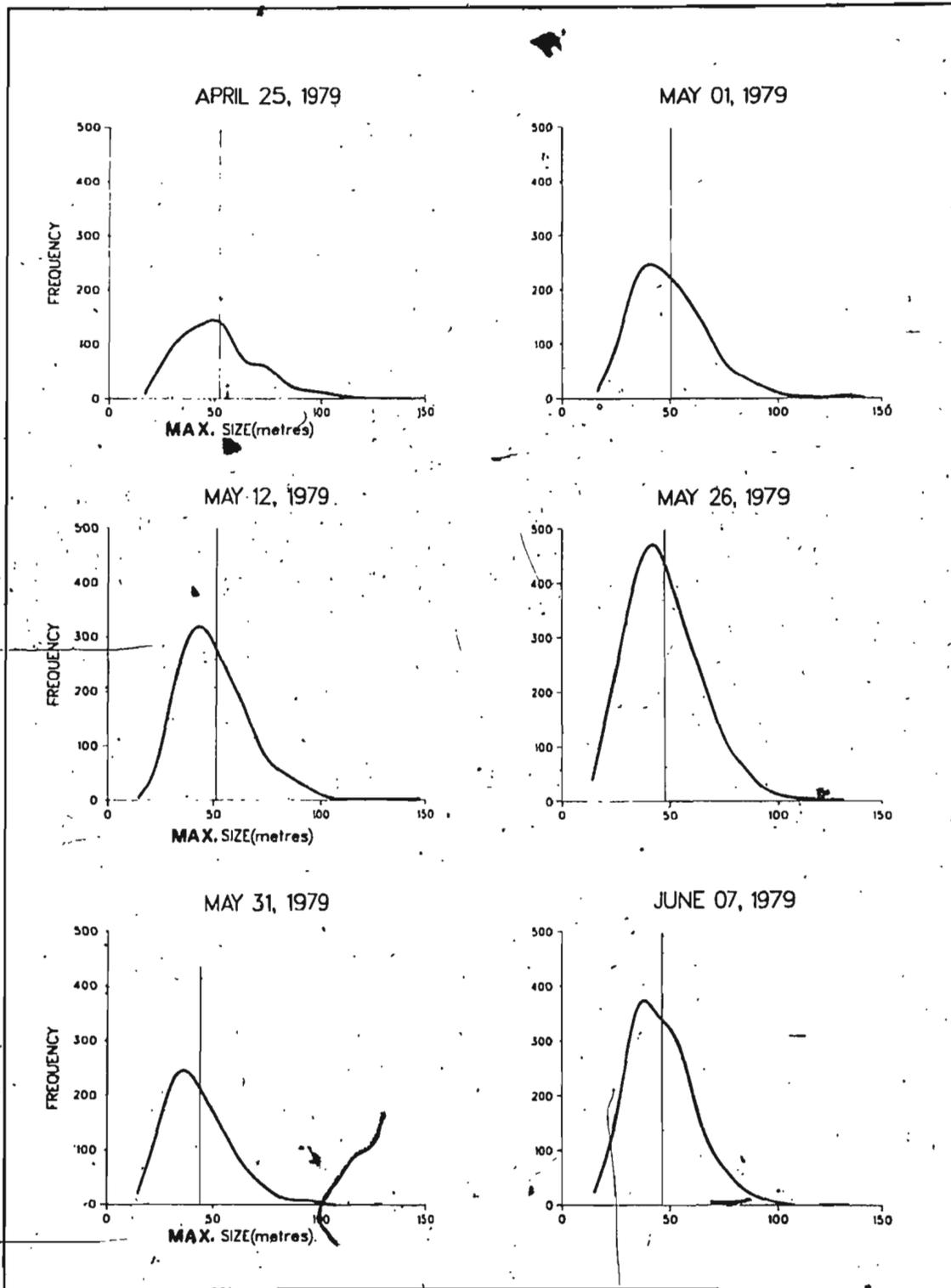
Figure 11 – Floe size frequency distribution curves for multi-
year ice by sample date.
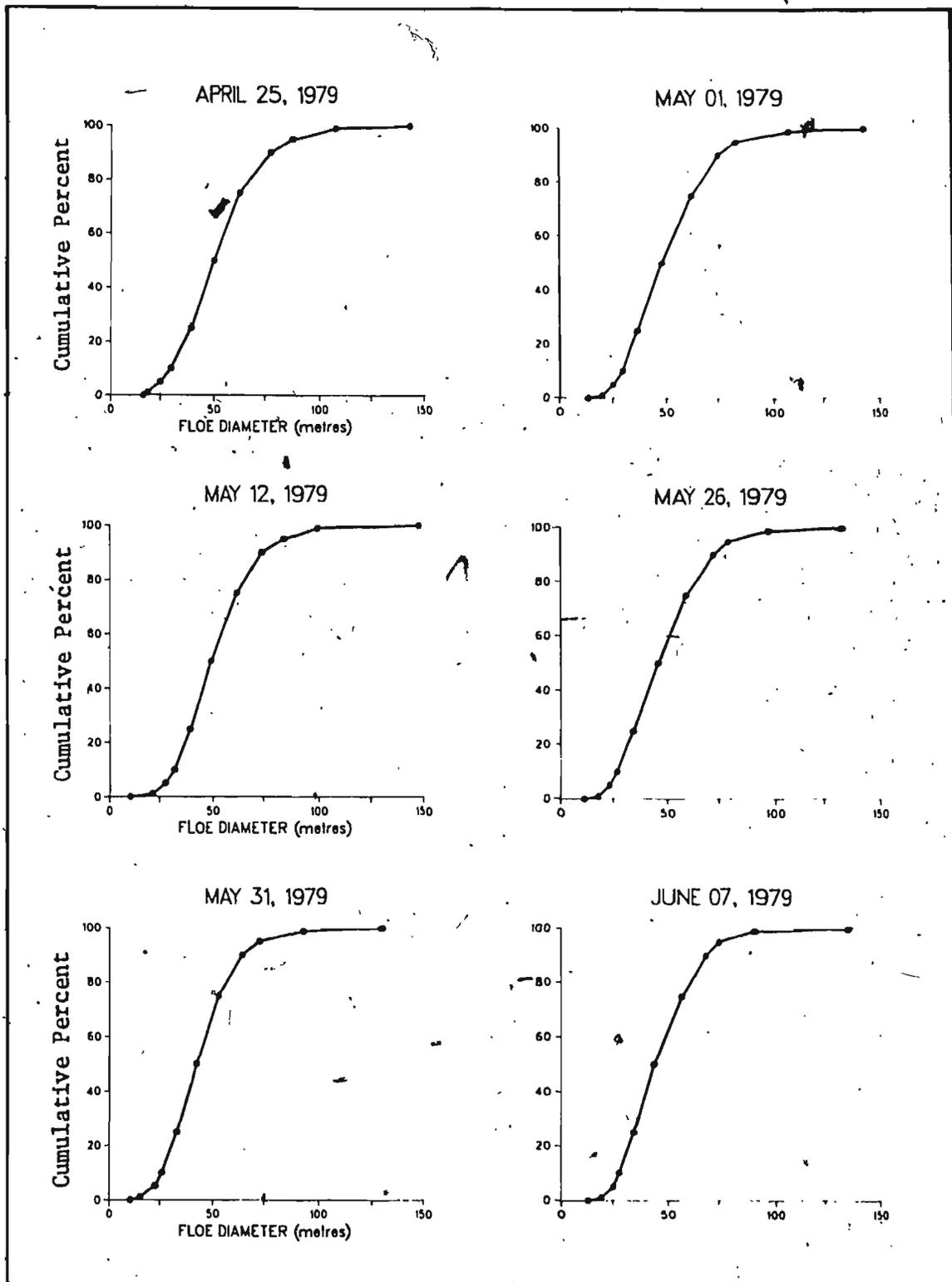
Figure 12 – Probability of occurrence for multi-year floe di-
ameters (m).

rence on each date, while Tables 2 and 3 (pp. 55, 56) summarize probability and descriptive statistics respectively. Although the individual values for the mean and the other statistical parameters of a given sample date lie near their corresponding values for the total sample, a distinct downward trend emerges when the daily values are compared in a time sequential manner. Referring to Table 3 (p. 56), between April 25 and June 07 the average floe size decreased from 52.4 to 46.4 m, with an intervening minimum of 44.0 m on May 31; over the same period the mode (except for May 12) dropped from 44 m to 38 m and the modal class midpoint shifted from 45 m to 35 m. Clearly, there was a decrease in overall floe size towards the end of the sampling period but, in conjunction with this, there was also a tightening of the size groupings around the mean which was reflected by a decrease in standard deviation from 19.22 m to 15.71 m and a decrease in the interquartile range from 24 to 21 m; the maximum and minimum sizes also reflected this downward trend.

Naturally, such a decrease would alter the size limits for percentile probability of occurrence; however, when the shape of the percentile distributions are compared in Figure 10c (p. 54), the size limit change near the 80th percentile appears to be almost twice as much as that near the 20 percent level. When plotted along a time series in Figure 10d (p. 54), the downward trend is evident, but the rate of change gradually levels off as the minimum probability levels are approached. Referring to Table 2 (p. 55), decreasing size limits at the 90th percentile ranged from 78 m on April 25 to 68 m on June 07, with an intervening low of 65 m and an overall net decrease of 10 m. At

59

the 10th percentile, sizes dropped from 30 to 28 m, with an intervening low of 26 m, for a net change of 2 m. The 75 th percentile had a net decrease of 7 m while the 25th percentile dropped by 4 m. The greatest decrease was at the 99th percentile with a net change of 17 m, and the smallest was at the 1% level which experienced a net change of 0 m. Obviously, there was a differential rate of floe size decrease between the upper and lower percentiles. The result of this would be to compress the size range as it became effectively caught between greater rates of decrease at the higher probability levels and smaller rates at the lower levels; it is this effect which explains the temporal decrease in the standard deviation from the mean. In response to this trend, the medium floe category, originally making up 2.2% of the April 25 sample decreased to containing only 0.3% by June 07; conversely, the number of small floes increased from an initial 96.5% to 98% while the ice cakes increased from 1.3% to 2.4% on May 31, and 1.7% on June 07.

4.3 Floe frequency vs. amount of ice

To test the relationship between floe frequency and amount of coverage, a one-tailed test of correlation was performed on the cell data from each flight. The null hypothesis was that the amount of ice, based on the aggregate sum of diameters per cell, varied only by chance from cell to cell, so that there was no response to an increase in the floe frequency which really reflected a cell region in which the ice had been broken into smaller pieces due to dynamic processes occurring in the pack. The alternative hypothesis was that an increase in floe frequency was positively correlated with a proportional increase in the

60

aggregate sums of diameters per cell, and therefore represented an actual increase in the amount of coverage. A more detailed discussion of these concepts is presented in Appendix A.

Correlation coefficients were calculated using the non-parametric Spearman's rank formula (Norcliffe, 1977; Hammond and McCullagh, 1978). The coefficients and their respective levels of significance are listed in Table 4, with the accompanying scattergrams shown in Figure 13. In all cases the calculated coefficients are greater than 0.97 and indicate a positive linear relationship which is significant at $\alpha=0.001$. We can therefore reject the null hypothesis in each case with 99.9% confidence that the observed linear relationship was not due to chance and conclude, with an equal level of confidence, that along each flight line, variations in floe frequency were strongly associated with, and therefore representative of, variations in amount. Table 4 also gives the slope values describing the rate of change in sums of diameter that is associated with a singular increase in floe frequency.

An extension of the original question however, asks if a similar relationship also exists between data for different flight dates and queries whether an increase in frequency along a line or portion of a line represents an increase in the amount of ice, which is equivalent to an increase that would occur along another flight line region having the same frequency. To find if a change in frequency from one data set to another represented a proportional change in amount, the same test was applied to data combined from the entire season's sample, using a null and alternative hypothesis incorporating the same logic as before.

61

TABLE4 — Spearman rank correlation between
floe frequency and aggregate sum
of diameters.

DATE	#CASES	COEFF.	SIG	SLOPE (metres)[*]	INTERCEPT (metres)
APRIL 25	86	0.9754	0.001	53.00	– 4.54
MAY 01	118	0.9794	0.001	46.70	34.24
MAY 12	94	0.9864	0.001	49.78	20.51
MAY 26	104	0.9901	0.001	49.40	-32.94
MAY 31	89	0.9852	0.001	40.74	31.64
JUNE 07	106	0.9800	0.001	43.19	42.25
FLIGHT TOTAL	6	1.000	0.001	46.43	2367.27
CELL TOTAL	597	0.9847	0.001	47.07	16.11

[*] Slope refers to the change in sum of diameters as a function of a
singular change in floe frequency. Slope value is derived from a
linear least squares fit.

APRIL 25, 1979

MAY 01, 1979

MAY 12, 1979

MAY 26, 1979

MAY 31, 1979

JUNE 07, 1979
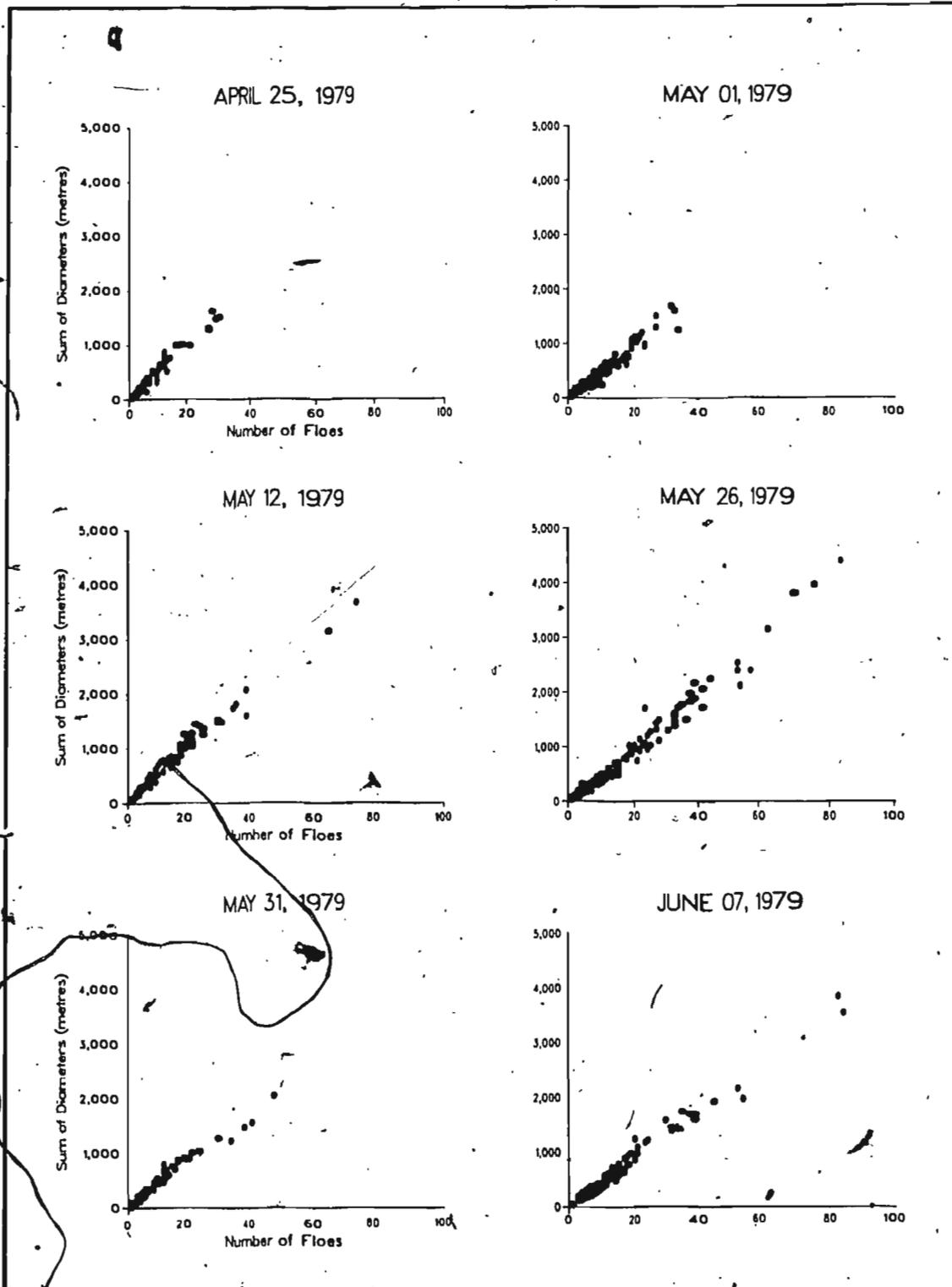
Figure 13 - Scattergrams showing relationships between the number
of multi-year floes and the aggregate diameter per
photographic cell.

Two different approaches were taken; one was to simultaneously test for a linear relationship between all the bivariate pairs of floe frequency and sum of diameters. In this way, if two equal frequencies were paired with two strongly differing aggregate diameter values then they would contribute to greater variance along the scatter of points. Numerous cases such as this would produce a greater precentage of the total variance which could not be explained by a linear relationship, thus reducing the calculated coefficient. The second method was more direct and simply tested for a linear relationship between the bivariate totals of frequency and aggegrate cell diameters for each date. Figure 10e and 10f (p. 54) illustrate the scatter of these respective relationships and the correlation coefficients are given in Table 4. Again, the relationship is strongly positive (0.98) and is significant at $\alpha = 0.001$ allowing for rejection of the null hypothesis, with 99.9% confidence that there is a linear relationship.

The final conclusion therefore, is that when making comparisons between flight line portions located differently both in space as well as time, variations in floe frequency are an adequate measure of the changing amount of ice. This has been drawn on the basis that all tested cases were capable of attributing more than 97% of their total variance as being due to a linear relationship between the two variables.

4.4 Floe size variation vs. distance from ice edge

A two-tailed test of correlation was applied to the cell data to determine how the average floe size and range varied by cell, if at

all, with increasing distance from the pack edge. For this test only

cells containing more than one floe were included in the data set.

Those having only one floe were rejected on the basis that any calcu-

lated measure (average or range) would be a deviant observation result-

ing from a formula specification error (Norcliffe, 1977). Although an

average and range could be mathematically computed from one observa-

tion, the result would not represent respectively either a measure of

central tendency or dispersal between a set of two or more observed

values. Attempts were made at collapsing the data into broader distance

categories; however, due to the nature of the spatial distribution of

the ice, single observations still occurred in some classes while a dis-

proportionately high percentage of the sample was favoured to fall into

a few other select classes. The test applied was the Spearman rank cor-

relation coefficient with a chosen level of significance at $\alpha = 0.002$.

The null hypothesis stated that there was no significant correlation

relating neither cell averages nor cell ranges to increasing distances

from the pack edge; the alternative hypothesis was that a significant

relationship did exist relative to the ice edge. The individual cell

averages and ranges for each date are shown in Figure 14; individual

average flags with no attached range bars denote those single observa-

tions which were not included in the test. Table 5 lists the correla-

tion coefficients and relevant statistics obtained.

For the test between average size and distance, the May 12,

the May 31, and June 07 data sets did not show a significant

relationship at $\alpha = 0.002$ leading to an acceptance of the null

hypothesis. The coefficients for April 25, May 01, and May 26
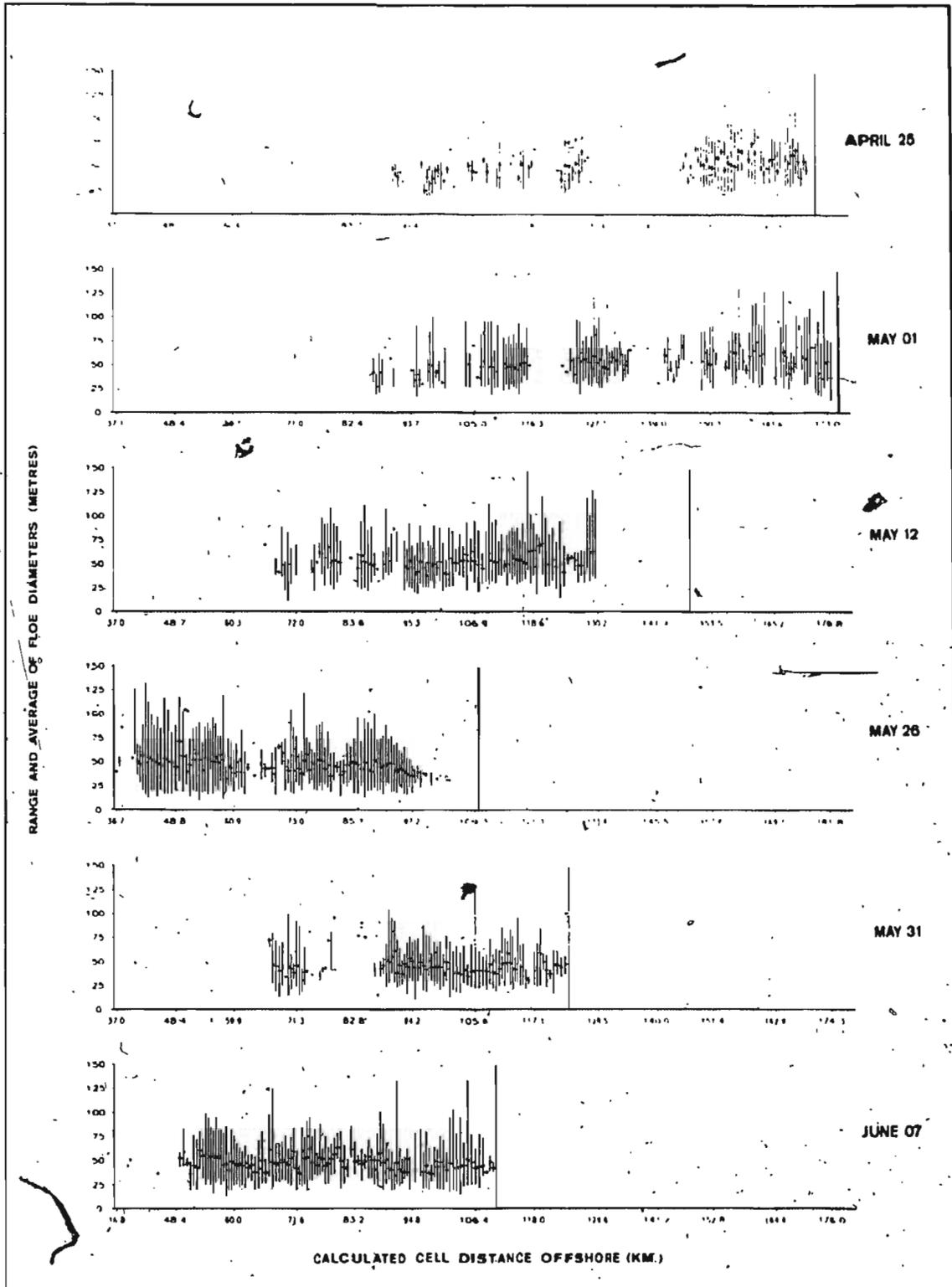
Figure 14 — Average and range of floe diameters by photographic cell along flight line.

TABLE 5 — Spearman rank correlation of cell average and range of sizes with distance from ice edge.

AVERAGE VS. DISTANCE

DAY	CASES	COEFF.	SIG.	SLOPE (m)	INTERCEPT (m)
APRIL 25	70	−0.5668	0.001	−0.217	59.54
MAY 01	100	−0.4701	0.001	−0.192	60.18
MAY 12	89	−0.1903	0.074	−0.076	55.82
MAY 26	97	0.5309	0.001	0.227	37.98
MAY 31	79	0.0199	0.862	0.298	43.58
JUNE 07	102	0.2874	0.003	0.101	44.06
TOTAL	537	0.0143	0.740	−0.022	49.87

RANGE VS. DISTANCE

DAY	CASES	COEFF.	SIG.	SLOPE (m)	INTERCEPT (m)
APRIL 25	70	−0.4165	0.001	−0.388	60.91
MAY 01	100	−0.1618	0.108	−0.165	53.92
MAY 12	89	−0.0745	0.488	−0.093	52.96
MAY 26	97	0.3872	0.001	0.542	30.70
MAY 31	79	0.0596	0.602	0.009	40.94
JUNE 07	102	0.065	0.513	−0.002	45.66
TOTAL	537	−0.0089	0.837	−0.028	48.01

67

however, although not strong, were significant and the alternative hypotheses was accepted, concluding that for these dates there was a relationship. For April 25 and May 01 the correlation was negative, with decrements in average floe size of 0.217 m and 0.192 m per kilometer away from the edge. The relationship is unusual in comparison to younger ice whose floe sizes generally increase (Wadhams, 1980). For May 26, the relationship is completely reversed and significantly positive, with an increase in average floe size of 0.226 m per kilometer. This coefficient had a value very close to that of April 25 and, considering the intervening period of May 12 when there was no correlation, there seems to have been a complete turn around representative of a seesaw effect. In addition, no significant correlation was found for the season's total sample, comprised of a combination of the six flight lines.

The test comparing cell ranges and distances from the ice edge yielded results significant at the $\alpha = 0.002$ level for only April 25 and May 26, leading to an acceptance of the null hypothesis for all other dates, including the combined total sample. For the significant dates, the coefficients, although not as strong, agreed with those obtained on the same respective dates for average size, being negative on April 25 and positive on May 26.

When considering the results of these tests, the only conclusion to be drawn is that the nature of the distribution of floe size average and range was variable for the 1979 data.

Although sometimes significantly correlated with distance, the observed conditions cannot be considered as being a consistent part of any representative trend.

CHAPTER 5

SPATIAL ASPECTS OF MULTI-YEAR ICE DISTRIBUTIONS, 1979

5.1 Overview

From the total of eight flight lines flown out of Saglek, Labrador during 1979, only the six sets of photos collected between April 25 and June 07 were found to contain sufficient data for spatial analysis. During the time period from April 25, 1025 photographs were taken, of which some 599 or 58.4% were found to contain multi-year ice; Table 6 lists the number of photos by date and their respective percentage of data content. It is this 58.4% for which the distribution statistics given in section 5.2 are calculated; as such, these are intended to describe the spatial characteristics of multi-year ice only where it occurred along the line. The statistics therefore, do not incorporate into their calculation cells which recorded zero frequencies. Such an approach would otherwise tend to deflate the calculated statistical values and compromise on their ability to describe the multi-year ice concentrations as they actually existed. Conversely, section 5.3, in an attempt to place the measured distributions within a spatial context relating to the overall pack ice coverage, does calculate average occurrence values which take into account the entire photographic line for any given date.

First-year and younger ice forms are ubiquitous in their occurrence across the entire Labrador MIZ. Prior to this study, and excepting vague qualitative assessments based upon casual

Table 6 – Photographic coverage and data content

DATE	# PHOTOS	# WITH RELEVANT DATA	% OF TOTAL
APRIL 25	236	86	36.4
MAY 01	242	118	48.8
MAY 12	160	96	60.0
MAY 26	121	104	86.0
MAY 31	144	89	61.8
JUNE 07	122	106	86.9
TOTAL	1025	599	58.4

observation, there was no hard evidence to indicate that multi-year floes, while albeit much smaller in number, did not occur throughout the pack in a similar fashion. Because of this, section 5.3 analyizes the six data sets by comparing the spatial patterns actually observed within each to a hypothetical spatial distribution of multi-year ice. This theoretical distribution is one which is uniformly spread across the pack, covering a distance equivalent to that of the flight line for the date considered and incorporating the same number of old floes.

5.2 Description of spatial patterns

Figure 15a illustrates the relative magnitudes of multi-year ice occurrence by cell for each flight. The floe occurrences appear highly variable, both in terms of frequency and location along the lines, as well as from one line to another. Referring to the cell frequencies in Table 7a, from 7179 floes recorded in 597 cells, the mean cell value was 12.0 floes per cell, with a standard deviation of 12.7, and a range of 84 lying between a cell minimum of 1 floe and a cell maximum of 85 floes. For individual dates, all cell minimums were 1 but the maximum values increased from 28 floes on April 25 to 83 on May 26, dropped to 48 on May 31 and climbed again to 84 on June 07; these fluctuations were commensurate with similar trends in fluctuation for the total, average and standard deviation of cell values for each date. Figure 15b illustrates the sum of diameters per cell as measured from these floes, with Table 7b listing the summary

72
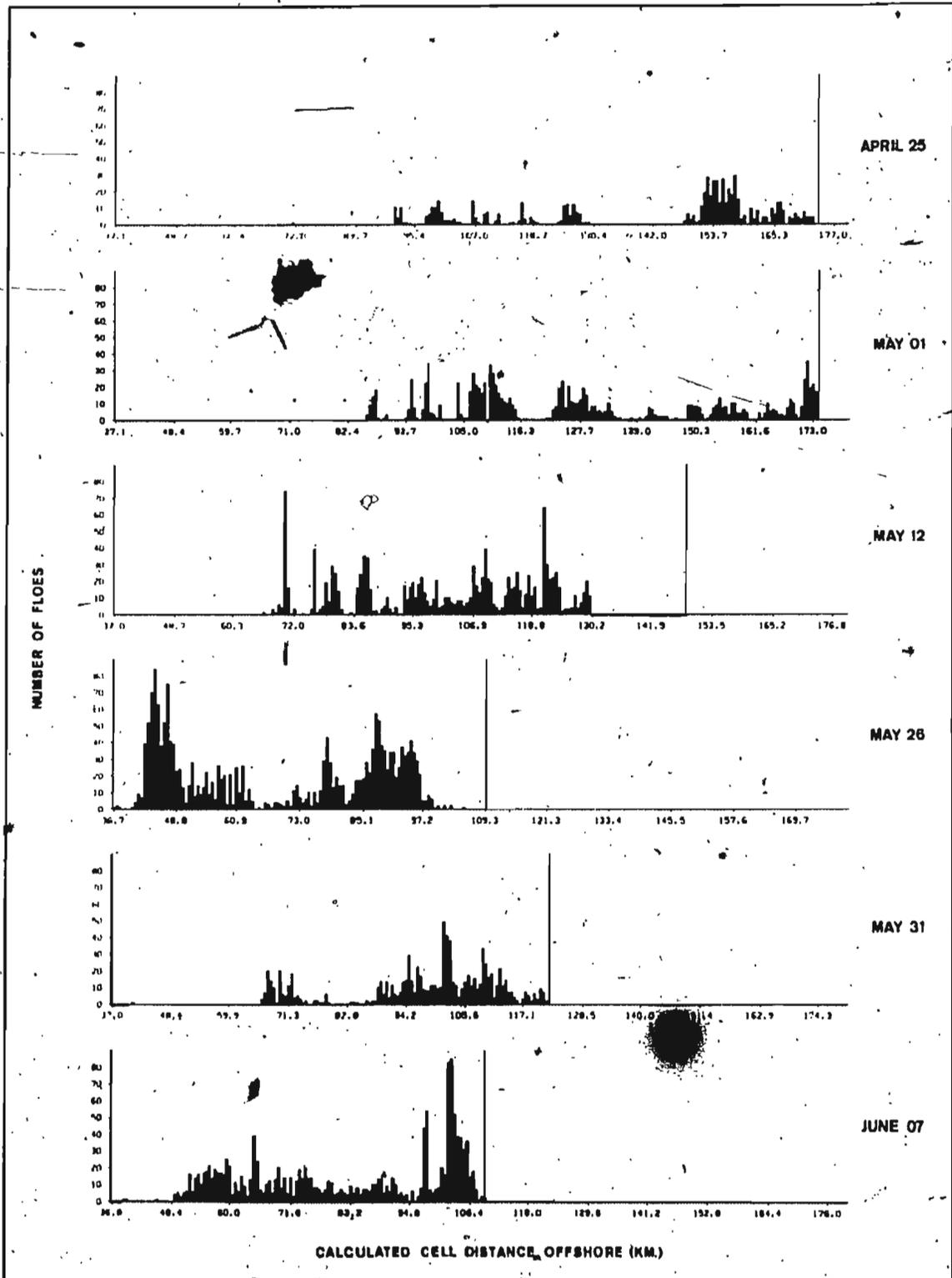
Figure 15 a – Number of multi-year floes occurring by photo cell
along flight line (bars projecting below 0 denote
missing data).
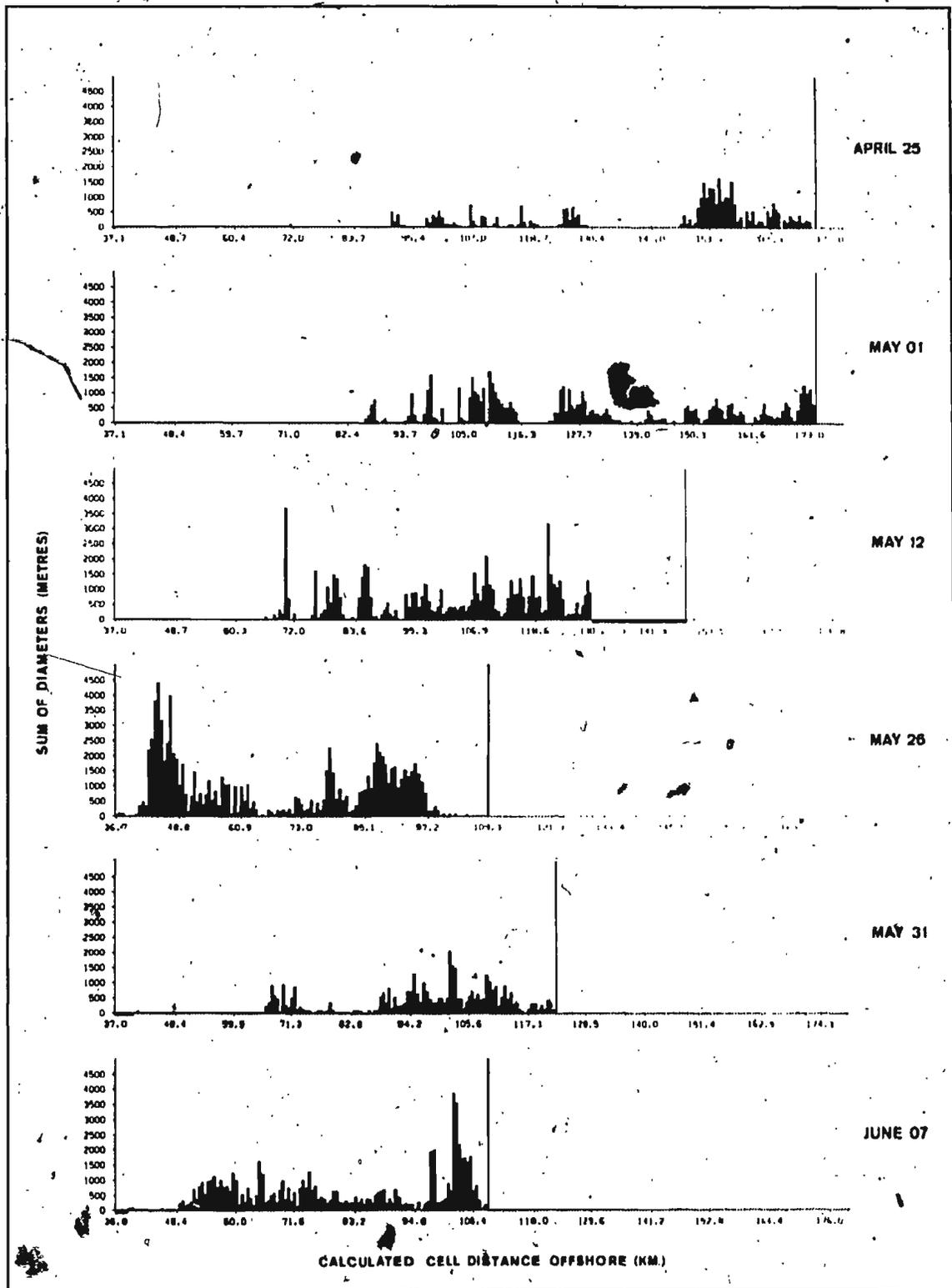
Figure 15b - Sum of multi-year floe diameters occurring by photo
cell along flight line.

Table 7a - Floe frequency by cell

	APRIL 25	MAY 01	MAY 12	MAY 26	MAY 31	JUNE 07	TOTAL
TOTAL	624	1061	1235	1957	872	1430	7179
MEAN	7.3	9.0	13.1	18.8	9.8	13.5	12.0
ST. DEV.	6.9	8.0	12.5	17.9	9.1	14.2	12.7
RANGE	28	34	73	83	48	84	84
MAX	29	35	74	84	49	85	85
MIN	1	1	1	1	1	1	1
STD. ERR.	0.749	0.734	1.287	1.750	0.965	1.383	0.520
KURT	1.965	1.201	7.515	1.874	5.053	10.93	8.258
SKEW	1.537	1.289	2.257	1.385	1.99	2.98	2.456

Table 7b - Sum of diameters by cell (in metres)

	APRIL 25	MAY 01	MAY 12	MAY 26	MAY 31	JUNE 07	TOTAL
TOTAL	32678.3	53585.9	63405.3	93244.6	38344.3	66241.6	347500.0
MEAN	380.0	454.1	674.5	896.6	430.8	624.9	582.1
ST. DEV.	374.1	381.2	626.9	892.8	375.3	621.9	606.6
RANGE	1599.0	1657.2	3631.6	4376.1	2026.0	3795.9	4391.6
MAX	1628.0	1686.7	3672.3	4401.1	2041.5	3832.1	4407.1
MIN	29.2	29.5	40.7	31	15.5	36.2	15.5
STD. ERR.	40.35	35.09	64.66	87.55	39.78	60.41	24.83
KURT	2.117	0.765	6.68	3.17	3.81	10.13	9.07
SKEW	1.567	1.143	2.13	1.643	1.685	2.765	2.50

75

statistics; because of the close correlation between floe fre-
quency and sum of diameters, both sets of bar charts are almost
identical and the descriptive statistics for aggregate diameters
incorporate the same trends as do those for floe frequency.

Reflecting the measured variability from cell to cell,
areal concentrations of multi-year ice also displayed these same
variations in density of occurrence per 0.5 square kilometer
along the line. Referring to Figure 16a for April 25, floe con-
centrations occurred in a series of grouped fluctuations between
0 and 9 floes/0.5 km^2 from 90 to 130 km offshore, but increased
to between 10 and 18 at 150-158 km, thereafter dropping to floe
density variations of between 0 and 8 seaward to the ice edge.
May 01 also experienced similar fluctuations but had increased
densities, as high as 20 floes/0.5 km^2 occurring between 90 and
130 km. However, near 153 km the values were low, around 4-7,
whereas for April 25 the floe concentration at this point had
been higher; inversely comparative, near the ice edge at 173 km,
the densities for May 01 were around 10-20 but were only at 2-5
for the previous flight. Furthermore, near 93.7 km (May 01),
there were two very narrow groups having strong increases from 0
to near 15-20 floes/0.5 km^2 which are indicative of the rapid
changes in the spatial characteristics of the distribution. May
12 also had extremes of fluctuation, one occurring in a narrow
band near 72.0 km where the densities abruptly jumped from 1-3
to 44 floes/0.5 km^2, and another near 120 km, where concentra-
tions increased from between 3 and 16 up to 38 floes per unit
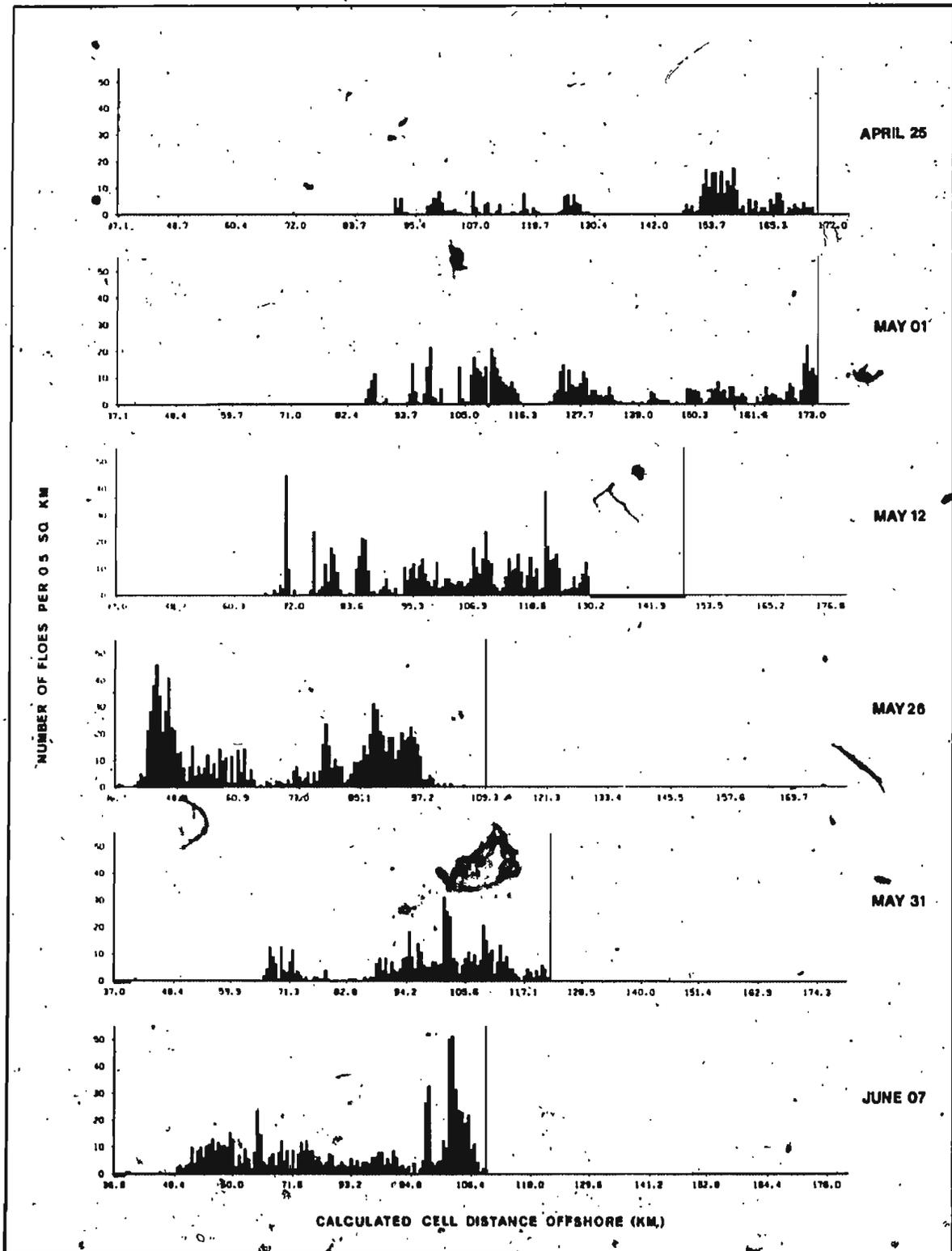
Figure 16 a – Number of multi-year floes occurring per 0.5 km^2 along flight line.

77
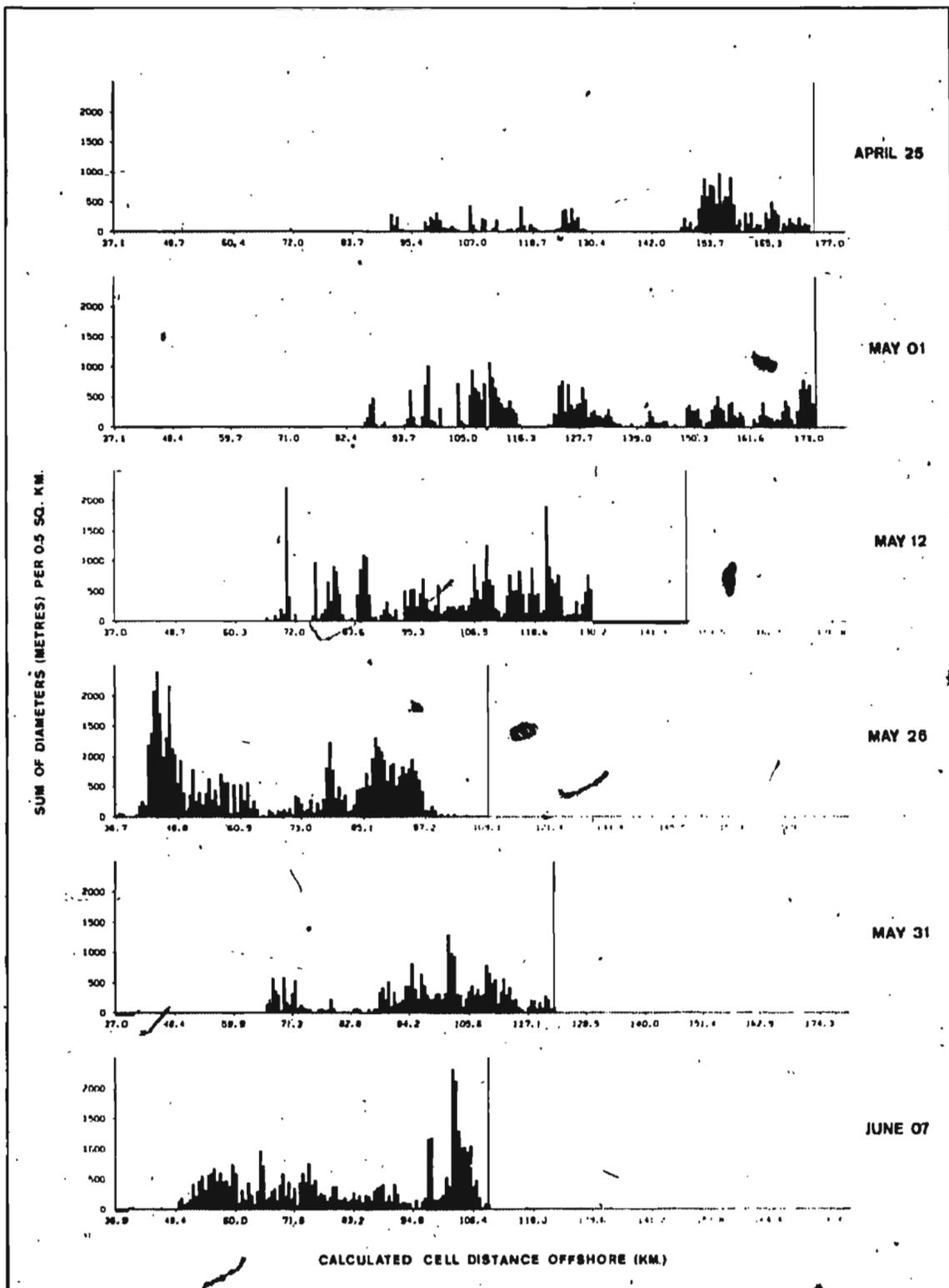
Figure 16b – Sum of multi-year floe diameters occurring per 0.5 km² along flight line.

Table 8a — Density of floe occurrence per 0.5 km^2

	APRIL 25	MAY 01	MAY 12	MAY 26	MAY 31	JUNE 07	TOTAL
TOTAL	371.8	661.3	741.2	1063.7	549.9	859.9	4246.8
MEAN	4.3	5.6	7.5	10.2	6.2	8.1	7.1
ST. DEV.	4.1	5.0	7.5	9.7	5.7	8.6	7.3
RANGE	16.6	21.2	43.9	45.2	30.3	50.5	50.6
MAX	17.2	21.8	44.5	45.7	30.9	51.1	51.1
MIN	0.6	0.6	0.6	0.5	0.6	0.6	0.5
STD. ERR.	0.445	0.458	0.773	0.952	0.609	0.832	0.300
KURT	2.00	1.168	7.570	1.875	5.062	10.92	8.050
SKEW	1.544	1.285	2.265	1.386	1.993	2.983	2.393

Table 8b — Density of aggregate diameter occurrence per 0.5 km^2 (in metres)

	APRIL 25	MAY 01	MAY 12	MAY 26	MAY 31	JUNE 07	TOTAL
TOTAL	19436.1	33444.2	39384.0	50685.8	24199.3	39846.4	205721.1
MEAN	226.0	283.4	405.4	487.4	271.9	375.9	344.6
ST. DEV.	222.5	237.9	376.8	485.3	236.8	374.1	349.1
RANGE	951.0	1034.3	2182.7	2378.7	1272.6	2283.3	2385.8
MAX	968.4	1052.7	2207.2	2395.6	1288.4	2305.1	2395.6
MIN	17.4	18.4	24.5	16.9	9.8	21.8	9.8
STD. ERR.	23.996	21.9	38.86	47.59	25.104	36.34	14.286
KURT	2.117	0.765	6.68	3.17	3.809	10.13	8.22
SKEW	1.567	1.143	2.131	1.643	1.685	2.764	2.37

79

area. On May 26 the locational variability was emphasized by
the occurrence of very high concentrations between 40 and 50 km,
a region in which multi-year ice had occurred neither previously
nor subsequently for the dates sampled. Here densities were
high, nearing 20 floes per 0.5 km^2 on average, with peak occur-
rences of 45 and 40 floes which dropped off rapidly to 2.2 floes
at 50 km; after this point and out to 78 km, it varied between 0
and 10 floes. Beyond 78 km, densities increased to 23 at 79 km,
dropped to 3 at 82 km, and then increased to fluctuating near 20
floes/0.5 km^2, with peak density concentrations of 28 and 31
near 88 km. On May 31 concentrations began near the 71.3 km
point and fluctuated around 5-10 floes/0.5 km^2; the only signifi-
cant previous occurrence at this point had been the 44 floe peak
on May 12. Peak occurrences for May 31 were densities of 30 and
25 floes per 0.5 km^2 near 102 km, 18.3 floes at 94 km and 20.8
floes/0.5 km^2 at 109 km; between 83 km and the ice edge at 122
km, floe concentrations mostly varied between densities of 3 and
8, with occasional drops to 0. On June 07 average densities
were 8 to 12 floes per 0.5 km^2 between 49 and 60 km, and 2 to 7
floes between 60 and 97 km; peaks were 26 and 32 floes per 0.5
km^2 at 98 km, and 49 and 51 floes at 102 km, dropping to 21
floes at 106 km.

Referring to Table 8a (p. 79), the average number of floes
occurring per 0.5 km^2 per data cell for the entire season's
sample was 7.1 with a standard deviation of 7.3 floes and a

range of 50.6 between the maximum and minimum cell densities of
51.1 and 0.5 floes per 0.5 km^2 respectively. For individual
dates these values varied between a maximum mean concentration
of 10.3 floes with a standard deviation of 9.7 on May 26 and a
minimum mean concentration of 4.3 floes per 0.5 km^2 with a stand-
ard deviation of 4.1 on April 25. By taking these values to
the second and third standard deviation and by comparing with
Figure 16a (p. 77), the grouped variability of multi-year ice
across the MIZ is obvious. Since several examples have shown
that peak concentrations are not always preceeded spatially by
an overall upward trend in floe concentration to either side,
the occurrence of these groups can be abrupt and spatially unpre-
dictable. Figure 16b and Table 8b (pp. 78, 79) deal with vari-
ations in sums of diameter per 0.5 km^2, which also varies in pat-
terns identical to that of the floes. Tables 9a and 9b sum-
marize probability levels for floe occurrence per photo cell and
per 0.5 km^2; Figure 17 graphs the probability for floe occur-
rence per 0.5 km^2.

Although the presence of floe grouping is constant from
flight to flight, there emerges two main patterns in which these
groups present themselves relative to the overall distribution.
In some cases, the groups are spatially "discrete", occurring as
a sharp increase from 0 to a peak magnitude and dropping off
sharply to 0 again, with intervening regions of multi-year ice
non-occurrence. In other cases, the peaks simply occur as a
series of higher concentrations projecting from a surrounding

Table 9a – Percentile probability levels for floe frequency
by photocell

PER	APR 25	MAY 01	MAY 12	MAY 26	MAY 31	JUNE 07	TOTAL SAMPLE
10	1.0	1.0	2.5	2.0	1.0	3.0	1.0
20	2.0	2.0	3.0	4.0	2.0	5.0	3.0
30	3.0	3.0	4.5	5.0	4.0	6.0	4.0
40	4.0	5.0	7.0	9.0	6.0	7.0	6.0
50	5.0	7.0	10.0	13.5	7.0	9.0	8.0
60	6.0	8.4	13.0	19.0	10.0	12.2	10.0
70	9.0	10.0	16.0	25.0	11.0	14.0	14.0
80	12.6	16.0	21.0	34.0	14.0	17.6	19.0
90	17.3	21.1	27.0	41.0	20.0	26.8	27.2
95	26.0	24.2	36.0	56.0	31.0	42.3	38.0
98	28.3	33.62	65.0	74.5	42.6	78.9	52.0
99	–	–	–	–	–	–	70.1
Q_3-Q_1	8.3	9.3	15.0	23.8	10.0	11.0	12.0

Table 9b – Percentile probability levels for floe frequency
by 0.5 km^2

PER	APR 25	MAY 01	MAY 12	MAY 26	MAY 31	JUNE 07	TOTAL SAMPLE
10	0.6	0.6	1.5	1.1	0.6	1.8	0.6
20	1.2	1.2	1.8	2.2	1.3	3.0	1.8
30	1.8	1.9	2.7	2.7	2.5	3.6	2.5
40	2.4	3.1	4.2	4.9	3.8	4.2	3.6
50	3.0	4.4	6.0	7.4	4.4	5.4	4.8
60	3.6	5.2	7.8	10.3	6.3	7.3	6.2
70	5.4	6.2	9.6	13.6	6.9	8.4	8.3
80	7.5	10.0	12.6	18.5	8.8	10.6	11.3
90	10.3	13.2	16.2	22.3	12.6	16.1	15.3
95	15.5	15.1	21.6	30.5	19.6	25.5	21.2
98	16.8	21.0	39.1	40.5	26.9	47.5	30.9
99	–	–	–	–	–	–	38.5
Q_3-Q_1	4.9	5.8	9.0	12.9	6.3	6.6	7.2
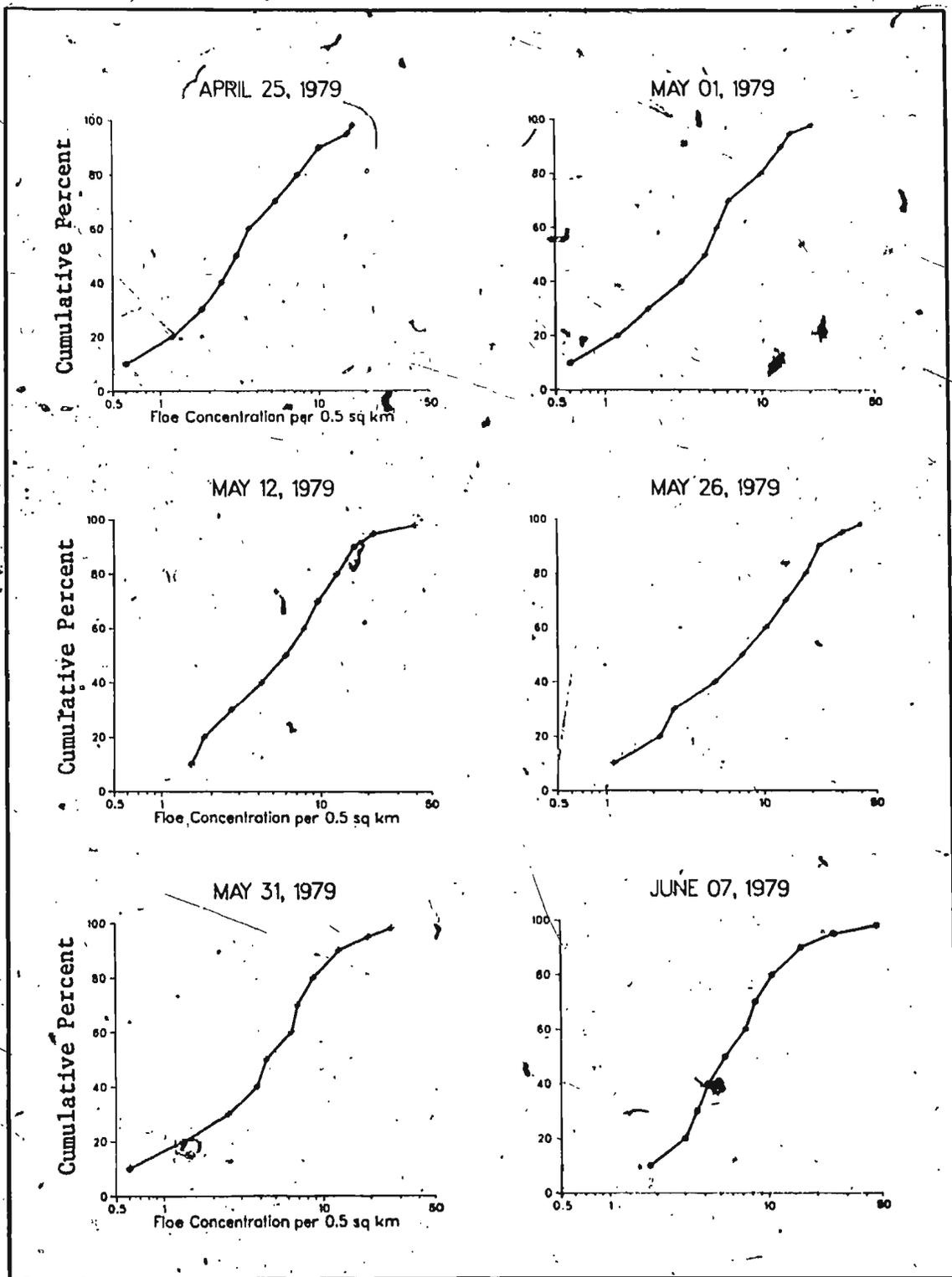
Figure 17 - Percentile probability for frequency of multi-year floes per 0.5 km^2.

pattern of lower or average values and are therefore, spatially "indiscrete". Since the peaks are of similar shape in terms of sharpness of increase and decrease no matter how they occur, and since they mostly lose their spatial discretion after May 12, the indication is that coverage by multi-year ice of near-average concentrations gradually spreads itself outward with time. This increases the occurrence of low density concentrations of multi-year ice in the spatial voids which would previously contain first-year and younger ice types intervening between the groups.

This pattern is illustrated by the diagrams in Figure 18. These are computer-drawn, mathematically-constructed surfaces responding in the Z dimension to the floe diameter measurements, which we know by previous correlation to incorporate the same cell to cell variations as floe frequency.

The software package utilized was Surface II; the procedure is described in Sampson (1978). In the initial stages, a uniform grid was "placed" over the spatially juxtapositioned data points and a value estimated for each point of intersection, or grid node. Each nodal value was determined from a distance-weighted average of the nearest eight data points (i.e. nearest eight floe positions). A scaled inverse distance squared function was used (Sampson, 1978):

$$W = (1 - D/(1.1 \times D_{max}))^2 / (D/(1.1 \times D_{max}))^2$$

where : W = weight of data point at distance D from grid node.

84
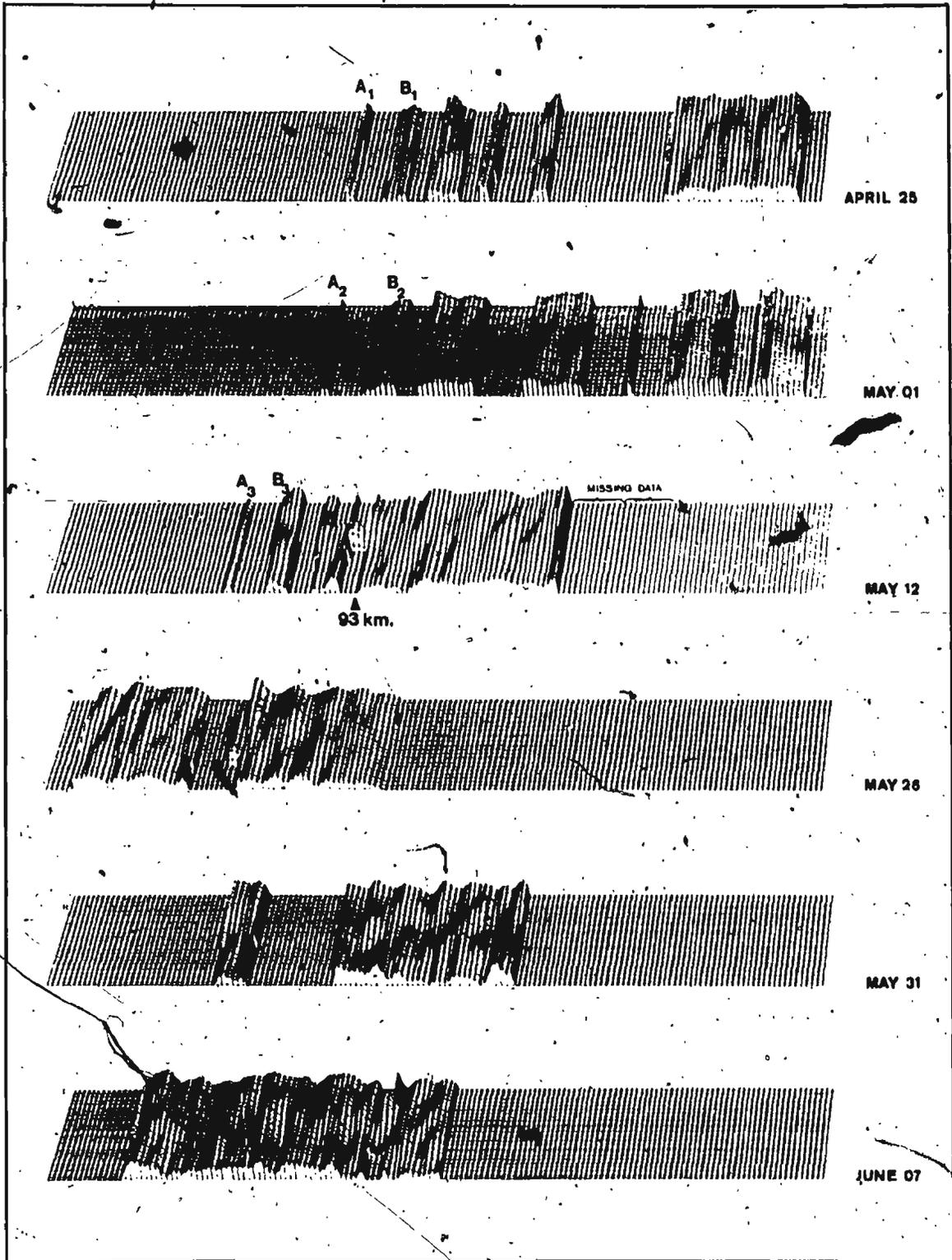
Figure 18 - Log_{10} - scaled surfaces showing multi-year ice distribution patterns of dates sampled. A and B indicate repeated occurrence of groups of multi-year floes crossing flight line.

D_{max} = distance from the grid node to the farther-
most of the eight data points used.

The calculated value of each node represented the Z dimension
of the surface at that point.

The surface was then subjected to two smoothings to dampen
small-scale variability. This was accomplished by averaging each
nodal value with the values of nodes contained in the nearest
two grid columns and rows on each side of the node. In the
final stage, the smoothed grid nodes were scaled by a log_{10}
transformation (Sampson, 1978). The resulting dominant visual
element is one which disregards differences in magnitude of
occurrence in favour of producing a clean separation between
areas of occurrence and non-occurrence.

Comparing this to Figure 15a (p. 73), for April 25, several
discrete groups are seen near the center of the flight line
which are also reflected in Figure 18 for this date. However,
near the outer end of the line, where the bar chart shows a
relatively high concentration grouped adjacent to a series of
low fluctuations, the log_{10}-scaled surface indicates that
instead of being spatially discrete, the group occurs in a
region of general multi-year ice coverage (i.e. it is an indis-
crete group). For May 01 all groups are discrete, but on May 12
a combination of patterns existed. Reference to Figure 15a
shows a series of groups along the entire length of the May 12
line, however Figure 18 shows that while those to the left of
center are spatially discrete, those to the right are not,

86

having instead become interspersed with lower density concentra-
tions contributing to a region of overall, but variable, multi-
year ice occurrence. For May 26 the pattern is slightly altered
since there are two regions of overall multi-year ice occur-
rence, themselves representing a grouping of sorts, but within
which occur several indiscrete examples of spatial grouping.
This carries over to May 31 which, for the most part, has a
series of spatially indiscrete groups in the outer portion of
the distribution, with a single discrete group making up the
inner portion. By June 07, with the bar charts showing a strong
degree of grouping near the edge and several smaller groups
along the inner portions, the zone of inter-group multi-year ice
occurrence as represented by the $\log_{10}$ surface is total, making
all groups spatially indiscrete.

The essence of portrayal by Figure 18 is that while such
groups are initially discrete both in terms of space and magni-
tude, due to the apparent dispersal of multi-year ice across the
MIZ as the season progresses, their inter-group voids are eventu-
ally infiltrated by occurrences of lower frequency. Therefore,
what was at first a series of individual strips of multi-year
ice is temporally transposed into a single belt of occurrence
within which groups are discrete only by magnitude. The dual
pattern shown in Figure 18 for May 12 suggests this surface to
represent a transitory phase in the dispersal process; since the
spatial discretion is lost in the outer portion of this particu-
lar distribution, the suggestion is that infiltration by lower

frequencies originates near the peripheral region of the pack and spreads inward. However, while the influence of general low frequency coverage eventually spreads across the entire spatial distribution of the groups, there seems to be certain extreme limits beyond which the spread does not permeate, as is suggested by the approximately equivalent coverage widths of the distribution for May 26, May 31, and June 07. Additionally, there was a contraction of the extreme limits between April 25 and June 07 indicating that as the strips merged into a belt, the limits of coverage by the entire distribution became narrower.

Figure 18 also emphasizes the temporal-spatial variability of the ice, especially with reference to April 25, May 01, and May 12 distribution surfaces. At the innermost portion of each of these lies two discrete groups which, when the three surfaces are compared, are identical in their juxtaposition to their respective distributions; however, because of a landward shift, no one pair is found at the same spatial location as its counterpart for either of the other two sample dates. In addition, the whole of the distribution shifted with a zig-zag motion between May 12 and June 07 which accounts partially for the spatial variability in occurrence of the groups.

5. Analysis of spatial patterns

To test the significance of the observed grouping, a runs test (Hammond & McCullagh, 1978; McCullagh 1974) was applied

88

which tested for random variations in the spatial order of occur-
rences of cell frequencies from the innermost to the outermost
portions of the flight line. (Application of this test involved
calculating the mean number of floes per cell for the entire dis-
tribution, taking into account also those cells containing no
multi-year ice. The frequencies observed were then isolated
into runs, with each run consisting of a sequence of adjacent
values, or even a single value, lying either above or below the
cutting line of the mean. The total number of these sequences,
or runs, was then found and transformed into a z-score describ-
ing how many standard deviations the total number of observed
runs lay from the mean number of runs which would be expected to
arise from a random sequence of occurrences. The significance
of the test is determined by finding the probability that the
calculated z-score could have been obtained from a random distri-
bution.

The null hypothesis assumed that the sequence of observed
frequencies along the cutting line was the result of chance, and
therefore, random; the alternative hypothesis stated that the
order of occurrence was significantly clustered. The test was
one-tailed, with a rejection level for the null hypothesis set
at $\alpha = 0.001$. Table 10 (p. 92) details the relevant statistics.
In all cases, after rounding to three decimal places, the calcu-
lated probability of having obtained the calculated z-scores
from a random sequence is near 0.000, indicating that we can
reject the null with at least 99.9% certainty that the observed

89

sequences are not random. Since the z-scores are all negative and lie at between 5 and 10 standard deviations to the left of the mean random value, we can accept the alternative hypothesis, concluding that the number of runs in each data set was far less than could have occurred for a random distribution, and therefore represents a significant element of clustering among the observed frequencies. Figure 19 illustrates the sequence of runs; in most cases each run has a high degree of cell contiguity for those values occurring above the mean and clearly isolates the regions of strong clustering.

Further investigation of the observed patterns incorporated a chi-square (X^2) goodness-of-fit test (Norcliffe, 1977; Hammond & McCullagh, 1978; Taylor, 1977; McCullagh, 1974). Rather than dealing with the sequential order of occurrence, this test compares the shape of the observed distribution to the shape of one which is expected or theoretical, and tests for a significant difference between the two. Since the calculated value is a measure of the differences between the values observed and those expected, the larger the value of X^2, the greater is the difference between the two distributions. To satisfy the minimum requirements for use of the test, the data were collapsed into categories with a chosen class width of 5 km; the test was one-tailed with a chosen rejection level at $\alpha = 0.001$. The null hypothesis stated that any difference between the observed and expected frequencies was purely due to chance variations and therefore not significant; the alternative hypothesis was that the observed distribution was significantly different from the
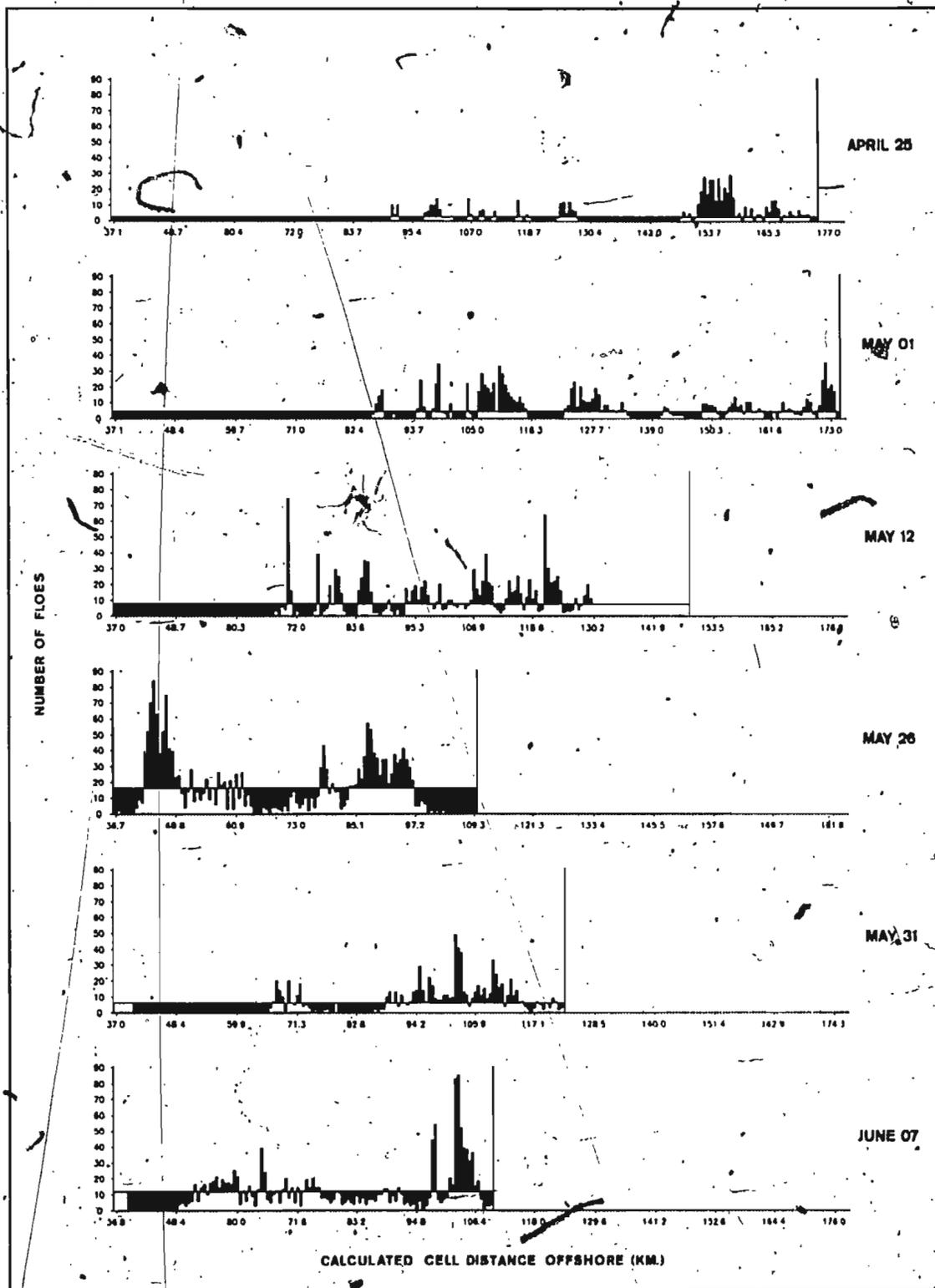
Figure 19 – Distribution of cell frequencies-above and below mean
cutting value for runs test on randomness.

91

Table 10 - Results for runs test of frequency

DATE	MEAN VAL.	TOTAL RUNS	CELLS	CELLS	Z-SCORE	SIG
APRIL 25	2.6441	31	175	61	-10.303	0.000
MAY 01	4.3843	33	167	75	-10.777	0.000
MAY 12	7.9125	30	103	57	$- 7.679$	0.000
MAY 26	16.174	21	75	46	$- 7.176$	0.000
MAY 31	6.056	23	93	51	$- 8.026$	0.000
JUNE 07	11.7213	31	77	45	$- 5.2368$	0.000

Table 11 - Results for X^2 test of frequency

DATE	EXPECTED	CRITICAL X^2	CALCULATED X^2	D.F.	SIG
APRIL 25	22.29	55.48	1866.833	27	0.000
MAY 01	37.89	55.48	1404.082	27	0.000
MAY 12	66.63	42.31	892.106	18	0.000
MAY 26	130.47	36.12	1669.896	14	0.000
MAY 31	48.44	40.75	1076.046	17	0.000
JUNE 07	95.33	36.12	1360.000	14	0.000
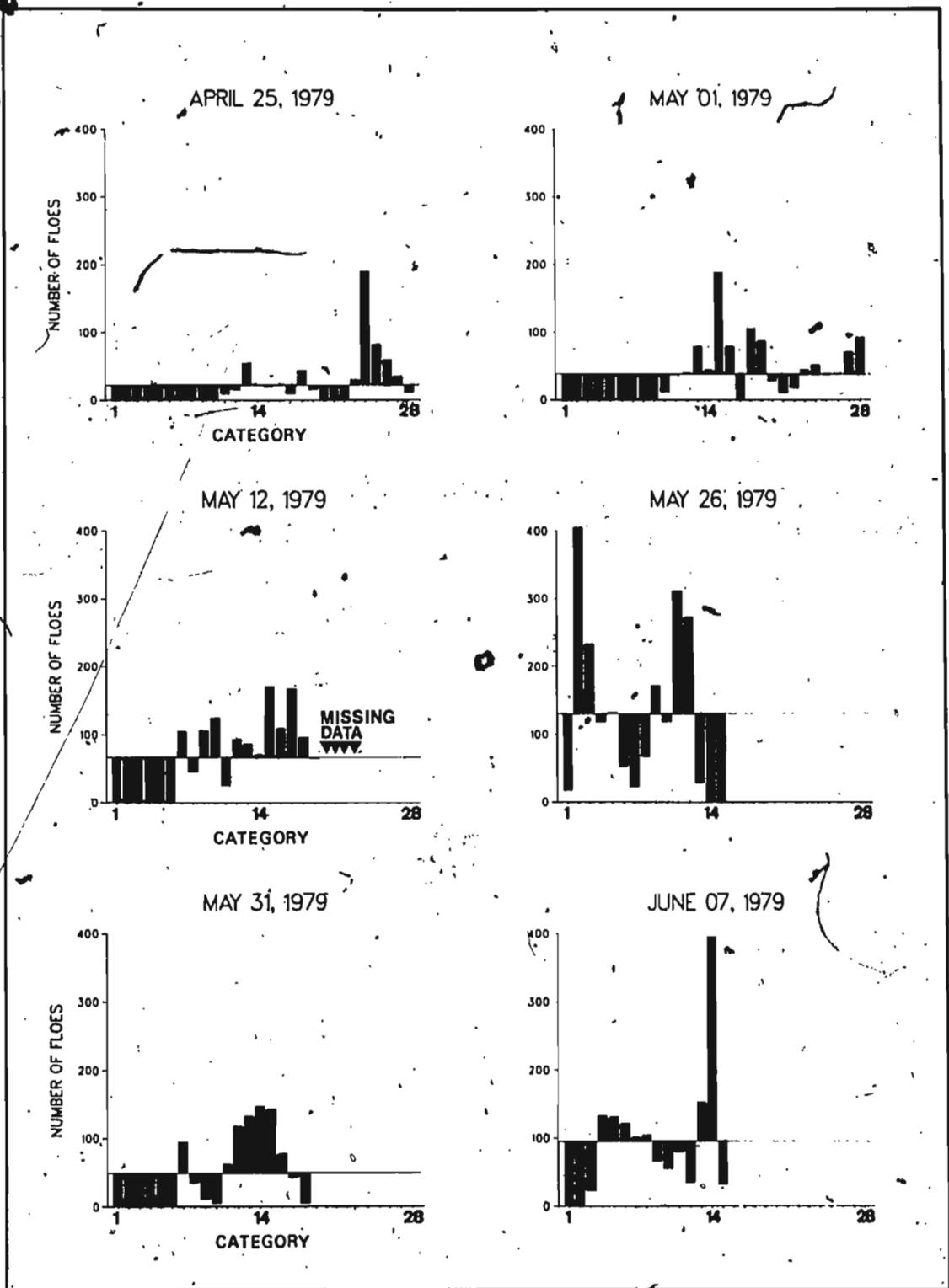
Figure 20 – Distribution of observed floe frequencies compared with expected values for X^2 test. "Category" denotes 5 km intervals into which data were collapsed; this is synomonous with n-1 degrees of freedom.

93

theoretical due to a clustering effect among the floes. Table 11 (p. 92) lists the summary statistics calculated from the test and Figure 20 (p. 93) shows the distribution of the observed frequencies around the expected mean value. In all cases, the calculated chi-square (X^2) values far exceeded the critical values necessary for a significant difference under the given degress of freedom, and the tests were calculated to have a level of significance at $\alpha = 0.000$ after rounding to three decimal places. We can therefore reject the null hypothesis with at least 99.9% confidence that the observed differences were not due to chance, and accept the alternative hypothesis concluding that the observed differences are significant and due to clustering effects within the multi-year ice distribution.

CHAPTER 6

TEMPORAL CHARACTERISTICS OF MULTI-YEAR ICE, 1979

6-1 Overview

Specific locations in the Labrador offshore should experi-
ence variations in multi-year concentrations they receive which
are related to the previously-discussed spatial and temporal
variations in the occurrence of multi-year floe groups.

To summarize these changes in concentration, Figure 21
shows the flux of floes across each flight line within the 10 km
intervals established to investigate this; Figure 22 is a sum-
mary of flux by average floe density per 0.5 km^2 over each 10 km
segment. Although Figure 16a (p. 77) indicates that individual
cell concentrations can have maxima higher than 50 floes per 0.5
km^2, when fluxes are averaged out over the full distance of each
10 km section, the average density is much lower. Average flux
densities higher than 10 floes per 0.5 km^2 per 10 km segment
occurred on May 26 with mean fluxes of 21.1, 13.1, and 12.4
floes per 0.5 km^2 at the 45, 85, and 95 km midpoints respec-
tively; on May 31 and June 07 respective average flux densities
of 11.8 and 16.3 floes 0.5 per km^2 occurred at the 105 km mid-
point. For 1979, all other 10 km regions of the flight line
experienced mean multi-year flux densities averaging between 0
and 10 floes per 0.5 km^2 per any aggregate 10 km of flight line
section. There are still however, strong variations between all

95
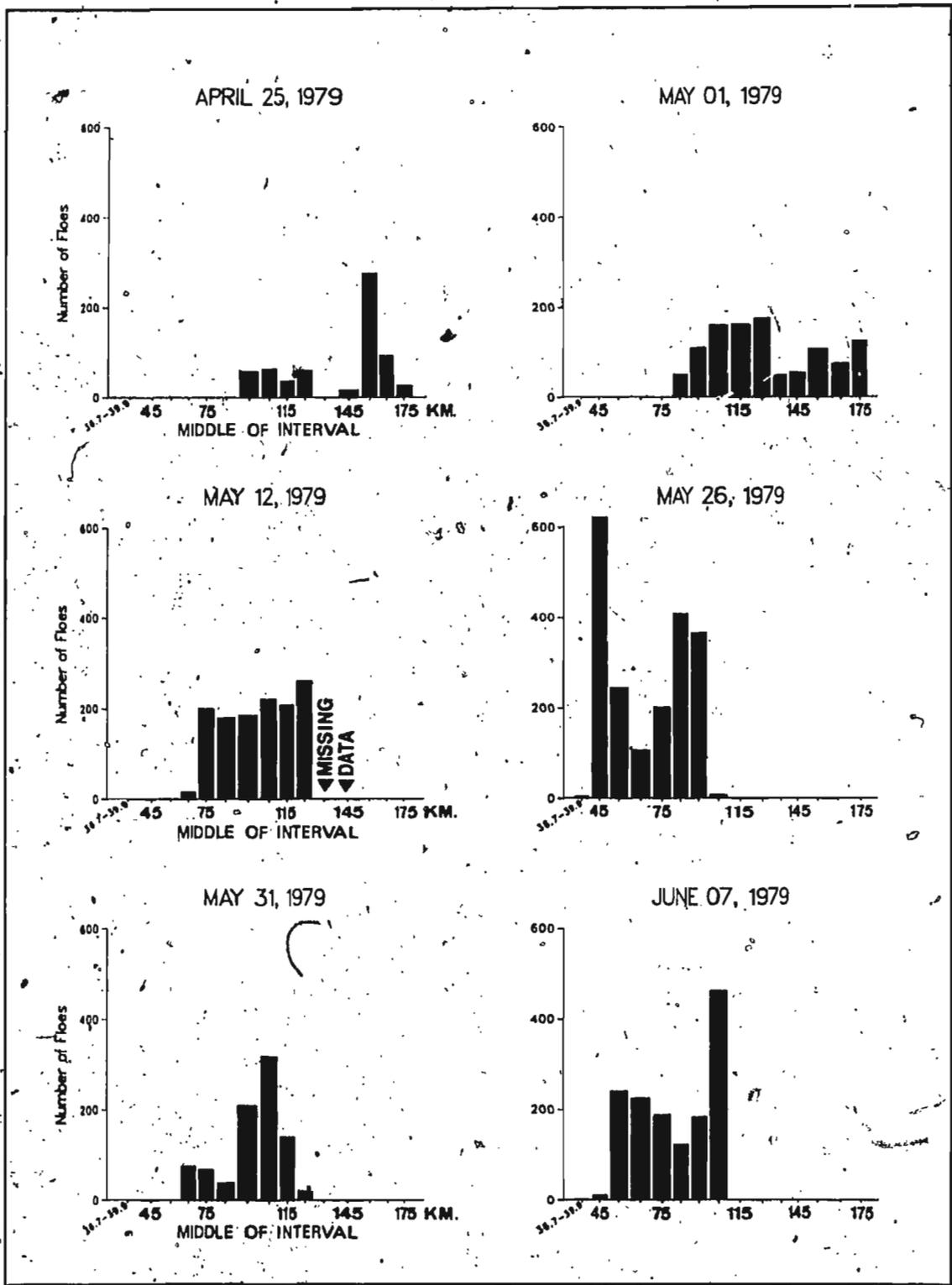
Figure 21 — Occurrence of multi—year floes per 10 km segment of
flight line. '36.7-39.9' refers to a distance
interval for which coverage was incomplete.
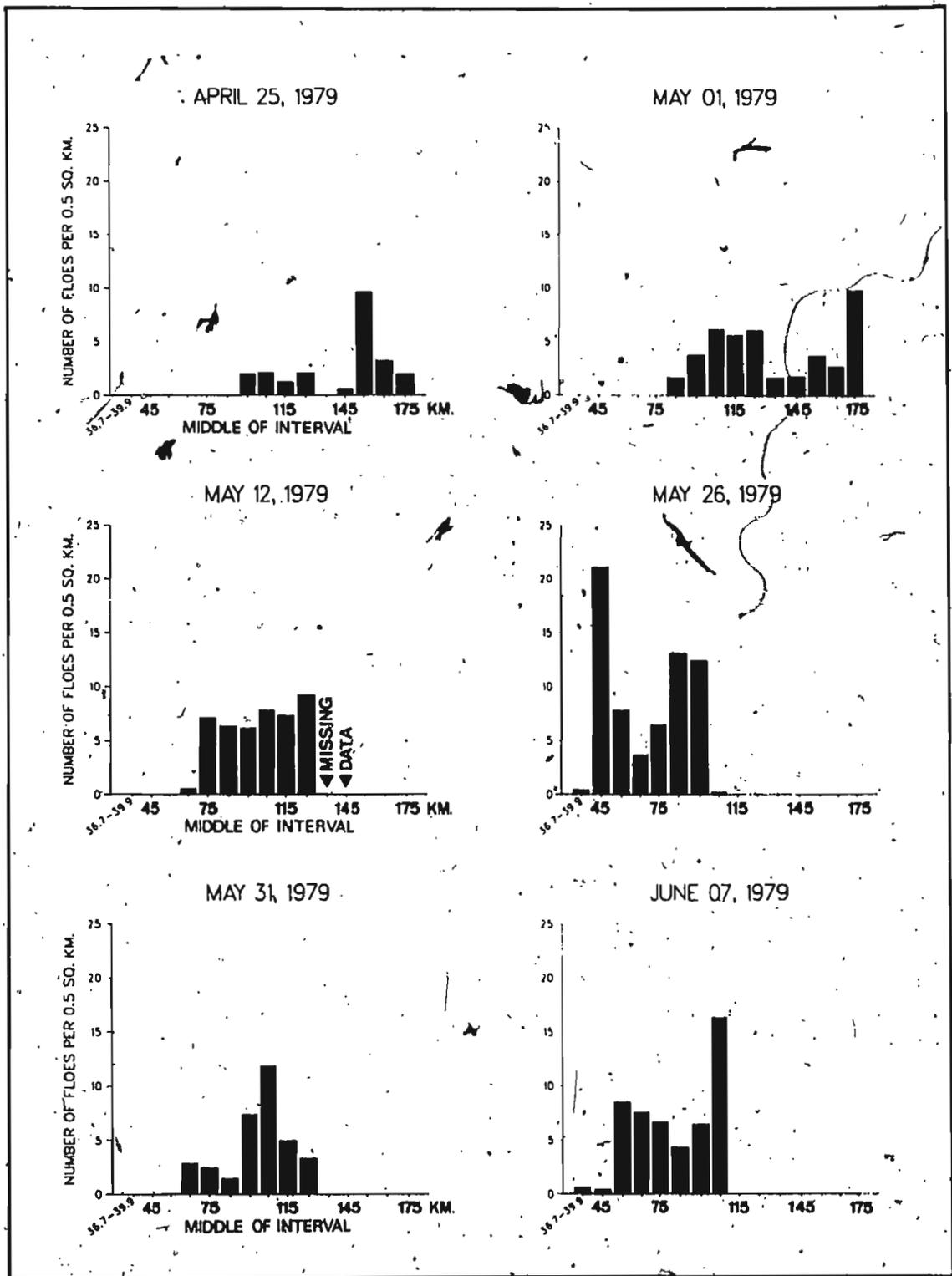
Figure 22 - Average density of occurrence of multi-year floes per 0.5 km² per 10 km length of flight line. '36.7-39.9' refers to a distance interval for which coverage was incomplete.

intervals and clearly some regions were favoured to have consistently higher concentrations of flux across the line than for others during the ice season.

6.2 Temporal variations in coverage

Reference to Figure 23 indicates that the observed shifts in the multi-year ice distribution corresponded almost exactly with changes in the position of the ice edge. Therefore, the positions of the multi-year distribution mean centers were closely tied to their respective asssociated ice edge position and, perhaps excepting May 01, did not vary as a series of independent movements within the pack. Table 12 details the relative ice edge and mean center locations by date. Between April 25 and May 26, both the ice edge and the mean center followed a similtaneous shoreward movement. A variation occurred between May 26 and May 31 when the mean center and ice edge moved slightly seaward, however both had approached land again by June 07, yet not as close as for May 26 which had been the closest shoreward approach of the entire sample. Overall, the projected lines of movement for both respective points approximately paralled one another, and coupled with each movement there was an internal lateral shifting of floe groupings relative to shore.

While ice edge fluctuations can often be closely compared to changes in wind direction over a few days, such associations did not explain the long-term trends observed in the adjustment of the ice edge and multi-year coverage centers for the 1979 ice

MEAN CENTER AND ICE EDGE LOCATIONS
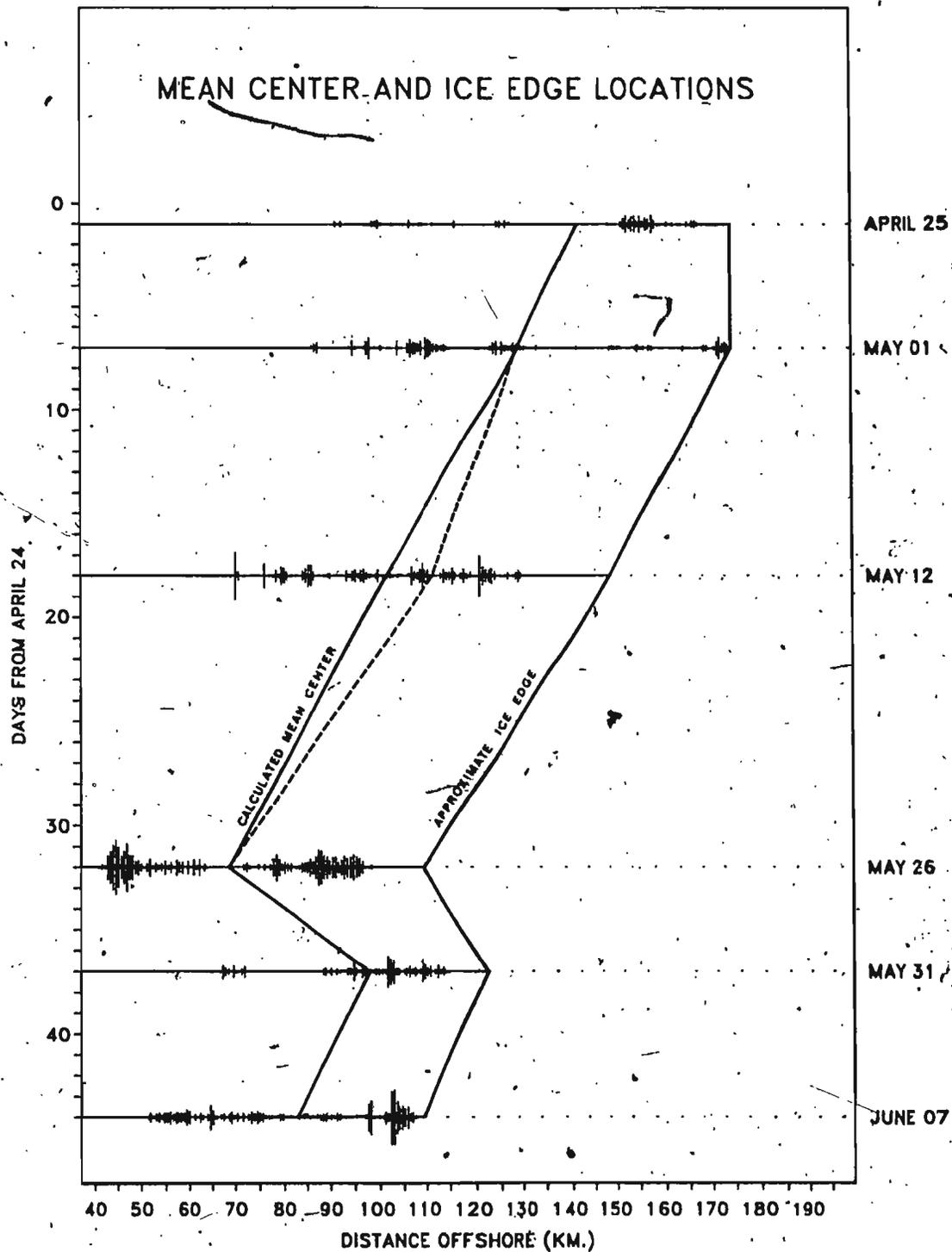
Figure 23 — Transient locations of ice edge and mean centers
of multi-year ice distributions during study
period. Dashed line indicates extrapolated posi-
tion of May 12 mean center, taking into account
missing data.

99

Table 12 — Mean center and ice edge
positions for 1979

DATE	MEAN CENTER (km Offshore)	ICE EDGE (km Offshore)
April 25	141.3	174.1
May 01	128.7	174.1
May 12	101.3*	148.3
May 26	68.6	109.3
May 31	97.9	122.2
June 07	82.8	109.3

* based on incomplete sample

season. Figure 24 is a summary of geostrophic wind conditions between April 25 and June 07, 1979; the data displayed were collected from surface air pressure charts at the 1:10,000,000 scale, each of which summarized synoptic weather conditions based on one of four observations taken at six-hour intervals from 0000 hrs GMT on each respective day. The direction and speed of the geostrophic wind was determined from the orientation and spacing of the isobars at a point on the map approximating the location at which the offshore edge of the pack intersected the zone of photographic coverage. The mean resultant wind vector for each day is shown in Figure 24a; the resultant vector represents the direction and speed obtained by addition of the component vector from each of the four daily observations. Figure 24b is a summary of wind directions by percent of frequency from the total of each individual observation over the entire period; Figure 24c summarizes the resultant geostrophic wind vector obtained from averaging the wind direction over periods of 1 to 6 days prior to the flight, as well as over the entire period intervening between a given flight and the previous one. Figures 24a and 24c give directions relative to the shoreline which, near Saglek, is oriented at 30° west of True North, while 24b relates directly to True North.

For the periods prior to May 12 and May 31 there is some agreement with Figure 23 (p. 99) in that the mean wind vector direction for each averaging period approximated the projected movement of ice over the time between flights. During the aver-
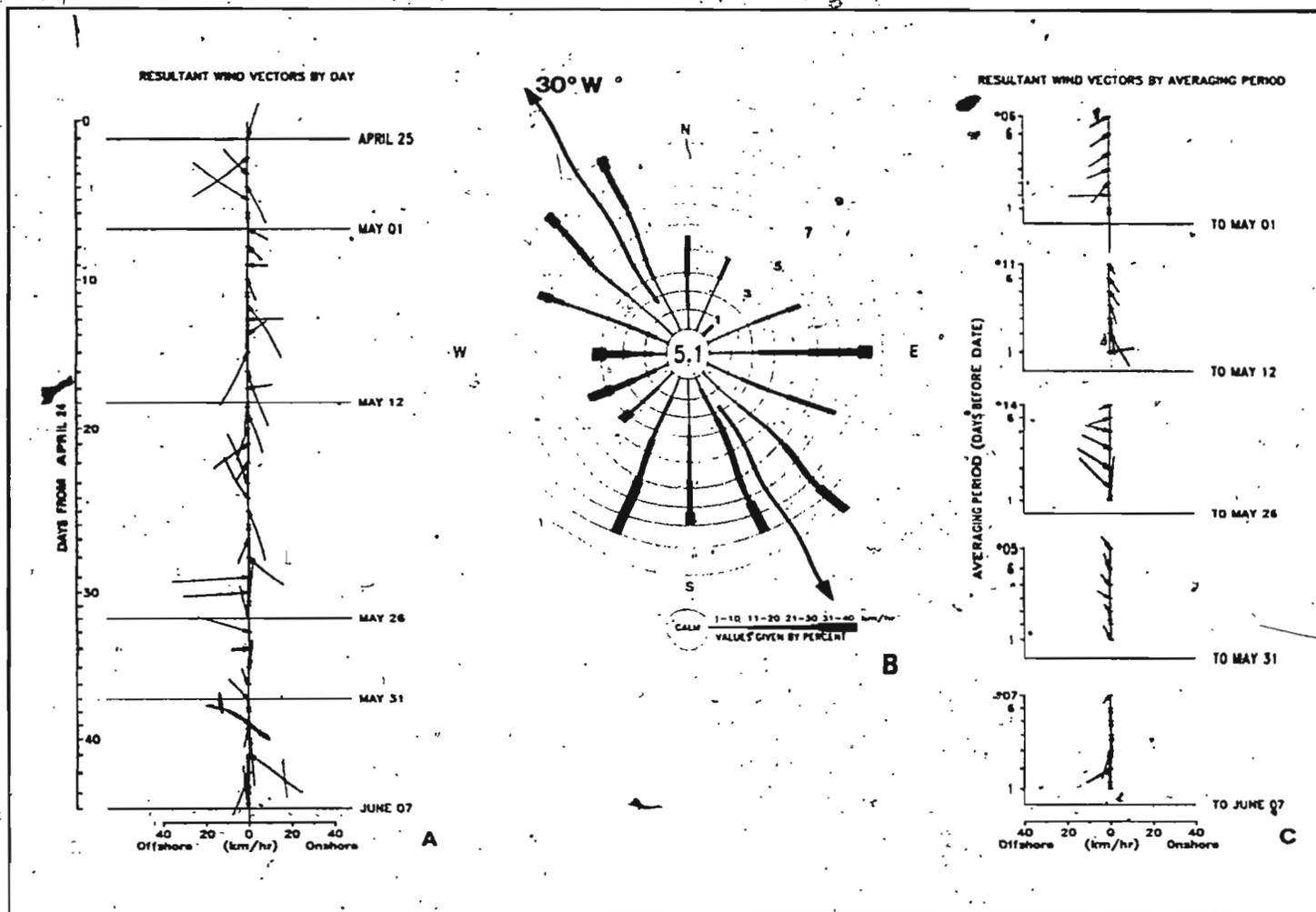
Figure 24 — Summary of Geostrophic wind data for Saglek region during April 25 – June 07, 1979. Numbers denoted by asterisk (*) indicate total number of days intervening since previous flight.

aging period prior to May 12 the geostrophic flow was onshore, albeit at a sharply acute angle from the southeast, and the ice had also moved shoreward relative to its May 01 position. For May 31 when the ice had moved offshore, all averaging periods between this date and May 26 also indicated an approximate off-shore geostrophic wind. However for both May 01 and May 26, when the mean center had moved shoreward relative to its previous flight position, there was no agreement since the geostrophic wind vectors for their respective preceeding averaging periods clearly indicated an offshore flow. June 07 also reveals contradictory ice movements since the averaged geostrophic vector resultants either paralled the coast or indicated an offshore wind, neither of which support the shoreward shift of ice which occurred. Although Figure 24a shows a day of strong onshore flow three days before June 07, it is not expected that this would have been significant in influencing this shoreward movement for the same reason that several days of prior offshore flow (also shown in Figure 24a) did not alter the shoreward movements of the mean centers for May 01 or May 26. Finally, considering the overall shoreward movement through the study period, when a line is drawn through Figure 24b, representing the coast at an angle 30° west of True North, we see that the distribution of all wind frequency percentages, to either side of the line, favours an onshore flow by a net frequency of only 2% - a negligible amount.

Conclusively, while there might be some agreement between the wind direction and ice movement (e.g. May 31), such a rela-

tionship appears to be weak and suggests that long-term ice movements during the study period were the product of other influencing factors. This tends to agree with the findings of Thorndike and Colony (1982) who estimate that, in the absence of a steady ocean current, Arctic pack ice moves in a direction of about 5° to the right of the geostrophic wind during fall, winter, and spring, and 18° to the right in summer. Their results suggested that over several months, only about half of the ice motion could be explained by geostrophic wind, with the other 50% being due to ocean circulation; over shorter intervals, about 70% of the ice motion was explained by variation in geostrophic wind. However, within 400 km of the coast the correlation was only about 50% effective in explaining ice velocities and in no case could any of the divergence be explained by geostrophic forces. Given these findings, coupled with the fact that the Labrador pack is within only 200 km of the coast and lies under the influence of a dominant southward flowing current, it is unlikely that any direct relationship would have existed for the 1979 data, even when the $5 - 18^\circ$ variation from the true geostrophic direction is taken into account.

6.3 Temporal variations in flux

Reference to Figure 25 indicates the relative variation, produced by shifts in distribution, of cumulative flux values across each 10 km segment of the Saglek flight line for 1979. Generally, no region from the point at which photographic cover-

104
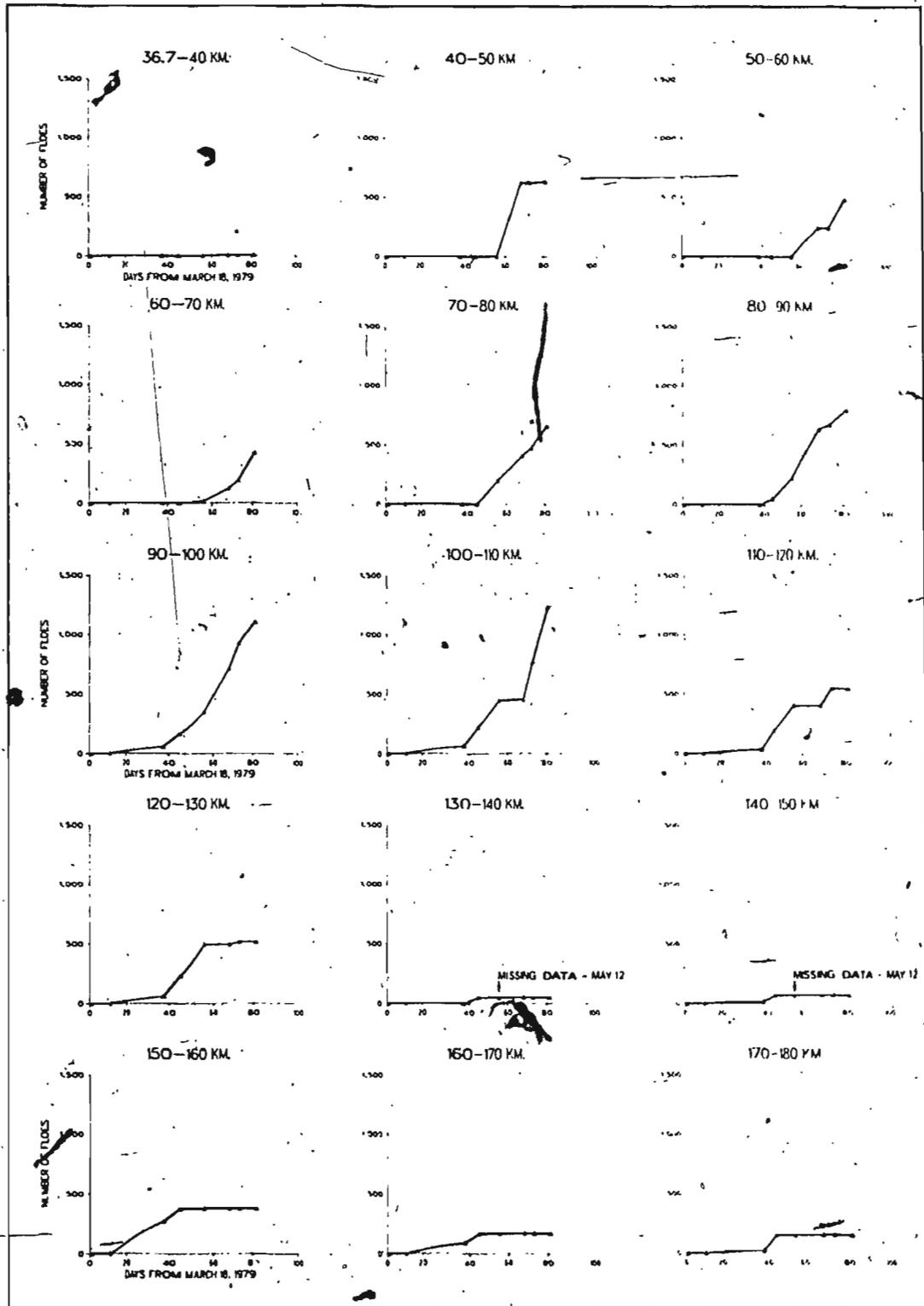
Figure 25 — Cumulative frequency curves for flux for multi-year floes across 10 km segments of flight lines during 1979.

age was begun, to 80 km offshore, received any multi-year ice until midway through the season, after May 01. This initial non-occurrence was due to the maximum offshore distance of the mean center of the distribution for May 01 and April 25. Inshore of this 80 km line, while the 60-70 and 70-80 km zones experienced different upward trends through May 12, the 40-50 and 50-60 km zones did not receive any multi-year ice until near May 26. The 50-60 km zone experienced a sporadicity of flux related to the May 26 and June 07 distributions; the inner portions of these crossed landward into this zone, respectively preceeding and following a seaward movement out of the area, which occurred on May 31. The 40-50 km zone experienced a similar single pulse when the May 26 distribution shifted landward, but experienced no measured significant occurrences thereafter. For the segments between 80 and 120 km, the 80-90 and 90-100 km zones experienced an approximately constant upward trend in cumulative frequency of flux beginning April 25. However, the 100-110 km graph reflects the absence of multi-year ice within this region for May 26, even though younger ice types were present. For this date, a plateau had been reached in the cumulative flux, which was to preceed a second upward trend within this zone for the two subsequent dates. The area between 110 and 120 km was most sensitive to the fluctuating ice edge which had alter-natively moved shoreward and seaward from this region between May 26 and June 07. This produced a series of steps on the curve which indicate a pulsating effect of flux southward across this zone. Outside of 120 km, multi-year ice concentrations had

begun by April 25 and increased until around May 12 (actual flux between 130 and 150 km for May 12 is unverifiable due to missing data), after which there was no further flux. An exception to the April 25 occurrence was in the 130-140 km zone which lay between major groupings for this date hence prolonging the non-receipt of multi-year ice for this area until near May 01. The region beyond 120 km is also reflective of the shifting ice edge which had moved inside of 120 km by May 26 and June 07, and only slightly extruded (122 km) on May 31. As a result, all measured multi-year flux after May 12 occurred to the landward of this point so that the observed season flux pattern for regions to seaward of 120 km consisted of a single pulse, increasing sharply from April 25 and levelling off to near zero after May 12.

For the 1979 season, three apparent zones of multi-year ice flux dominated the offshore region near Saglek. More specifically: -

   (i)   Regions inside of 80 km which experienced initial occurrence approximately midway through the season, near May 12, and which had continued flux thereafter.

   (ii) Regions between 80 and 120 km which experienced varying degrees of flux throughout the entire sample period after sometime prior to April 25.

   (iii) Regions beyond 120 km which experienced flux early in the season, prior to April 25, but none after May 12.

Within these regions, zones sometimes experienced a sporadicity of flux which resulted in alternating periods of occurrence and non-occurrence of multi-year floes. This phenomenon

was due to fluctuations in the ice edge position which were

coupled with a synchronous shifting of the multi—year ice dis-

tributions within the pack.

MULTI-YEAR ICE DISTRIBUTIONS OFFSHORE SAGLEK, LABRADOR, 1979:
A SUMMARY REVIEW

7.1 Total daily flux

In 1979, measured multi-year ice concentrations began enter-
ing the region near Saglek Bank in significant proportions some-
time after March 29 and increased in an apparently constant up-
ward trend through April 25, May 01, and May 12, reaching a peak
occurrence sometime near May 26. Reference to Figures 26e and
26f indicates that after May 26, concentrations began a downward
trend which incorporated an upward fluctuation between May 31
and June 07, indicative of a pulsating effect in the actual rate
of delivery of the multi-year ice to the study area between
these dates. Whether this upward fluctuation reached a greater
amplitude after June 07 is unknown since no data exist. How-
ever, for the data available, the overall downward trend after
the May 26 peak is in agreement with Markham (1980b) and Nordco
(1979) who also document similar downward trends after a central
peak in seasonal multi-year ice flux. The actual shape of the
curve between May 01 and May 26 is also unclear, owing to miss-
ing data for a portion of the May 12 flight line, and occur-
rences were probably higher for this date than available data
suggest.

While the 1979 data might not be representative of the
multi-year ice concentration occurring in the region over a
period of years, it is interesting to note that the 1979 peak
flux period occurred sometime near the middle of May, approxi-
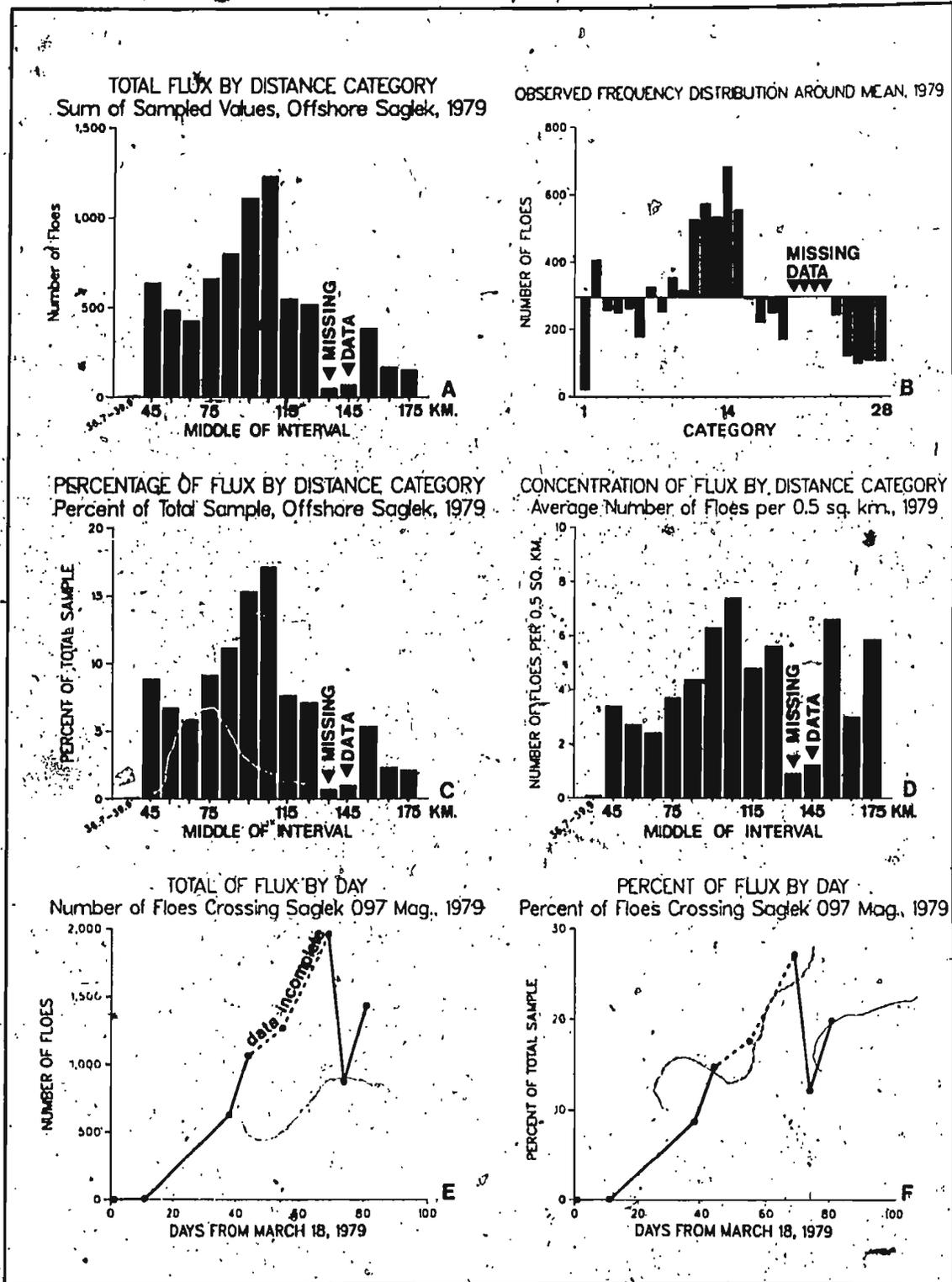
Figure 26 — Summary of sampled multi-year floe flux across Saglek 097° Mag. during 1979. '36.7-39.9' refers to a distance interval for which coverage was incomplete.

110

mately one month prior to a multi-year flux peak which occurs
off Groswater Bay in mid-June as reported by Nordco (1979).
Such a time difference might be indicative of the temporal lag
occurring between the arrival of multi-year ice in the northern
region and its eventual transport to the southern areas of the
pack.

7.2   Total of sampled flux by distance category

Reference to Figures 26a and 26c indicates that the main
concentrations of sampled multi-year ice flux for the season
occurred in a central core between 80 and 110 kilometres off-
shore, a zone which accounted for 43.5% of all sampled values,
with total flux values decreasing to either side. However, the
decrease is more rapid in the region seaward of 110 km due to
the spatially-dynamic nature of the ice edge, the progressive
shoreward movement of which increasingly lessened the probabil-
ity of multi-year ice occurring in this region later in the sea-
son. For a similar reason, the total values inside the 80 km
region drop off more slowly because the shoreward movement of
the multi-year ice distribution approximately coincided with the
season's two highest-recorded flux values on May 26 and June 07.
This resulted in much higher flux rates in the inner regions on
those dates than had occurred at the outer edge during the lower
flux rates of April 25 and May 01. Again, the true shape of the
distribution is obscured by the absence of complete data for the
region between 130 and 150 km on May 12.

Comparison of the shape of Figure 26a with the shape of the distributions in Figure 21 (p. 96), indicates that as the concentrations shifted from the outer offshore region to the inner offshore, this central core represented a common zone shared initially by the inner edge of the distribution during April 25 and May 01, and later by the outer edge of the distribution during May 26 and June 07. During the apparent period of spatial transition surrounding May 12, and the seaward shift of May 31, this zone nearly coincided with the center of the spread of multi-year ice occurrences.

Furthermore, Figure 26d indicates that despite the lower frequency of floes which occurred in regions seaward of the core, the mean concentration in floe density per 0.5 km^2 (based only on the dates when these areas were inside of the ice edge), was close to and sometimes exceeded the average densities occurring within the 80-110 km zone. With the exception of the 160-170 km zone, the average seaward densities were actually higher than the average seasonal densities occurring landward of 90 km.

Reference to Figure 27a reveals that most of the sampled flux was found landward of the 200 m depth contour which is located at the seaward edge of Saglek Bank. Therefore, a far greater portion of the multi-year ice for the season was drifting in the shallower waters over the bank rather than in the deeper water along the continental slope. Exceptions to this were the April 25 and May 01 flights when approximately 75% and 55% of the respective individual distributions lay seaward of

Occurrence of Multi-year Ice Relative to 200m Depth
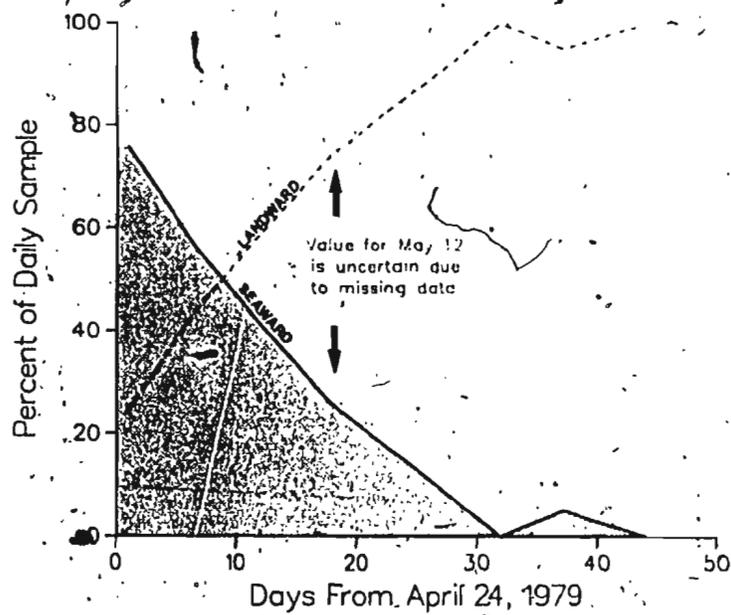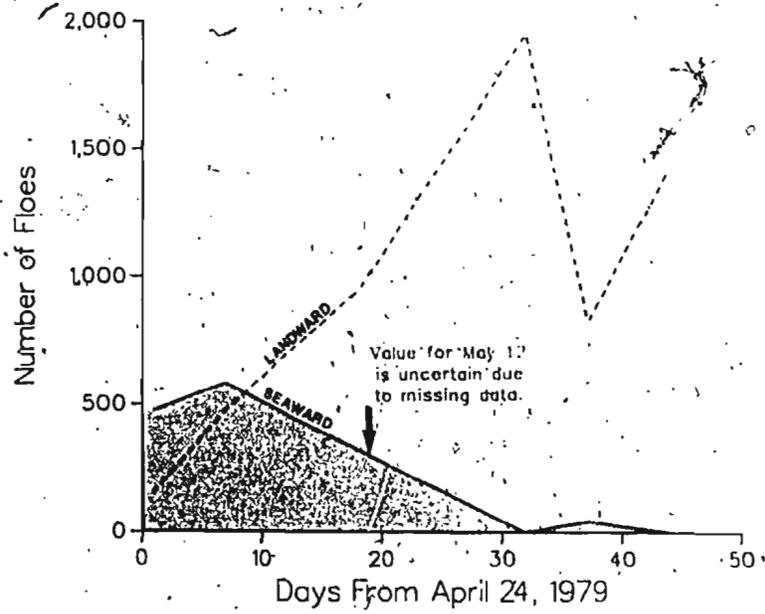
Figure 27 - Frequency of occurrence of multi-year ice relative
to the seaward edge of Saglek Bank during 1979.

113

this line, as shown in Figure 27b.

7.3 Temporal clustering of multi-year flux

To test the significance of the apparent grouping in the total flux values, a chi-square test was applied to seasonal data at the 5 km interval, using the same null and alternative hypothesis as in section 5.3. Again, the test was one-tailed with a chosen level of significance at $\alpha = 0.001$; incomplete data from the 130-150 km region were not included because they would have resulted in an inflated value for x^2. Testing of the observed frequencies against the expected mean category value of 295.17 yielded a x^2 value of 2316.88 which at 23 degrees of freedom, exceeded the critical value of 41.64 with a calculated level of significance at $\alpha = 0.000$. The resulting decision was to reject the null hypothesis with at least 99.9% confidence that the observed differences were not due to chance variations, concluding therefore that there was a significant clustering of total flux values for the season. Figure 26b shows the distribution of observed frequencies around the expected mean value and clearly isolates the central core of seasonal multi-year ice flux which was observed at 80 to 110 km in Figure 26a (p. 110).

CHAPTER 8

OCEANOGRAPHIC INFLUENCES ON MULTI-YEAR ICE DISTRIBUTIONS DURING
1979

8.1 Overview: general oceanographic conditions in the Labrador
     Current

While little information exists regarding the exact nature

of water circulation and transport in the Labrador Current (Bob-

bitt, 1983; Fissel and Lemon, 1982), the general pattern of cur-

rent distribution has been well-documented.

Northern Davis Strait is a mixing area for the Cold Baffin

Current and the westward-flowing warm West Greenland Current

which join and flow south along the east coast of Baffin Island.

North of Resolution Island this flow splits, with a branch moving

west, on both sides of the Island, into Hudson Strait (LeBlond,

et al., 1981; Bailey and Hachey, 1950). The eastern branch con-

tinues flowing southward with warm West Greenland water in its

eastern section and some cold water of the Baffin current in the

western section. The water entering Hudson Strait penetrates

west for about 250 km (Matthews, 1976) before recurving and even-

tually exiting along the south side of the strait after having

taken on the brackish and cold characteristics of Polar Basin

water. In the northern region of Saglek Bank this joins with

the eastward branch to form the Labrador Current which flows

southward in two main bands along a direction parallel to the

isobaths (Matthews, 1976; Lazier, 1979).

The outer band is comprised of warm west Greenland water,

in excess of $4^{\circ}C$, along its eastern side and colder east Green-

115

land water of less than 3°C along its western side. The inner band is made up of cold water from Hudson Strait and Baffin Bay and has a temperature of less than -1°C; it flows over the Labra-dor shelf, along Saglek Bank (Allen, 1980). From assimilation of historical records, Matthews (1976) concluded that the inner band actually consisted of two sub-component bands which made for a total of three southward-flowing bands as shown in Figure 28. Of these two, the inner component band follows the marginal depression along the inner edge of the banks, and it is composed of water from Hudson Strait as well as local run-off from the coast. The outer component band of the main inner band is made up of Baffin water and Hudson Strait water which follows the outer edge of the banks along the 200 m isobath (Matthews, 1976).

Located within these water masses, Fissel and Lemon (1982) identified four main circulation regimes in the Labrador offshore region:

(i) Regions on or near the continental slope where strong, very steady flow exists, having moderate vertical shear between water types.

(ii) Regions in the marginal trough where flow is slightly less stronger than on the slope, with large vertical shear.

(iii) Regions over the banks where flow is unsteady and weak with low vertical shear and moderate energy.

(iv) Regions in the saddles, between banks, where flows are unsteady with high energy and moderate vertical shear.

A strong flow situated over the continental slope was also identified by Smith, Soule and Mosby (1937), and Lazier (1982)

116
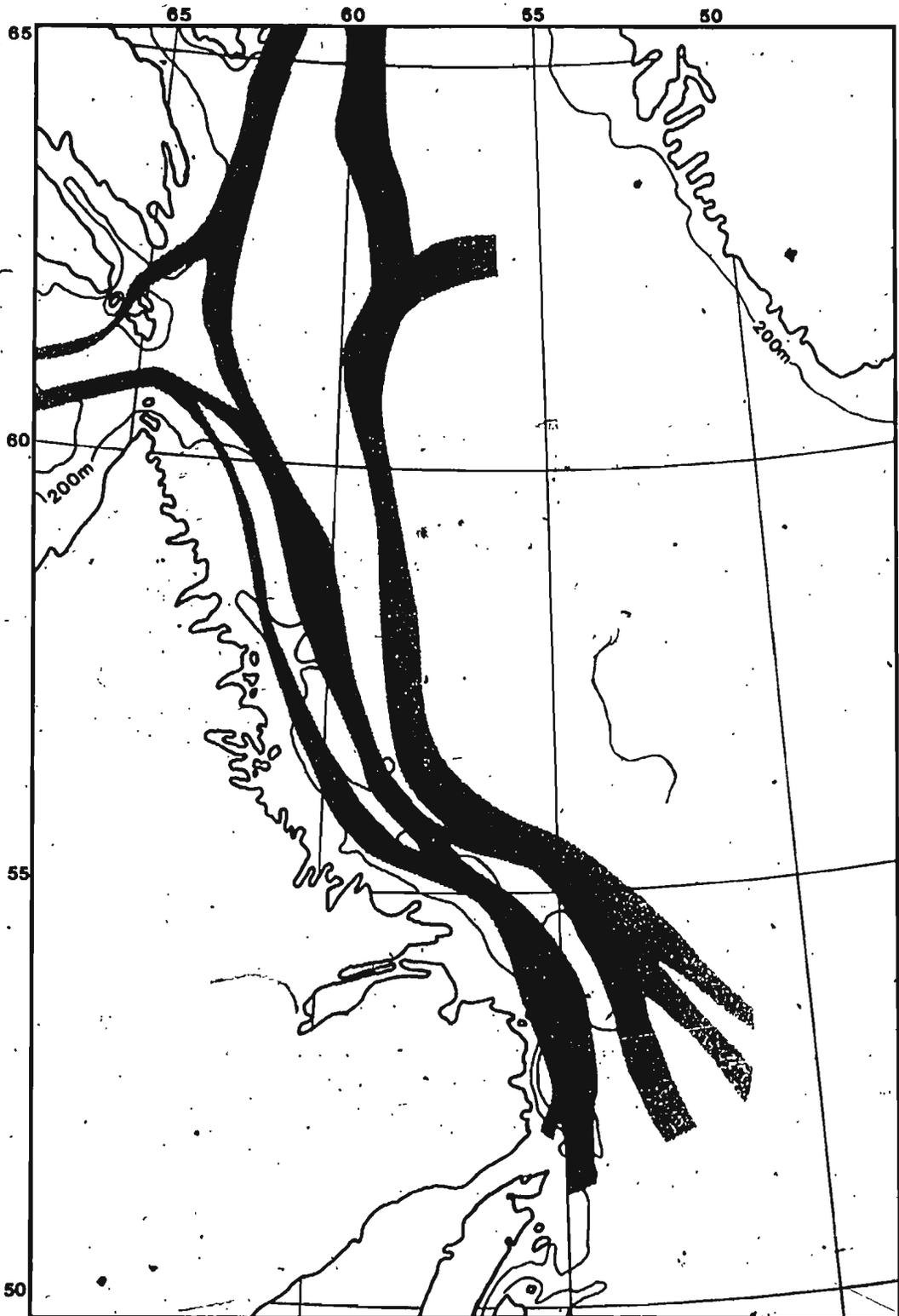
Figure 28 – General patterns of flow within the Labrador Current
as described by Matthews (1976). 200 m isobath has
been added for purposes of this report.

indicates that near-surface velocities here are 0.5 to 0.8 ms^{-1}.
The flow in this zone is therefore much faster than over the
shelf where average speeds of 0.17 ms^{-1} have been recorded
(Petro-Canada, 1982). This strong flow acts as a boundary
between the water of the shelf and the offshore water mass
(Lazier, 1982).

Salinities in the main outer band are between 34.7 and
34.9^{o}/oo while the main inner band has values of between 32.6
and 33.7^{o}/oo (Fissel and Lemon, 1982). Lazier (1982) found a
strong positive gradient for both temperature and salinity with
increasing distances from shore across the shelf, slope and
outer areas. However, the sharpest temperature and salinity gra-
dients occur along the boundary separating the cold water of the
shelf from the warmer Greenland water farther offshore. This
demarks the location of a thermal front across which Islen
(1927) noted a temperature change of 5°F (2.8^{o}C) over a distance
of 15 miles (24 km). The frontal zone between the two main
water masses has been illustrated by Legeckis (1978a) and
LeBlond (1982), from interpretation of satellite imagery, and
lies along the edge of the continental shelf (LeBlond, et al.,
1981).

Large scale spatial perturbations usually occur along such
frontal zones and are well-documented for other regions of the
world having an eastern coastal current similar to that of Labra-
dor. For example, meanders have been observed in the front of
the Gulf Stream (Flagg and Beardsley, 1978), and Niller and Mysak

118

(1971) predict that for the southeastern coast of the U.S.,
unstable waves in this front can have wavelengths of near 150 km
with periods of 10 days; propagation in either direction along
the current axis is considered possible. Large-scale undula-
tions have also been observed in the Gaspe Current. Over a 3-5
day period during 1978, the axis of the current moved offshore
for several days and, when it again began to approach its near-
shore position, a wavelike structure developed which eventually
broke after reaching a wavelength of 60 km (Tang, 1980). In
ice-free waters around the United Kingdom meanders have been
observed to evolve, over a four-day period, into full scale
eddies which then separated from the frontal zone and moved off
into the warm water zone as a cell of cooler water (Simpson,
Allen, and Morris, 1978). Formation of cold-core eddies is also
known to occur in the Kamchatka Current (Solomon and Ahlnas,
1978) and warm-core eddies have been observed in the Gulf Stream
(Halliwell and Moores, 1979) where they are thought to be the
driving force behind topographic Rossby waves observed at depth
(Thompson, 1971).

Bane and Brooks (1979), Brooks and Bane (1978) and Legeckis
(1979) all indicate that, for the Gulf Stream, such frontal undu-
lations are capable of propagating warm water up onto the conti-
nental shelf and into shallower depths landward of the 200 m iso-
bath. Associated with these Gulf Stream meanders, Vukovich, et
al (1979), Lee and Mayer (1977), Legeckis (1975) and Lee (1975)

119

all note that warm-core eddies formed along the front spin off onto the continental shelf and extend into regions inside of the 100 m isobath. While several of these authors consider bottom topography to be the instigating force behind eddy and wave formation, Huthnance (1981) suggests that the actual movements are compensatory occurrences intended to conserve mass by drawing up water from the slopes to replace that which has been lost from the shelf.

In the Labrador Current, meanders and eddies are seen in Legeckis' (1978) illustration of the frontal zone and meanders have also been produced in Tee's (1978) numerical model of a homogeneous Labrador Sea. LeBlond (1982) also presents evidence of frontal undulations in the Labrador Current which he observed from a thermal infrared satellite image. This image is shown in Figure 29, and the wave-like features along the front are clearly visible. Near the northern part of Labrador we see a finger of warm water (see arrow) extending as a southward curve into the cold water zone. This structure is almost identical to the configuration of eddies as described by the previous authors studying the Gulf Stream, and in this case indicates the formation of a similar feature along the Labrador Current frontal zone near Saglek Bank.

Evidence of meanders based on direct measurement in the Labrador Current has been given by Weir (1979) who, using three

120
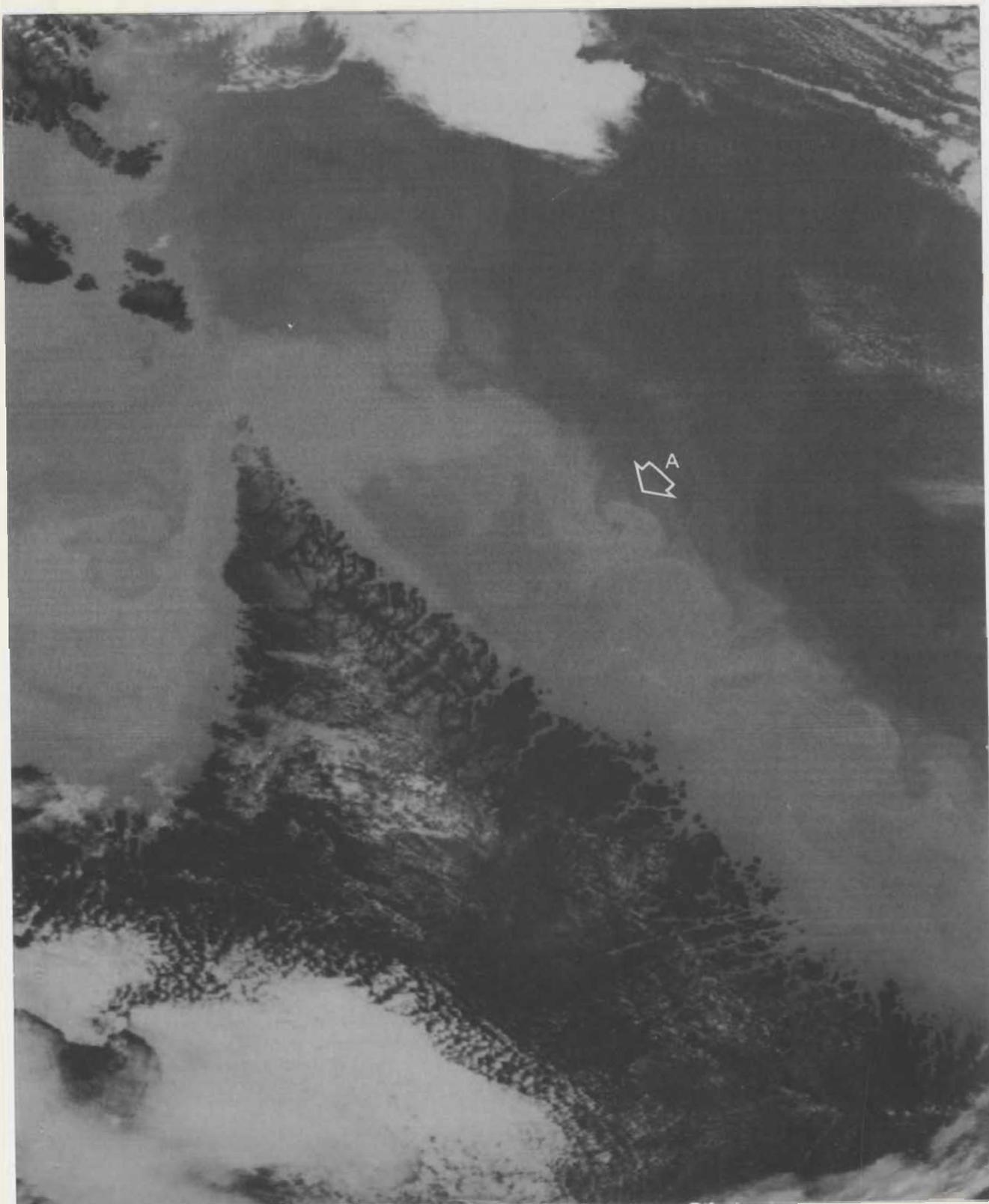
Figure 29 – NOAA-5 infrared image showing meanders in the frontal zone of the Labrador Current as seen at 1355Z on September 3, 1977; lighter tones denote colder water. For explanation of arrow, see page 120. (Photograph courtesy of Dr. P.H. LeBlond)

121

year's of data from satellite-tracked buoys also found undulations in the current; the crests of these waves varied east to west over distances of up to 90 km during a period of 2-4 days. Other evidence is given by Fissel and Lemon (1982) who observed large variations in current direction over periods of 7 to 30 days, with shorter variations also occurring over 4 to 7 days. At the 4-7 day interval, meanders were detected along the main core of the current at the shelf break (i.e. near the continental slope in the region of the 200m isobath), as well as in the Cartwright Saddle. These meanders occurred on the inner edge of the main band and were identified by an increase in current speed as well as temperature and salinity. Temperature and salinity readings were also strongly indicative of warm-core eddies spun off from the main current band. The distance of penetration by such formations onto the shelf was not known, however comparison with the Gulf Stream examples suggests that landward penetration beyond the 200 m isobath might be possible.

Similar variability in current has been described by Allen (1979, 1980) and Allen and Huntley (1977). Using two current meter sets at 2600 m and 3000 m in the Hopedale Saddle, Allen and Huntley found a mean southward flow of $0.20 - 0.40$ ms^{-1} with the occurrence of four northward reversals over a 27.9 day period. During this study, temperature records indicated the advection of warm parcels of water past the recording instruments. Initial analysis of these results indicated possible causes as being due to either a meander, a net counter-current flow in the offshore section of the current, or eddies propagating along the

outer edge of the Labrador Current. Later reports (Allen, 1979; Allen, 1980) revealed the influence of bottom-trapped Rossby waves occurring in the frontal zone. Over 4 to 8 day periods these waves produced cross-slope movements only in the bottom flow, however during 8 to 10 day periods, the waves extended throughout the water column and were responsible for major current fluctuations at the surface. Other instances of vortical flow can be found in Anderson (1968) who observed at least two vorticies near Southern Labrador which he thought were produced by depressions in the bottom topography near Hamilton Bank.

The relationship between spatial variations in sea ice patterns and fluctuations in the southward flow of the Labrador Current has been studied by LeBlond (1982). From interpretation of satellite images, meanders were observed in the outer edge of the marginal ice zone which corresponded well with the meanders observed in the oceanic front from infrared imagery. These ice edge meanders moved southward with an amplitude of 15 km and a wavelength of 75 km, however it was not possible to determine if the thermal front meandered synchronously. Peripheral evidence of sea ice relationships with the Labrador Current has been given by MES (1974) who observed that the edge of the pack probably marked the boundary between the cold and warm sections of the current; drift measurements taken inside and outside of the edge yielded distinctly different patterns of movement.

In the marginal ice zone of eastern Greenland, similar eddy motions have been observed along the ice edge by Johannessen, et

al., (1983). These were small eddies of 5 to 15 km seen as rotational patterns extending out from the edge of the ice; at least one was embedded in the oceanic front. Additionally, ice edge meandering was greatly enhanced during periods of off-ice wind or calm while an on-ice or down-ice (blowing parallel to the edge with ice on the right) wind caused floe convergence and straightening of the edge.

Wadhams and Squire (1983) also report a large scale eddy of about 60 km diameter in the east Greenland MIZ. Within this feature, lenses of warm water having temperatures of up to 443°C were found centered at the 40 m depth at a distance of 60 km inside the Polar Front. Within the eddy, zones of reduced ice concentration were closely related to the warm water region. Submarine transects of the Greenland MIZ by Wadhams, Gill and Linden (1979) during 1976 also revealed patches of warm water contained within the polar water behind the frontal zone. These patches were also considered to be the result of eddies, and while one eddy did have a significantly thinner ice cover lying over it, no causal relationship could be established.

Descriptions provided by these scientists indicate that frontal meanders and the associated eddy formation do have an effect upon the distribution of ice within a marginal ice zone. In the simplest case such eddies are capable of drawing floes laterally across the MIZ from one section to another and can also advect warm parcels of water into the MIZ leading to accelerated melt rates (Wadhams, 1981). However, few data are available

regarding the properties of eddy production, their resulting

internal structure, or how such features eventually deteriorate

(Wadhams, 1981).

8.2 A theory on the grouping of multi-year ice in the Labrador Current.

Wheeler (1981) suggests that for Arctic regions the occur-
rence of multi-year floes in groups is a result of the weakening
of larger floes during the summer which are then broken apart
during storm conditions in the fall. Floe fracture is undoubt-
edly responsible for the smaller overall multi-year floe sizes
occurring off Labrador. However, the phenomenon of spatial
separation in which relatively lower or zero magnitudes of occur-
rence are found between groups of high concentration appears to
be coupled with oceanographic conditions.

Figure 30 is a plot of individual multi-year floe positions
recorded from the 1979 flight lines. Owing to the extremely nar-
row nature of the actual flight line relative to its length, the
width of the plotted flight line is severely exaggerated in
order to make individual floe positions distinguishable. Because
of this, the patterns they depict are not literal representa-
tions of the actual patterns observed. However, when making com-
parisons from one flight to another the relative changes observ-
ed in pattern are real and the diagrams are therefore useful in
high-lighting the extent of change from one date to another.

The positions of multi-year floes in both discrete and non-
discrete spatial patterns are clearly visible. The strongly
linear nature of the patterns is due mostly to the exaggeration
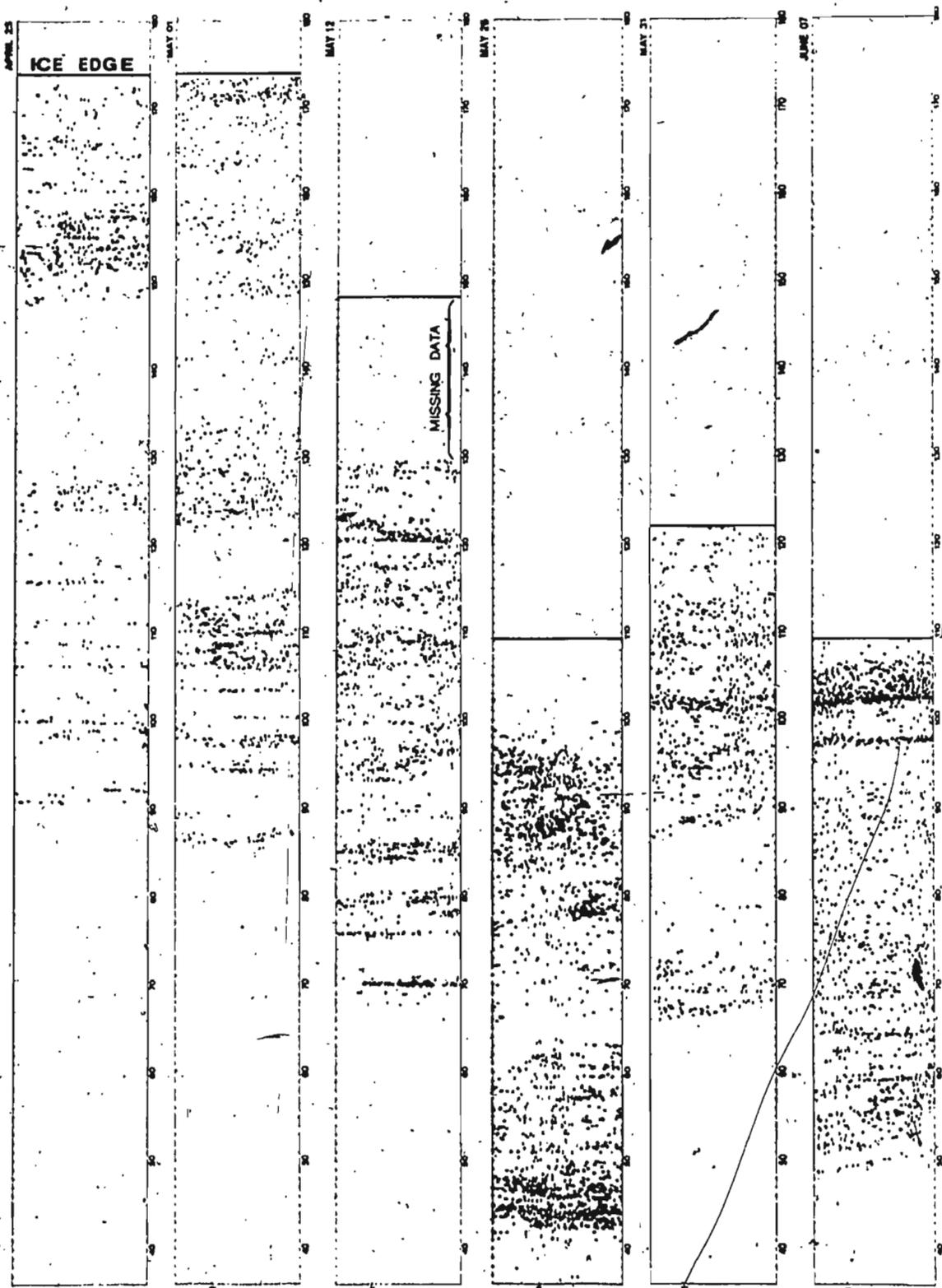
Figure 30 - Plots of individual multi-year floe positions as identified on flight lines.

of the Y-axis and as such must be interpreted with care (although some linearties in floe distributions across the flight lines were actually observed from the photographs). What is real and constant from flight to flight however, is that the groups are seen as extending from the top of the coverage region to the bottom. On the basis of this observation, an extrapolation of these patterns beyond the region of coverage would suggest that the observed groups are actually bands of multi-year ice crossing the flight line, with similar banded regions of reduced or zero multi-year ice occurrence lying between them. This is also supported by Figure 18 (p. 85) which consistently shows a pair of bands on the innermost portion of the multi-year floe distributions for the first three flights. The recurrence of these features suggests that flux of multi-year ice was constant in this area, albeit with some landward deflection, and that a more or less continuous band of old floes crossed this zone during the time period between flights; similar recurrences of bands can be observed from Figure 30.

Lepparanta and Hibler (1984) indicate that variations in floe thickness will produce banding effects in a marginal ice zone. The basis of their explanation is that heavier floes will drift slower and more to the right of the wind direction than will smaller floes. Clusters occur in situations where lighter floes either catch up with the heavier ones, or drift apart from them. These authors note that originally-adjacent first-year and multi-year floes can drift apart by several kilometers in a single day. The assumption is that the differential drift of the heavier floes will eventually separate them from the younger types.

127

Two considerations make this an unlikely mechanism for
explaining the grouping of multi-year floes observed during 1979.
First, the clustering phenomenon observed by Lepparanta and Hib-
ler (1984) occurred mainly near the ice edge, whereas many of
the examples of discrete grouping seen during 1979 occurred well
landward of the ice edge. Second, for 1979, the observed bands
crossed the photographs from the top to bottom for all days sam-
pled. Since the sorting mechanism described by Lepparanta and
Hibler assumes a differential drift of floes which is relative
to the wind direction, then in order for wind effects to have
caused the phenomenon observed during 1979, the wind would need
to have blown from a constant direction in order to maintain
the same orientation of the bands from day to day. Reference
to the wind data shown in Figure 24 (p. 101) shows this was not
the case. Moreover, Lepparanta and Hibler observed the best
differential drift between two floes to have occurred during a
several-day period of offshore wind; reference to Figure 24 shows
that the period of strongest offshore wind occurred just prior
to May 26, a day on which the occurrence of discrete groups of
multi-year ice was minimized. Therefore, it seems unlikely that
wind effects could have been the dominating factor controlling
the 1979 multi-year ice grouping phenomenon.

However, if the explanation given by Lepparanta and Hibler
is modified to consider effects of the Labrador Current, instead
of the wind, then it becomes more plausible. In this case the
current becomes the forcing mechanism, acting with greater
influence on the deeper multi-year floes than on the shallower
first-year floes. Since the Labrador Current flows in a mean

128

southward direction, then this could explain why the bands of multi-year floes would have retained the same orientation from one flight to another.

Structurally, the Labrador Current has usually been described as a series of bands (see Figure 28, p. 117), with each band representing a core of flow within which velocity is greatest near the center and decreases towards the peripheral annuli. For the Saglek Bank region, this banding is evident in the findings of Smith, Soule, and Mosby (1937). For the Hamilton Bank area, this structure has been observed by Scobie (1972) and by Anderson (1968) who noted a banding based on temperature data. Kollmeyer, McGill, and Corwin (1965) further suggest that cold cores of the Labrador Current are actually intrusive filaments of water moving through the shelf water which is slower-moving and considered to be a resident water mass. Figure 31 illustrates the geostrophic velocity structure of the cold core of the Current at the seaward margin of Makkovik and Hamilton Banks as depicted by Fissel and Lemon (1982) for specific dates of observation during the summer of 1980. Since most findings tend to support this banded cold core structure then, in the simplest terms, the flow of water within the current can be likened to the flow of water within a pipe or a trough. In this case, the wall of the pipe would be represented by the zone of contact between the core of flow and the slower-moving shelf water.

For some cases, the flow of water in a pipe is laminar. However, in other situations, there exists three distinct flow
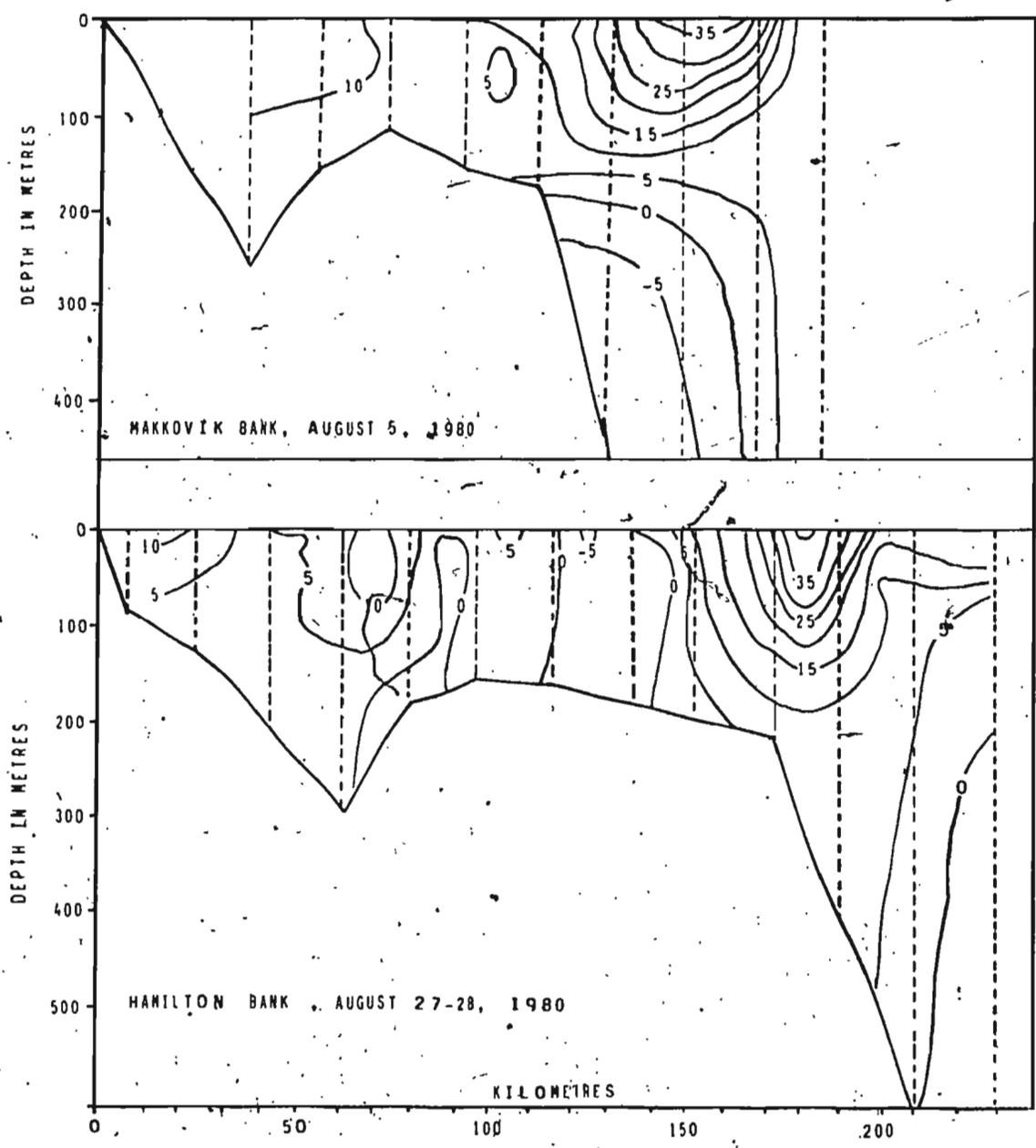
Figure 31 – Structure of cold core of the Labrador
Current at the seaward margin of Makkovik and Hamilton
Banks for specific dates during 1980, as illustrated
by Fissel and Lemon (1982). Contours denote geo-
strophic velocities (cm s⁻¹); negative values indi-
cate northward flow. Dashed vertical lines show
positions of current meter arrays.

130

regimes as described by Duckworth (1977):

(i)   a laminar flow region next to the pipe wall where flow
      width (y) is $0< y <\delta$; where δ is the thickness of this
      laminar sublayer.

(ii) a transition region where $\delta <y <6\delta$

(iii) a turbulent region of $6<\delta y<R$, where R is the radius
      of the pipe.

For all situations, the onset of turbulent flow is predicted

by the Reynolds number, Re (Fox and McDonald, 1973):

$Re = \rho DV/\mu$ where: ρ is density of the fluid
                     D is pipe diameter
                     V is average flow velocity
                     μ is viscosity of the fluid.

It is generally accepted that for Re < 2300 flow is usually turbu-

lent and for Re> 2300 it is laminar. However, no single value

of Re is taken as representing the cutting line between laminar

and turbulent flow (Fox and McDonald, 1973).

Holding density and viscosity constant for the Reynolds for-

mula, it is seen that in a pipe of small diameter, a high veloc-

ity is required for turbulent flow. However, if the diameter

is extended to a value approximating tens of kilometers, hence

corresponding to the scale of Labrador Current cores, then very

small velocities can induce turbulent flow. There is therefore

a basis for intuitively assuming the possible existence of turbu-

lent flow in the Labrador Current.

For purposes of simplification only, consider a flow condi-

tion during which laminar and turbulent flow coexist as shown

in Figure 32. This diagram illustrates the change in flow veloc-

ity as distance increases seaward from the inner boundary of the
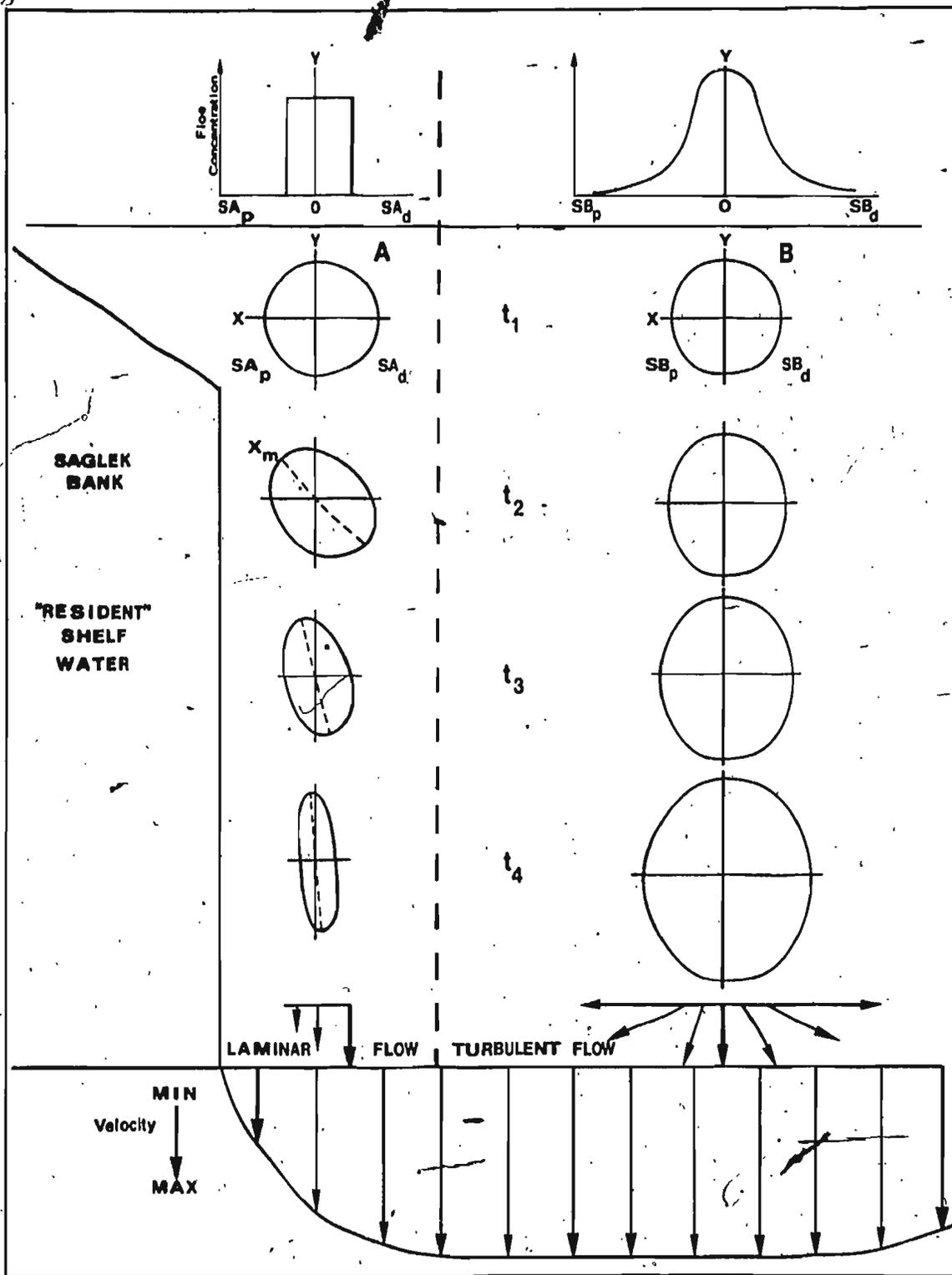
Figure 32 – Schematic representation of the deformation of two initially uniform fields of multi-year floes, one lying within a zone of laminar flow and another in a turbulent flow. Vectors at the bottom of the diagram denote relative velocities.

132

current core. Using the analogy of water flowing in a pipe at Re < 2300, the velocity curve rises steeply in the laminar flow region, but flattens out to a slope of zero in the zone of turbulent flow. For the turbulent zone, where $\delta < \delta y < R$, this means that the axial velocity component is roughly constant at any distance (d) from the pipe wall, assuming $d > 6\delta$; however, in the laminar zone, where $0 < y < \delta$ and $d < \delta$, velocity decreases rapidly as d approaches 0. This produces high rates of axial shear across the zone of laminar flow.

Consider initially, two uniformly-shaped fields of multiyear floes, fields A and B (Figure 32), existing at a time t_1, and located at an undefined distance upstream from the Saglek flight line; both fields are assumed to be in a state of free drift. Field A is located within the region of laminar flow in the peripheral region of the current core, while field B is drifting southward within the region of turbulent flow. Relative to the zone of contact between the shelf water and the current core, the proximal sides of fields A and B are denoted SA_p and SB_p respectively, while the distal sides are SA_d and SB_d; each field is also given a X and Y axis as illustrated.

Taking field A, by the time it has reached its t_2 location, the higher current velocity at SA_d relative to the velocity at SA_p will have resulted in shear deformation of the field, producing an ellipse which now has a major axis denoted x_m. A continued higher rate of drift at SA_d will cause it to move even farther downstream relative to SA_p. This further elongates field A so that by time t_3, the orientation of axis X_m will have begun to approach the orientation of the Y axis. Additionally, since

133

SA_d has a higher velocity component than SA_p, it will correspondingly have a higher Coriolis component. This would cause the floes at SA_d to drift to the right of the direction of flow at a faster rate than those in SA_p, further aiding X_m in its approach to Y. Continued elongation due to differences in drift and Coriolis deflection between SA_p and SA_d will have caused X_m to assume the same orientation as Y by time t_4. Hypothetically therefore, an originally circular field of multi-year floes can be temporally transposed into a narrow, elongated strip due to shear stresses induced across the region of laminar flow.

For field B, lying in the region of turbulent flow, the effects would be different and severe elongation would not occur. Since the relative velocity between SB_p and SB_d would be roughly equal and constant across the X axis of B, then there would be no deformation from shear - though the field might be slightly affected by the slower drift of heavier floes. In a turbulent flow condition, however, there are trans-axial velocity components (Duckworth, 1977) which transfer momentum and mass across the axis of flow. The effect of these cross-flow components would be to disperse the floes, causing field B to broaden its perimeter between times t_1 and t_4 as is shown in Figure 32. The turbulence which produces this dispersal effect is of a small-scale nature when compared to the large-scale turbulence which produces the structure which is shown in Figure 29 (p. 121).

The occurrence of cross-flow components in turbulence is random (Fox and McDonald, 1973), and approximately equal over

time as defined by the equality (Davies, 1972):

$$\tilde{V}'_x = \tilde{V}'_y = \tilde{V}'_z \quad \text{where:} \quad \tilde{V}' \text{ represents the root mean square fluctuation velocity in the x, y, and z dimensions.}$$

This equality defines isotropic turbulence, in which there are numerous small eddies of random orientation, having no preferred direction of flow within their population, but which are all travelling as a turbulent envelope in a down-stream direction.

Since turbulence is a stochastic process, then like most stochastic processes, the frequency distribution of its fluctuations should approximate a Gaussian density function. This is supported by Cousteix, Desopper and Houdeville (1977) who find that, for turbulent flow in a boundary layer, fluctuations in the axial velocity component do indeed tend to a Gaussian distribution. It has also been shown from lab studies, that when a dye tracer is injected into a turbulent flow, the cross-flow or orthogonal dispersal of the tracer also approximates a Gaussian curve which is initially narrow and peaked, but becomes wider and flatter as distance increases downstream (Davies, 1972).

In a similar manner, the random intensity and duration of cross-flow components in an isotropic turbulent flow acting upon multi-year ice field B (Figure 32) would cause the dispersal of floes relative to the center of the field to approximate a Gaussian density. In this case, floes near the edge of the field would have a lower spatial concentration than those near the center. For field A however, the distribution of floes relative to the center of its X axis would hypothetically approximate a uniform density distribution which is box-shaped and has no tails, since there are no cross-flow components to act as a mechanism of dispersal.

If several uniform fields of multi-year ice exist, each located an equal, undefined distance upstream and in the zone of laminar flow, then by time t_4 each will ideally produce a discrete box-shaped curve which is separated from its neighbour by some undefined distance D. If, however, the fields are in the region of isotropic turbulent flow at time t_1, they will have each produced a Gaussian-shaped distribution by t_4. Due to the dispersal processes in turbulence, as the Gaussian curves become flatter and wider, the tails of adjacent curves will eventually meet and overlap. This produces a region having a more or less constant presence of multi-year floes within which there are peak and trough variations in magnitude.

Unfortunately, the concept of laminar and turbulent flow coexisting as ideally illustrated in Figure 32 does not properly explain the April 25 and May 01 distributions. On these days, the groups were all spatially discrete (see Figure 15a, p. 73 and Figure 18, p. 85), and the merging which is expected during isotropic turbulence is not apparent. A better explanation is that for these two dates the flow was completely laminar.

Figure 33 illustrates the horizontal velocity profile for a fully-developed laminar flow as described by Bober and Kenyon (1980). The change in velocity is less rapid close to the wall (i.e., the zone of contact between the current core and the shelf water) than for the turbulent case. In fact, it increases in an almost linear fashion, but the slope again becomes very gentle at a distance from the wall, roughly equal to 1/3 of the diameter. Reference to multi-year ice fields A and B in Figure
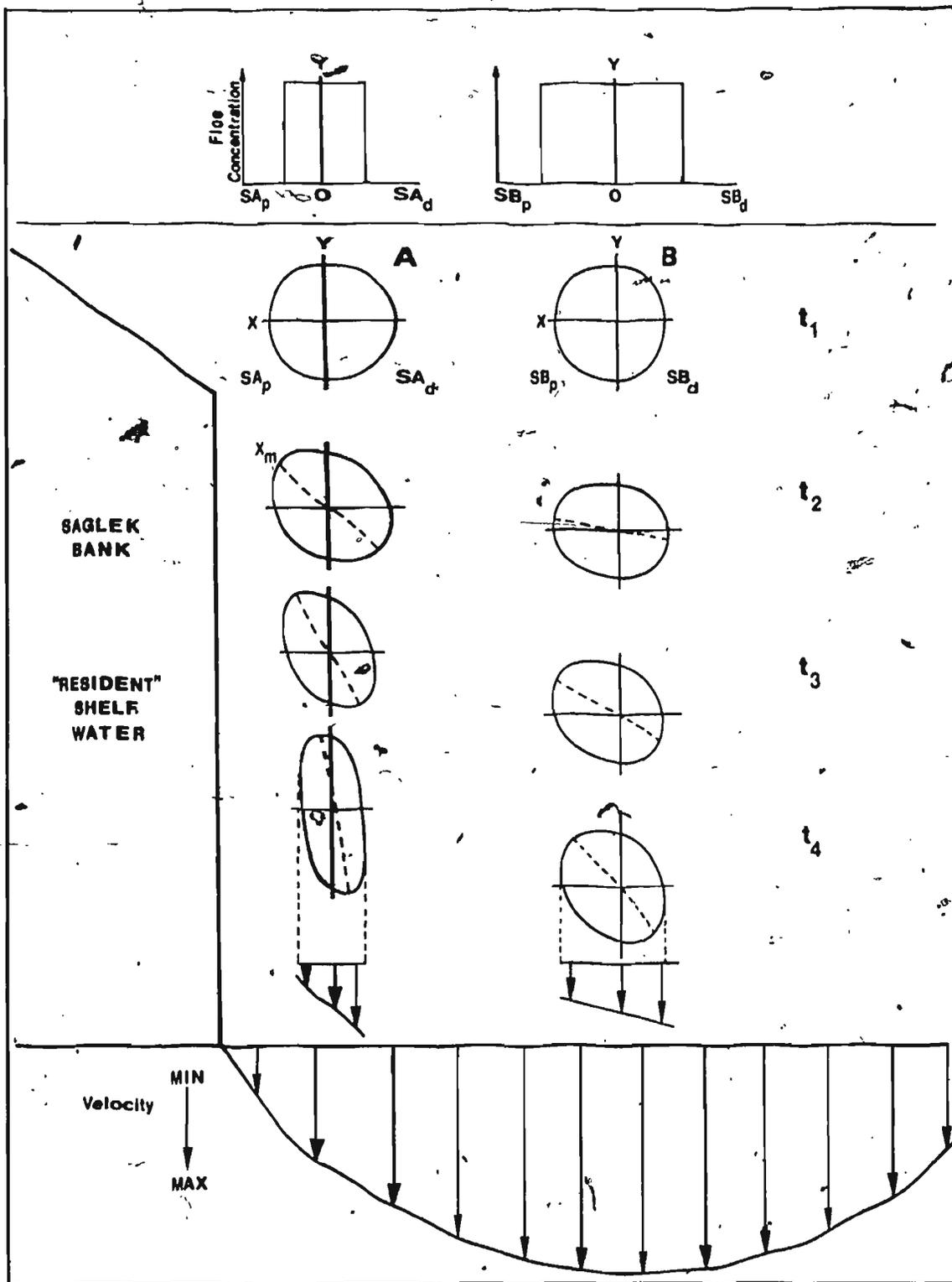
Figure 33 — Schematic representation of the deformation of two
initially uniform fields of multi-year floes located
in different regions of a current dominated by lami-
nar flow. Vectors at the bottom of the diagram
denote relative velocities. See text for explana-
tion.

33, shows that the difference in velocity between SA_p and SA_d would be greater than the differences between SB_p and SB_d. The outcome is that field A would be subject to a higher rate of shear deformation than field B, causing A to form a much narrower band than B. These differences would explain why the bands located in the landward half of the April 25 and May 01 distributions in Figure 18 (p. 85) are generally narrower than those to the seaward. However, for the seaward half of the May 12 distribution, the discrete banding phenomenon is less evident, as it is also for May 26, May 31, and most of the June 07 distribution. The indication, therefore, is that the laminar flow conditions of April 25 and May 01 became less dominant during subsequent days.

Referring again to the case of water flowing in a pipe, it is possible to have a flow condition which is in a state of transition between the totally laminar mode and the fully developed turbulent mode (Reynolds, 1974; Stuart, 1979). Under these conditions, periods of laminar flow are intermittently alternated with a period of fully-developed isotropic turbulence, referred to as a turbulent slug (Teitgen, 1979). The change between the two modes is quite abrupt; generally a frontal zone at the leading and trailing edges of the slug marks the change from laminar to turbulent and back to laminar once more as the turbulent section propagates downstream past a fixed point (Teitgen, 1979). The leading edge of the slug is bullet-shaped, while the trailing edge has a cavitation of the same shape. Any such turbulent flow will consist of a spectrum of eddy lengths,

with the largest eddy being approximately equal to the diameter
of the pipe (Davies, 1972). Interaction between large eddies
will generate intermediate eddies, which in turn generate small
eddies, hence developing a wide range of sizes. If it is
assumed that the Labrador Current was flowing in a similar state
of transition, with alternating modes of flow during the study
period, then it might be possible to schematically explain the
changes which were observed in the multi-year floe distribution
patterns during 1979.

8.3 Reconstruction of events during 1979 multi-year ice flux across Saglek 097° magnetic.

Figure 34 reconstructs the time series of events thought
to have occurred in the Labrador Current as extrapolated from
the distribution patterns of multi-year floes observed during
the 1979 study period. Study of the distribution patterns for
April 25 and May 01 from Figure 34 (also shown in Figure 30,
p.126) suggests that most of the flow within the current was
nominally laminar on these dates. Under these conditions,
individual fields of multi-year floes would have responded to
shear stresses as illustrated in Figure 33 (p.137). Therefore,
it is the decrease in differential shear across the horizontal
laminar velocity gradient which leads to wider bands of old
floes as distance increases seaward on these days. If the posi-
tion of the ice edge also coincides with the seaward margin of
the current core, where the cold core water makes contact with
the warmer water offshore, then according to Figure 33 (p.137);
one would also expect to find the occurrence of narrow bands
very close to the ice edge. This, however, does not occur for

139
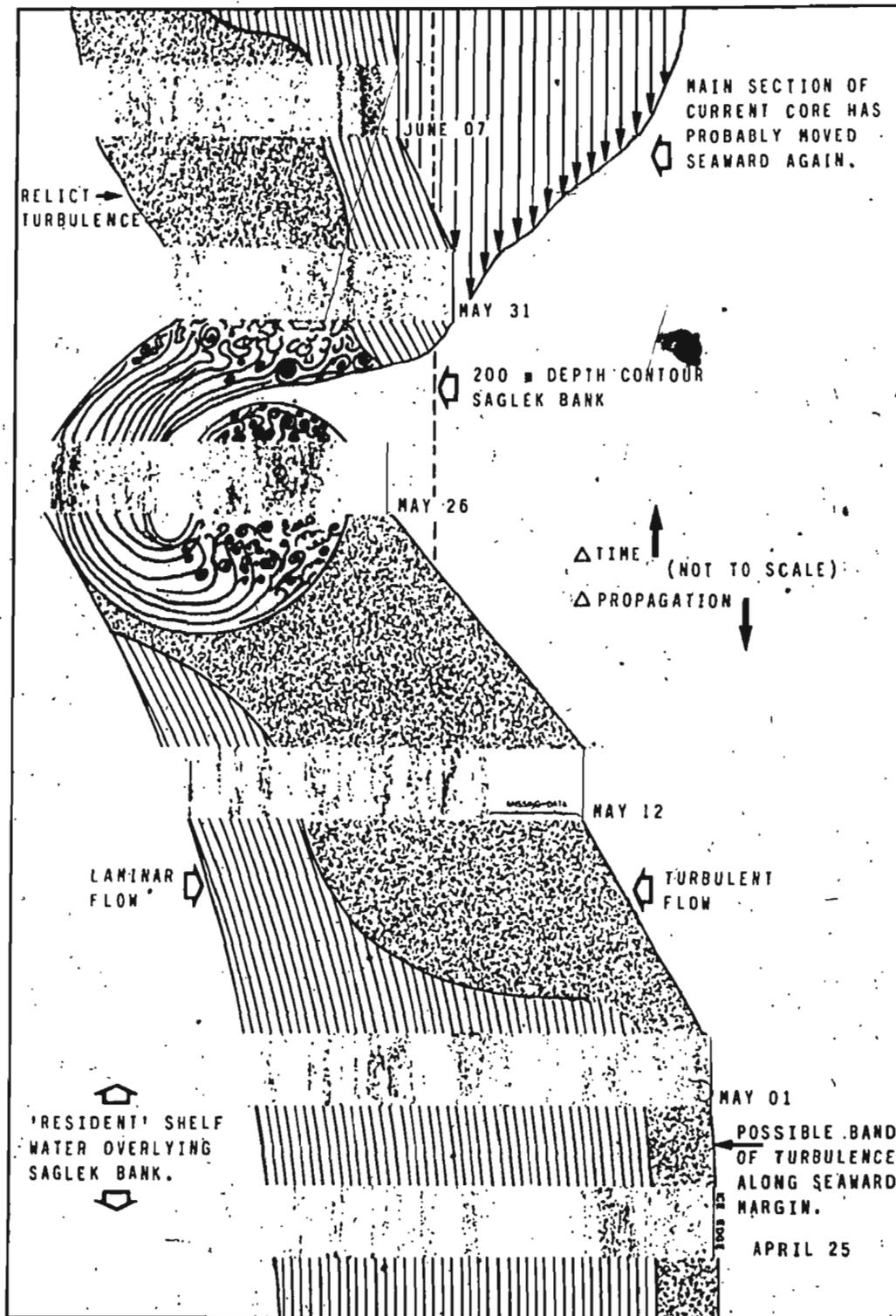
Figure 34 - Illustration of nominal oceanographic conditions
occurring during April 25 - June 07, 1979 as inferred
from the distribution patterns of multi-year floes.

April 25 and May 01. Reference to Figure 29 (p. 121) suggests
that there is usually a zone of turbulence near the seaward
margin of the core. It is possible that the existence of a
similar zone on April 25 and May 01 prevented the occurrence of
narrow bands of old floes along the seaward edge of the distribu-
tion. The effects of such a turbulent zone, plus swells and
waves from the open ocean, would have caused the dispersal of
any band of multi-year floes which passed through it.

The landward shift of the distributions after April 25 was
probably due to a wave structure (meander) propagating along the
thermal front. This would have caused the current to be deflec-
ted shoreward. Evidence for east-west variations in the current
near the seaward edge of Saglek Bank is shown in Figure 35
(after Seaconsult, 1977). Shown are paths taken by satellite-
tracked drogue buoys which were released on two separate
occasions during August and September, 1977. The diagram is a
composite plot of drift trajectories following the releases;
east-west meanders in the mean southward track are clearly
evident.

Because of the frontal meandering, the zone of turbulence
along the front would have been widened and forced landward as
the frontal zone meandered in this direction; for the pipe
scenario, the turbulent intrusion would be analogous to an iso-
tropically-turbulent slug. This would have occurred at a time
after May 01, so that the leading edge of the turbulence would
have begun to approach the study region as shown in Figure 34.

By May 12, the leading edge would have intruded into the
study region near the seaward margin, but had not yet extended
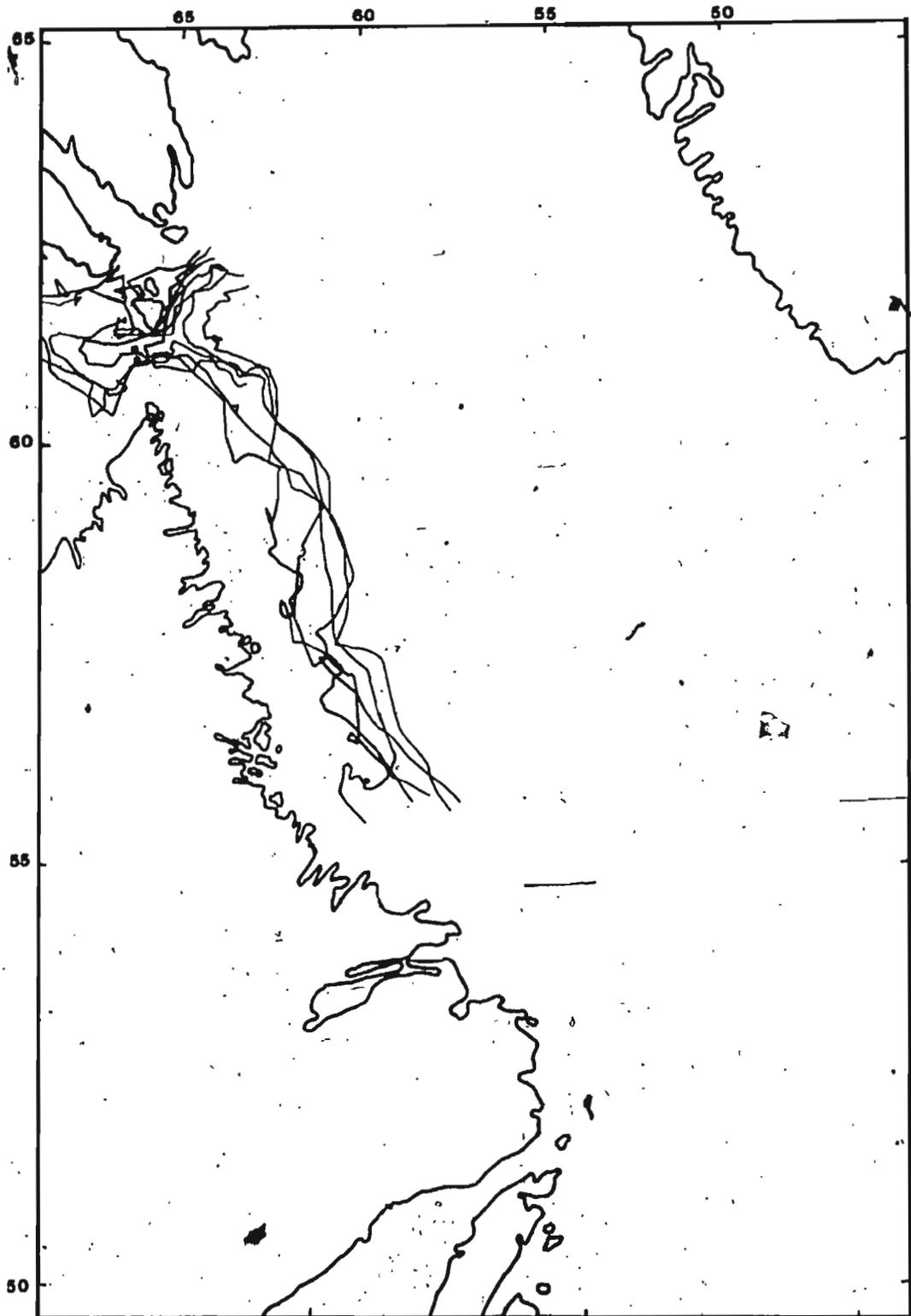
Figure 35 - Composite plot showing drift trajectories of buoys
released during August and September, 1977 by Sea-
consult Ltd. (Seaconsult, 1978).

142

sufficiently landward to incorporate the entire region of multi-year floe occurrence. As a result of this, Figure 34 shows a frontal zone passing through the May 12 distribution, probably located near 93 km offshore. Seaward of 93 km, turbulent flow conditions would exist; the random nature of cross-flow components would have caused each previously discrete group of floes to disperse in a pattern approximating the Gaussian density function which is characteristic of dispersal in isotropic turbulence. In the analogue sense, the outward spreading floes caused the tails of adjacent Gaussian curves to overlap so that the groups merged to form a zone of continuous coverage (with reference to the 90 km point, see Figure 30, p. 126). Within this zone, the formerly spatially discrete groups were now identified only by positive departures from the mean magnitude of floe concentration for May 12 (Figure 19, p. 91). Landward of 93 km, flow would remain nominally laminar. The absence of significant cross-flow components, and the presence of differential rates of shear across the laminar velocity gradient in this region, kept the groups separate and spatially discrete in the form of bands. The distinction between the laminar and turbulent flow regimes relative to the 93 km point for May 12 is better illustrated by reference to Figure 15a (p. 73) and Figure 18 (p. 85).

Because of the two week period intervening between the May 12 and May 26 flights, it is difficult to evaluate the actual sequence of events occurring between photo missions. Perhaps the turbulent section receded downstream, allowing laminar flow to return for a short period, before being interrupted by a second such zone just prior to May 26. Alternatively, the tur-

bulence might have persisted throughout the entire period.

Referring to Figure 33 (p.137), an interpretation of the floe distribution pattern for May 26 would suggest the presence of a large eddy encompassing most of the distribution. Since we know that a large spectrum of eddy sizes exists within a turbulent section, then the transition from numerous small eddies, which could have produced dispersal on May 12, to a large eddy on May 26 is not implausible.

The suspected configuration of this feature is represented by the eddy shown at arrow A in Figure 29 (p. 121). In this image we see a lobe of cold water extending northward along the edge of the thermal front; coupled with this is a finger of warm water which has penetrated southward into the cold water zone, and thus separates the cold northward lobe from the main cold water mass. Note that, due to the presence of the eddy as it is shown in Figure 29, a large portion of the cold water stream has been deflected shoreward over Saglek Bank in the region denoted by arrow A. By May 26, the multi-year ice distribution had achieved its farthest shoreward advance of the study period, and the distribution in its entirety lay to the landward of the 200 m isobath which is at 117 km offshore, along flight line 097.° mag. from Saglek. It is thought that this shoreward advance was due to a portion of the current having been deflected shoreward by the eddy as it folded over, in much the same manner as the eddy which appears in Figure 29 (p.121). Several of the authors cited in Section 8.1 indicate that water originating along the shelf break can be propagated onto a continental shelf into depths of less than 200 m due to the occur-

rence of an eddy. Furthermore, an ice-water vortex measuring

60 km in diameter, and similar in structure to the one suggested

here, was observed at the edge of the East Greenland MIZ by

Wadhams and Squire (1983). Reference to Figure 30 (p. 126) indi-

cates that the eddy suggested by the distribution of old floes

on May 26 is also on the order of 60 km in diameter.

Comparison of the May 26 distribution in Figure 30 (p. 126)

with the structure illustrated in Figure 29 (p.121) suggests

that the region of very low multi-year ice occurrence located at

between 60 and 70 km actually represents an intrusion of warm

water, perhaps from the north, similar to that which is shown in

Figure 29. Delivery of multi-year ice to this warm water zone

would probably not occur owing to the shoreward deflection of

the current caused by its intrusion.

Referring to Figure 15b (p. 74) for May 26, we see that the

shape of the barchart in the region seaward of this void zone

is in sharp contrast to all other distributions since there are

no sharp fluctuations along a series of narrow groups as is

usually the case. While two groups exist in this outer region,

the outermost is broad and low, suggesting the occurrence of a

dispersal process. Reference to the pattern of individual floes

in Figure 30 (p. 126) seems to confirm this interpretation. The

floes in the seaward portion of the distribution appear as non-

linear clusters which are relatively different from any pattern

observed either in the landward zone of May 26 or on any other

flight lines prior or subsequent to this date. The patten sug-

gests drift which is confused in relation to all other patterns

and does not suggest movement in any preferred direction.

Study of the portion of the May 26 distribution which is landward of 65 km (Figure 30, p. 126) suggests the presence of two sub-regions. Between 42 and 48 km, the floes are tightly banded, similar to patterns from previous flights. From 48 to 63 km, the floes appear somewhat dispersed; however, a close scrutiny of the pattern suggests that fine streamers of old floes might be extending across the flight line from top to bottom in this region also.

This can be explained when it is realized that the eddy considered for the May 26 distribution probably represents the maximum size which can occur in the spectrum - i.e., in this case it approximates the diameter of the conduit through which it passes, as defined in Davies (1972). For isotropic turbulence, such as on May 12, the flow within each small eddy is in a preferred, spiralling direction. Only when the vector velocity components of the numerous tiny eddies in the turbulent envelope are averaged over time does the flow become truly isotropic. Therefore, since we are dealing with what appears to be a single large eddy for May 26, the flow is actually anisotropic. In this case, the flow of water in the eddy is southward for regions landward of approximately the 65 km point, and nominally northward for regions to the seaward (see Figure 34, p.140).

The banding phenomenon observed in the landward zone (i.e. 40-63 km) probably represents an elongation of fields of old floes due to differential shear induced across a horizontal velocity gradient. The gradient might be caused by contact between the faster-moving core water and the slower shelf water.

146

Given that the most intense banding is found at the innermost edge of the multi-year floe distribution, then this is actually where it would be expected to occur if the zone of contact between the core and the shelf water was located here also. The dynamics of shear would then be as illustrated in Figure 33 (p.137); the less-concentrated banding between 50 and 63 km would be due to a decrease in diffential shear as a function of flattening in the slope of the velocity gradient.

The dispersal process observed in the zone seaward (70-100 km) of the warm water intrusion is probably due to some of the water in the main, southward-flowing core (at 40-63 km) having been recurved into the northward-extending lobe of cold water. Due to a decrease in velocity and less shear, movement of water in such a lobe would be different from the main core and more variable, leading to a scattering of floes.

Further evidence for a warm water intrusion is also found in the relatively strong positive correlation between increasing average floe diameter and distance from the ice edge for May 26, as described in Chapter 4. The northward extension of a cold lobe in the manner described would result in this cold water being effectively located within a region of ambient warm water. If interchange occurred between these water masses along their zones of contact, then melt rates in the outer region would have been accelerated due to increasing temperatures within the lobe. This would produce smaller floe sizes than would occur in the innermost region of cold water, a pattern which is consistent with the spatial distribution and correlation of average floe sizes observed for May 26 (Figure 14, p. 66). The occurrence of

a zone of younger ice between the multi-year distribution and the ice edge for this date is probably due to this area having been farthest from the main zone of delivery on the shoreward side of the warm water intrusion; because of the high variability of current in the lobe, floes which depart from the main zone (at 40-63 km) are not advected all the way to the ice edge. First-year ice thus predominates here because its occurrence does not depend upon advection by current and therefore could have formed in situ. Similarly, the absence or occurrence of younger ice types in the suspected warm water zone is likewise not important since such ice could still exist over a region of warm water. This would be similar to examples of sea ice known to overlie parcels of warm water in the Greenland MIZ (Wadhams, Gill, and Linden, 1979).

For May 31 the total number of floes (872) is less than half of the total count for May 26 (1957). If an eddy had existed during the time surrounding May 26, it would have tended to collect any transient multi-year ice within its vortex, thereby preventing it from continuing southward, and hence leading to an overall increase in floe concentration in the study area. A strong eddy existing in the thermocline will tend to retain its internal water mass, albeit with some entrainment and mixing (Robinson, 1983). Because of this, as the eddy moved southward after May 26, those floes lying within its perimeter would have been transported out of the study area, causing the subsequent drop in frequency which is observed on May 31.

Study of the May 31 distribution pattern (Figure 30, p. 126) reveals the floes to be scattered, with no pronounced banding apparent. A possible reason is that most of the multi-year floes now lie over Saglek Bank where current flow is known to be variable (Fissel and Lemon, 1982). However, the existence of two faint bands at 102 and 110 km indicates that banded flux is beginning to re-occur. The seaward deflection of the ice edge for May 31 might represent the passage of another meander along the thermal front, or it might possibly be coupled with the offshore wind which existed at this time (Figure 24, p. 101).

The distribution for June 07 is still strongly scattered, with low magnitude concentrations for about 80% of the region covered by old floes. Again, this is probably due to their location within the variable current regime over the Bank where remnants of isotropic turbulence have not yet been attenuated. However, at 98 and 102 km, the recovery of banded flux which was hinted at in the May 31 pattern is now obvious and indicates a return to laminar flow in this region as illustrated in Figure 34 (p.140). The juxtaposition of these two bands is very similar to the two weaker bands observed on May 31 and suggests that flux of old floes through this region might have been constant since that date; however, actual floe concentrations have increased. An interesting observation is that evidence of a return to laminar flow has appeared first at the extreme seaward edge of the distribution, which is closest to the edge of Saglek Bank. This is where a return to the original flux pattern should initially occur since it is closest to the current core which runs southward along the shelf break. Given that an eddy

on May 26 forced some cold-core water onto Saglek Bank inside of the 200 m isobath, then it is likely that as the eddy moved southward, a trail of isotropic turbulence would have occurred behind it, accounting for the dispersed pattern of most of the floes in the May 31 and June 07 distributions. However, after the occurrence of the May 26 eddy, the current core probably moved seaward and stabilized once more at the edge of the Bank. Since velocities are higher closer to the current core, then the frontal zone which marks the change from the turbulent back to the laminar mode of flow would have passed across the flight line near the seaward edge first, allowing laminar flow to return first near the ice edge as illustrated in Figure 34. In short, return to a banded flux of old floes has occurred approximately where one would expect it, based upon the position of the current core relative to the edge of Saglek Bank as it is shown in Figure 28 (p. 117), and Figure 29 (p. 121).

An interesting feature of the overall pattern of multi-year ice occurrences for 1979 is the landward edge of the distribution. This is seen on all flight lines (Figure 30, p. 126) as an abrupt zone where coverage by concentrations consisting entirely of first-year ice ends and coverage containing a portion of multi-year ice beings. This lends good support to the idea that the multi-year floes are drifting southward under the influence of the cold core of the Labrador Current. Reference to Figure 29 (p. 121) indicates that the separation between the water of the cold core and the relatively warmer water of the shelf is very distinct near Saglek. If one accepts that multi-year floes are being transported southward within the cold core

150

of the Labrador Current then it seems likely that the landward

point at which the presence of multi-year ice ends would also.

mark the landward limit of the flow regime dominated by waters

of this cold core.

The implications for the occurrence of multi-year ice are

now clear. The cold section of the current which delivers old

ice to the Labrador Coast generally stays well offshore in the

Saglek Bank region. Therefore, the occurrence of multi-year ice

in the nearshore area of the Bank is not normally expected,

owing to the presence of a different and variable flow regime,

which does not have its origin in a multi-year ice source

region. This is supported by Figure 35 (p. 1+2); in all cases,

the paths followed by the drifting drogue buoys lay well off-

shore along the northern Labrador coast and did not penetrate

close to land. Variability in the east-west location of the

multi-year ice distribution however, can occur when the current

is deflected shoreward by a meander or eddy structure in the

thermal front which separates the cold core from the warmer

water to seaward.

Reference to Figure 29 (p. 121) suggests that, near Saglek,

the cold current stays well offshore due to the topographic

influence of Saglek Bank. Farther south, the cold portion of

the current spreads out and moves much closer to land; it is pos-

sible therefore that south of Saglek Bank, the multi-year floes

might also behave in a similar manner.

The sequence of events and interaction of controlling fac-

tors as described in this section and illustrated in Figure 34

(p.140) regarding the 1979 multi-year ice distribution are

surely nominal. It is felt, however, that the events and
mechanisms discussed are, in principle, reflected in the actual
distributions observed during 1979. Discrepancies between con-
ditions actually observed and those hypothesized can be quali-
fied by realizing that other, undefined, environmental factors
(e.g. tidal influences) might also have affected the distribu-
tion of multi-year floes during the study period. The oceano-
graphic environment and current regime of the seaward edge of
the Labrador Shelf are intricate and not capable of full explana-
tion using simple models. However, it is often the utilization
of an analogue context which provides the key to understanding
the complexities of macro-scale stochastic phenomena.

8.4 Floe size variations and oceanographic influences during 1979

Analysis of multi-year floe diameters in Chapter 4 indi-
cated that the expected floe sizes for a given probability level
of occurrence experienced a greater rate of decrease at the
higher probability levels than at the lower. With reference to
Table 2 (p. 55), the 90th percentile multi-year floe size for
April 25 was 78 m, while for June 07 the 90th percentile size
was 68 m. Simply stated, this means that on April 25, 90% of
the multi-year floes were less than or equal to 78 m, while on
June 07 90% were less than or equal to 68 m. For the 10th per-
centile on April 25, 10% of the multi-year floes were less than
or equal to 30 m, while on June 07 10% were less than or equal
to 28 m.

The indication is that as the season progressed and tempera-
tures increased, the multi-year floes weakened and were now

152

more susceptible to being broken into smaller pieces. However it is apparent that the large floes (i.e. those above the 50th percentile) were disappearing at a faster rate than the smaller ones (below the 50th percentile); Figure 10d (p. 54) reaffirms this possibility. This suggests a two-stage process of deterioration for multi-year floes in a marginal ice zone. Large floes are initially broken into smaller pieces by mechanical processes involving the tensile stresses produced by flexure (Weeks and Assur, 1967; Goodman, 1978), especially if cracks are already present (Parmerter, 1975). However, the probability for fracture from these processes becomes increasingly less as a lower size limit is approached, below which floe flexure is not sufficient for inducing the necessary fracture stress. This would account for the floe size frequency distribution being skewed to the left of the mean (Figure 10a, p. 54), with the majority of old floes being smaller than the average, yet greater than a certain lowest 1% size limit of approximately 20 m in diameter (Table 2, p. 55). Beyond the lower size limit for flexure-induced fracturing, the dominant deterioration process is thermodynamic and depends upon the ambient water and air temperatures as well as the degree of pack-ice compactness. This would control the rate of lateral melt which generally occurs along the floe edge in the upper 1-2 m layer of warmer water, as well as the degree of wave-induced melt caused by oscillating shear currents at the ice/water interface, as described by Wadhams (1981).

In open water, an individual floe would deteriorate quite rapidly, however in a marginal ice zone where lower temperatures

153

are perpetuated by the presence of other ice floes (especially during conditions of pack-ice compression), deterioration by melt processes would be slow. Therefore, for multi-year floes in pack ice, the net difference between the number of 20-30 m multi-year floes created by mechanical fracture and the number destroyed by melt processes is large, and produces the skewed floe size frequency distributions observed in the 1979 data.

When compared to the Arctic, at a given level of probability for floe size occurrences, Labrador Sea multi-year floe diameters were much lower. During 1979, the floe size expected at the 50% probability level of occurrence for the entire sample was 46 m; in contrast to this, Wheeler (1981) predicts a 152 m diameter at the 50% level for Arctic regions. Additionally, the maximum measured diameter of 147 m for Labrador during 1979 is much lower than the size for large multi-year floes in the east Greenland MIZ where Wadhams (1980) indicates that larger diameters sometimes exceed 400 m; maximum diameters near 3000 m have been measured in the Arctic (Wheeler, 1981). This overall smaller size found in Labrador Sea multi-year ice is due to floe fracture occurring during transport both from the Arctic source region as well as within the dynamic environment of the marginal ice zone.

CHAPTER 9

CONCLUSIONS

Multi-year ice distributions, recorded from air photographs
taken during six overflights of the Labrador Sea marginal ice
zone, during the ice season of 1979, have been analyzed for the
region of the pack overlying Saglek Bank. The average floe size
diameter for the season was 48.5 m with the diameter expected
at the 50th percentile probability level of occurrence being
46 m. Floe diameters on the whole are much smaller than those
of multi-year floes found in the Arctic; this is due to frac-
turing during transport. Study of trends in the floe size occur-
rences suggests that larger floes are broken into smaller pieces
by fracturing which does not occur below a certain size; beyond
this size limit, floe deterioration is mainly the result of melt
processes.

Statistical analysis shows that, within the pack, these
floes have a significant tendency to occur in groups which have
high concentrations, with voids of few or zero multi-year floe
occurrences intervening; this is in contrast with younger sea
ice types which are approximately homogenously distributed. These
groups appeared as bands, crossing the photographs from top to
bottom; relative to True North, the bands occurred with an
approximate NW/SE orientation.

An application of the general principles of fluid dynamics
shows that such bands can be produced when an hypothetically cir-
cular field of multi-year floes undergoes deformation due to
shear stresses. When these stresses are applied differentially

155

across a horizontal velocity gradient in a current dominated by laminar flow, the field of floes experiences progressive elongation. This is due to differences in velocity across the axis which is orthogonal to the direction of flow.

Interpretation of the distribution patterns of old floes from flight to flight suggests that periods of laminar flow occurred within the Labrador Current; it also appears that these periods were interrupted by conditions of turbulent flow. The turbulence altered the floe distribution patterns associated with laminar flow by destroying the banding effect. The most severe disturbance of pattern is thought to have been due to a large eddy in the thermal front which separates the cold current core from warmer water offshore. This eddy might have propagated cold-core water onto the continental shelf inside the 200 m isobath.

The mean center of the multi-year floe distribution also varied from date to date. Fluctuations in its position are thought to have been partially due to the propagation of meanders along the thermal front; an eddy which existed on May 26 also contributed. While evidence can be found to support the occurrence of meanders and eddies in the Labrador Current, their intensity and potential for propagation onto the Shelf are unknown. Comparison with other regions of the world, such as the Gulf Stream, indicates that frontal wave and eddy propagation into depths less than 200 m does occur and is therefore highly likely for the Labrador Shelf.

The continual east-west shifting of floe groups in response to these influences resulted in a core region which had a constant delivery, and hence a high concentration of total flux values for the season, while areas to either side experienced lower and sporadic degrees of flux. This central region showed a statistically significant clustering of old floes when the sampled values for the season were totalled and tested. This is because it represented a zone of coverage common to all of the observed multi-year floe distributions, regardless of their spatial fluctuations. Regions to either side were more sensitive to the fluctuations and therefore received overall less ice as multi-year floe groups temporally changed position, moving variably east-west, into and out of these zones. A summation of season flux values revealed three main zones of multi-year ice occurrence for the 1979 season:

(i)   Regions between approximately 40 km and 80 km offshore which experienced initial occurrences approximately midway through the season, near May 12, and which had continued flux thereafter.

(ii)   Regions between 80 and 120 km which experienced varying degrees of flux throughout the study period after a time prior to April 25.

(iii) Regions beyond 120 km which experienced flux early in the season, prior to April 25, but none after May 12 as the ice edge moved landward of this area.

While no photographic coverage exists for areas landward of 40 km offshore it is thought that multi-year ice might not usually occur here. Study of the inner edge of the multi-year floe distribution for the sampled dates strongly suggests that it did not move shoreward of this point. This is probably due to the nature of currents delivering multi-year ice to the

157

Labrador Sea, which tend to remain offshore near the edge of the continental shelf. Exceptions to this might be expected when perturbations along the frontal zone cause shoreward deflection of the transporting currents.

Although many of the conclusions presented here are original in their suggestion and verification, an interpretation of the patterns observed in the distribution of multi-year floes strongly supports them. Clearly, more detailed oceanographic surveys are needed, preferably during the ice season, before relationships between the occurrence of multi-year ice (and possibly younger ice types in general) and the movement, as well as distribution, of currents in the Labrador offshore is understood.

REFERENCES

Allen, A.A., and Huntley, D.A., 1977. "Currents at the Offshore Edge of the Labrador Current". In: POAC '77, _Proceedings of the Fourth International Conference on Port and Ocean Engineering Under Arctic Conditions_, September 26-30, Memorial University of Newfoundland, St. John's, Nfld., (Vol. II). Edited by D.B. Muggeridge; p. 927-937.

Allen, A.A., 1979. "Current Variability at the Offshore Edge of the Labrador Current". Thesis submitted in partial fulfillment of the requirements for the degree of Master of Science, Dalhousie University, December 1979.

Allen, A.A., 1980. "Observations of Topographic Rossby Waves in the Labrador Current." _EOS Transactions_, Vol. 61, No. 17 (April 22), p. 252.

Anderson, H.S., 1968. "The Labrador Current Between Hamilton Inlet and the Strait of Belle Isle". U.S. Coast Guard Oceanographic Report No. 41 (CG. 373-41) (July). United States Coast Guard Oceanographic Unit, Washington, D.C.

Avery, T.E., 1977. _Interpretation of Aerial Photographs_. (Minneapolis: Burgess Publishing Company).

Bauer, B.J. and Martin, S., 1980. "Field Observations of the Bering Sea Ice Edge Properties During March 1979". _Monthly Weather Review_, Vol. 108, No. 12 (Dec.), p. 2045-2056.

Bailey, W.B. and Hachey, H.B., 1950, "The Vertical Temperature Structure of the Labrador Current". _Proc. Nova Scotia Institute of Science_, Vol. 22, Pt. 4, p. 34-48.

Bane Jr. J.M.; and Brooks, D.A., 1979. "Gulf Stream Meanders Along the Continental Margin From the Florida Straits to Cape Hatteras". _Geophysical Research Letters_, Vol. 6, No. 4 (April), p. 280-282.

Bennington, K.O., 1967. "Desalination Features in Natural Sea Ice". _Journal of Glaciology_, Vol. 6, No. 48, p. 845-857.

Bobbitt, J., 1983. "The Implications of the Physical Environment Offshore Labrador on Arctic Tanker Traffic". Presentation to Beaufort Sea Environmental Assessment Panel, for Labrador Inuit Association (October).

Bober, W. and Kenyon, R.A., 1980. _Fluid Mechanics_. (New York: John Wiley & Sons, Inc.)

Bradford, D., 1973. "Newfoundland Coastal Transportation Study, Vol. 5, Survey of Environmental Conditions Affecting Navigation in the Newfoundland-Labrador Coastal Area". Transport Canada, Canadian Surface Transport Administration, Ottawa.

Brooks, D.A. and Bane Jr., J.M., 1978. "Gulf Stream Deflection by a Bottom Feature Off Charleston, South Carolina". Science, Vol. 201, No. 29 (September), p. 1225-1226.

Bursey, J.O., et al., 1977. "The Climate of the Labrador Sea". In: POAC '77, Proceedings of the Fourth International Conference on Port and Ocean Engineering Under Arctic Conditions, September 26-30, Memorial University of Newfoundland, St. John's, Nfld., (Vol. II). Edited by D.B. Muggeridge; p. 938-951.

Butt, K.A., Gamberg, D.B., and Rossiter, J.R., 1979. "Remote Estimation of the Properties of Sea Ice, Impulse Radar Study of Lake Melville, Labrador". C-CORE Data Report 79-7, August, 1979.

Campbell, N.J., 1958. "The Oceanography of Hudson Strait". Fisheries Research Board of Canada, Manuscript Report Series (Oceanographic and Limnological), No. 12, Atlantic Oceanographic Group, March 31.

Cousteix, J.; Desopper, A.; Houdeville, R., 1977. "Structure and Development of a Turbulent Boundary Layer in an Oscillatory External Flow". In: International Symposium on Turbulent Shear Flows, 1st., Pennsylvania State University, April 18-20, edited by F. Durst, et al., p. 154-171.

Crane, R.G., 1978. "Seasonal Variations of Sea Ice Extent in the Davis Strait — Labrador Sea Area and Relationship with Synoptic Scale Atmospheric Circulation". Arctic, Vol. 31, No. 4 (Dec.), p. 434-447.

Crarey, A.P., 1960. "Arctic Ice Island and Ice Shelf Studies, Part II". Arctic, Vol. 13, No. 1 (March), p. 32-50.

Culshaw, S.T., 1977. "An Examination of Marine Transport in the Ice-Season Off the Labrador and North Newfoundland Coasts". In: POAC '77, Proceedings of the Fourth International Conference on Port and Ocean Engineering Under Arctic Conditions, September 26-30, Memorial University of Newfoundland, St. John's, Nfld., (Vol. I). Edited by D.B. Muggeridge; p. 425-439.

Davies, J.T., 1972. Turbulence Phenomena. (New York: Academic Press, Inc.)

Dinsmore, R.P., 1972. "Ice and its Drift into the North Atlantic Ocean". In: Symposium Proceedings on Environmental Conditions in N.W. Atlantic 1960-1969. International Committee for N.W. Atlantic Fisheries (ICNAF), Special Publication No. 8, Dartmouth, N.S., p. 89-127.

Duckworth, R.A., 1977. Mechanics of Fluids. Introductory Engineering Series, under editorship of G. Webster. (London: Longman Group, Ltd.).

Dunbar, M., 1973a. "Ice Regime and Ice Transport in Nares Strait". Arctic, Vol. 26, No. 4 (December), p. 282-291.

Dunbar, M., 1973b. "Winter Regime of the North Water." Transactions of the Royal Society of Canada, Series IV, Vol. XI, p. 275-281.

Dunbar, M., 1978. "Interpretation of Ice Imagery From Original and Modified Versions of a Real-Aperture SLAR". Defense Research Establishment Ottawa, Research and Development Branch, Department of National Defense, Canada, DREO Report No. 770, Project No. 97-67-05 (Special Assignments Unit, February, 1978).

Ebdon, D., 1977. Statistics in Geography, A Practical Approach. (Oxford: Basil Blackwell, Publisher).

Evans, R.J. and Untersteiner, N., 1971. "Thermal Cracks in Floating Ice Sheets". Journal of Geophysical Research, Vol. 76, No. 3 (January 20), p. 694-703.

Evans, R.J., 1971. "Cracks in Perennial Sea Ice Due to Thermally Induced Stress". Journal of Geophysical Research, Vol. 76, No. 33 (November 20), p. 8153-8155.

Fenco Ltd., 1975. "Spring Field Ice Survey, Offshore Labrador". Report submitted to Total Eastcan Exploration Ltd., by Fenco Consultants Ltd. (July).

Fenco Ltd., 1976. "1976 Winter Field Ice Survey, Offshore Labrador". Report submitted to Total Eastcan Exploration Ltd.; by Fenco Consultants and Innovative Ventures Ltd.

Fenco Ltd., 1978. "Multi-year Ice Floe Population Offshore Labrador, 1978", cited in Fenco (1979), "Multi-year Floe Population, Offshore Labrador, 1979". Report submitted to Total Eastcan Exploration Ltd., Calgary, Alta., by Fenco (Nfld.) Ltd.

Fenco Ltd., 1979a. "Multi-year Floe Population, Offshore Labrador, 1979". Report submitted to Total Eastcan Exploration Ltd., Calgary, Alta., by Fenco (Nfld.) Ltd.

Fenco Ltd., 1979b. "1978-79 Freeze-Up Study Offshore Labrador". Report to Total Eastcan Exploration Ltd., Calgary, Alta., by Fenco, Consultants Ltd.

Fissel, D.B. and Lemon, D.D., 1982. "Analysis of Physical Oceanographic Data From the Labrador Shelf, Summer, 1980". Report prepared by Arctic Sciences Limited for the OLABS (Offshore Labrador Biological Studies) Program, Vols. I and II.

161

Flagg, C.; and Beardsley, R.C., 1978. "On the Stability of the Shelf Water/Slope Water Front South of New England". Journal of Geophysical Research, Vol. 83, No. C9 (September 20), p. 4623-4631.

Fox, R.W. and McDonald, A.T., 1973. Introduction to Fluid Mechanics. (New York: John Wiley and Sons, Inc.)

Goodman, D.J., 1978. "Fracture Toughness of Ice: A Preliminary Account of Some New Experiments". Journal of Glaciology, Vol. 21, No. 85, p. 651-660.

Goodman, D.J.; Wadhams, P.; and Squire, V., 1980. "The Flexural Response of a Tabular Ice Island to Ocean Swell". In: Annals of Glaciology I, 1980. Conference on the Use of Icebergs, Cambridge, 1-3 April, 1980. International Glaciological Society, p. 23-27.

Gustajtis, A., and Buckley, T.J., 1977. "A Seasonal Iceberg Density Distribution Along the Labrador Coast". In: POAC '77, Proceedings of the Fourth International Conference on Port and Ocean Engineering Under Arctic Conditions, September 26-30, Memorial University of Newfoundland, St. John's, Nfld., (Vol. II). Edited by D.B. Muggeridge; p. 972-983.

Gustajtis, K.A., 1977. "Iceberg Hazard". In: Oil Spill Scenario for the Labrador Sea. Edited by B.R. LeDrew and K.A. Gustajtis. Economic and Technical Review Report EPS 3-EC-79-4, Environmental Impact Control Directorate, November 1979, p. 221-238.

Halliwell, G.R. and Moores, C.N.K., 1979. "The Space-Time Structure and Variability of the Shelf Water - Slope Water and Gulf Stream Surface Temperature Fronts and Associated Warm-Core Eddies". Journal of Geophysical Research, Vol. 84, No. C12 (December 20), p. 7707-7725.

Hammond, R. and McCullagh, P.S., 1978. "Quantitative Techniques in Geography, An Introduction". (Oxford: Clarendon Press).

Hanson, R.J., 1961. "The Albedo of Sea-Ice and Ice Islands in the Arctic Ocean Basin". Arctic, Vol. 14, No. 3 (September), p. 188-196.

Hibler, W.D. III, et al., 1972. "Top and Bottom Roughness of a Multi-year Ice Floe". In: I.A.H.R. International Symposium on Ice and its Action on Hydraulic Structures, 2nd., Leningrad, U.S.S.R., 26-29 September, 1972, p. 130-142.

Holden, B.J., 1974. "Some Observations on the Labrador Current at Saglek, Labrador". A project submitted to the Committee on Graduate Studies in Partial Fulfillment of the Requirements for the Degree of Master of Engineering, Memorial University of Newfoundland, St. John's, Nfld.

Huthnance, J.M., 1981. "Waves and Currents Near the Continental Shelf Edge". Progress in Oceanography, Vol. 10, p. 193-226.

Imperial Oil Ltd., 1977. "Report on Ice and Meteorological Observations in the Davis Strait During April, May, and June 1977". Arctic Petroleum Operators Association (APOA) Project Report 138-13.

Iselin, C.O., 1927. "A Study of the Northern Part of the Labrador Current". Transactions of the American Geophysical Union, Eighth Annual Meeting, April 28 and 29, 1927, Washington D.C. Bulletin of the National Research Council, No. 61, July 1927, p. 217-222.

Johannessen, O.M., et al., 1983. "Oceanographic Conditions in the Marginal Ice Zone North of Svalbard in Early Fall 1979 with an Emphasis on Mesoscale Processes". Journal of Geophysical Research, Vol. 88, No. C5 (March 30), p. 2755-2769.

Jordon, F. and Neu, H.J.A., 1982. "Ice Drift in Southern Baffin Bay and Davis Strait". Atmosphere-Ocean, 20 (3), p. 268-275.

Kollmeyer, R.C.; McGill, D.A.; and Corwin, N., 1967. "Oceanography of the Labrador Sea in the Vicinity of Hudson Strait in 1965". U.S. Coast Guard Oceanographic Report No. 12 (CG. 373-12) (March). United States Coast Guard Oceanographic Unit, Washington, D.C.

Kovacs, A. et al., 1973. "Structure of a Multi-year Pressure Ridge". Arctic, Vol. 26, No. 1, p. 22-31.

Kovacs, A. and Sodhi, D.S., 1980. "Shore Ice Pile up and Ride up: Field Observations, Models, Theoretical Analysis". Cold Regions Science and Technology, 2 (1980), p. 209-288.

Lazier, S.S. and Metge, M., 1972. "Observations on Thermal Cracks in Lake Ice". In: I.A.H.R. International Symposium on Ice and its Action on Hydraulic Structures, 2nd., Leningrad, U.S.S.R., 26-29 September, 1972, p. 99-104.

Lazier, J.R.N., 1979. "Recent Oceanographic Observations in the Labrador Current". In: Proceedings of Symposium on Research in the Labrador Coastal and Offshore Region. May 8-10, 1979, Memorial University of Newfoundland, p. 195-204.

Lazier, J.R.N., 1982. "Seasonal Variability of Temperature and Salinity in the Labrador Current". Journal of Marine Research, Vol. 40, Supplement, p. 341-357.

LeBlond, P.H., et al., 1981. "Surface Circulation in the Western Labrador Sea". Deep Sea Research, Vol. 28A, No. 7 (July), p. 683-693.

LeBlond, P.H., 1982. "Satellite Observations of Labrador Current Undulations". <u>Atmosphere-Ocean</u>, Vol. 20, No. 2 (June), P. 129-142.

Lee, T.N., 1975. "Florida Current Spin-off Eddies". <u>Deep Sea Research</u>, Vol. 22, No. 11 (November), p. 753-765.

Lee, T.N. and Mayer, D.A., 1977. "Low-Frequency Current Variability and Spin-off Eddies Along the Shelf off Southeast Florida". <u>Journal of Marine Research</u>, Vol. 35, No. 1 (February), p. 193-220.

Legeckis, R., 1975. "Application of Synchronous Meteorological Satellite Data to the Study of Time Dependent Sea Surface Temperature Changes Along the Boundary of the Gulf Stream". <u>Geophysical Research Letters</u>, Vol. 2, No. 10 (October), p. 435-438.

Legeckis, R., 1978. "A Survey of Worldwide Sea Surface Temperature Fronts Detected by Environmental Satellites". <u>Journal of Geophysical Research</u>, Vol. 83, No. C9 (Sept. 20), p. 4501-4522.

Legeckis, R., 1979. "Satellite Observations of the Influence of Bottom Topography on the Seaward Deflection of the Gulf Stream Off Charleston, South Carolina". <u>Journal of Physical Oceanography</u>, Vol. 9, No. 3 (May), p. 483-497.

Lepparanta, M., and Hibler, W.D. III, 1984. "A Mechanism for Floe Clustering in the Marginal Ice Zone", In: <u>Modelling the Marginal Ice Zone</u>, MISEX Bulletin No. 3, April; W.D. Hibler III, ed. U.S. Army Cold Regions Research and Engineering Laboratory, Hanover, New Hampshire, U.S.A. CRREL Special Report 84-7, p. 73-76.

Lister, H., 1962. "Heat and Mass Balance at the Surface of the Ward Hunt Ice Shelf, 1960". Terrestrial Sciences Laboratory, Geophysics Research Directorate, Air Force Cambridge Research Laboratories, Office of Aerospace Research, U.S. Airforce, Bedford, Massachusetts. AFCRL-62-219 Research Paper #19.

MANICE, 1980. <u>Manual of Standard Procedures and Practices for Observing and Reporting Sea Ice Conditions</u>. Manual of Sea Ice Reporting, 5th Edition. Environment Canada, Atmospheric Environment Service, Toronto, Canada (January).

Markham, W.E., 1980a. "Ice Conditions on the Labrador Coast". In: <u>Labrador Ice Dynamics Experiment. LIDEX Workshop Report</u>, March 6-8, St. John's, Nfld. (Memorial University of Newfoundland, NICOS), p. 63-66.

Markham, W.E., 1980b. "Ice Atlas Eastern Canadian Seaboard". Environment Canada, Atmospheric Environment Service, Toronto, 1980. Ministry of Supply and Services.

Markham, W.E., 1981. "Ice Atlas Canadian Arctic Waterways".
Environment Canada, Atmospheric Environment Service, Ministry
of Supply and Services, Canada. Canadian Government Publishing
Center.

Marschall, E., 1977. "Free Convection Melting of Glacial Ice in
Saline Water". Letters in Heat and Mass Transfer, Vol. 4, p.
381-384.

Martin, S., 1981. "Frazil Ice in Rivers and Oceans". Ann. Rev.
Fluid. Mech., 13, p. 379-97.

Martin, S. and Kauffman, P., 1981. "A Field and Laboratory Study
of Wave Damping by Grease Ice". Journal of Glaciology, Vol.
27, No. 96, p. 283-313.

Masterson, D.M. and Wright, B.D., 1982. "Pack Ice in the Labrador
Sea". In: Proceedings of Workshop on Sea Ice Ridging and Pile-
Up, 22-24 October 1980, Calgary, Alberta. Edited by R. Freder-
king and G.R. Pilkington. NRC Associate Committee on Geotechni-
cal Research, Tech. Memo. 134, (January 1982), p. 85-95.

Matthews, J.B., 1976. "Oceanography of the Labrador Coast - A
Review". Unpublished report, Bedford Institute of Oceanography,
19p.

McCullagh, P., 1974. Data Use and Interpretation, Vol. IV: Science
in Geography, edited by B.P. FitzGerald (London: Oxford Univer-
sity Press).

MES Ltd., 1974. "Offshore Labrador Environmental Conditions, Summer
1974". Report submitted to Total Eastcan Exploration Ltd. by
Marine Environmental Services Ltd., Calgary, Alberta.

Metge, M., et al., 1982. "Extreme Ice Pile-Ups and Multi-year Hum-
mock Fields". In: Proceedings of Workshop on Sea Ice Ridging
and Pile-Up, 22-24 October, 1980, Calgary, Alberta. Edited
by R. Frederking and G.R. Pilkington. NRC Associate Committee
on Geotechnical Research, Tech. Memo. 134 (January 1982), p.
96-106.

Milne, A.R.; Herlinveaux, R.H.; and Wilton, G., 1977. "A Field Study
on the Permeability of Multi-year Ice to Sea Water With Implica-
tions on Its Permeability to Oil". Report submitted to Research
and Development Division, Environmental Emergency Branch,
Environmental Impact Control Directorate, Environmental Pro-
tection Service, Dept. of Fisheries and the Environment. Tech-
nology Development Report EPS-4-EC-77-11 (October).

Niiler, P.P. and Mysak, L.A., 1971. "Barotropic Waves Along An East-
ern Continental Shelf". Geophysical Fluid Dynamics, Vol. 2,
p. 273-288.

Nolte, K.G. and Trethart, W.E., 1971. "North Atlantic Sea Ice Survey
In Southern Labrador Sea, March 8-27, 1971". Amoco Petroleum
Co. Ltd.

Norcliffe, G.B., 1979. Inferential Statistics for Geographers.
(London: Hutchinson & Co. (Publishers) Ltd.).

Nordco Ltd., 1980. "Lake Melville/Offshore Labrador Year Round Navi-
gation Study, 1978-1979". Report to Department of Industrial.
Development, Government of Newfoundland and Labrador.

Oceanographic Atlas of the North Atlantic Ocean, 1968. Naval Oceano-
graphic Office, Washington, D.C. 20390.

Parmerter, R.R. and Coon, M.D., 1972. "Model of Pressure Ridge
Formation in Sea Ice". Journal of Geophysical Research, Vol.
77, No. 33 (Nov. 20), p. 6565-6575.

Parmerter, R.R., 1975. "On the Fracture of Ice Sheets with Part-
Through Cracks". AIDJEX Bulletin No. 30 (November), p. 94-118.

Petro-Canada Inc., 1982. "Offshore Labrador Initial Environmental
Assessment". Report prepared by the Environmental and Social
Affairs and Offshore Engineering Sections of Petro-Canada on
behalf of the Labrador Group of Companies.

Reynolds, A.J., 1974. Turbulent Flows in Engineering. (New York:
John Wiley & Sons, Inc.).

Robinson, A.R., 1983. "Overview and Summary of Eddy Science." In:
Eddies in Marine Science, (Berlin: Springer-Verlag, 1983),
edited by A.R. Robinson; p. 3-15. Topics in Atmospheric and
Oceanographic Sciences series; M. Ghil, R. Sadourny, and J.
Sundermann, series editors.

Sampson, R.J., 1978. "Surface II Graphics System". Computer Ser-
vices Section, Kansas Geological Survey, Lawrence, Kansas.

Scobie, R.W., 1972. "A Comparison of Current Velocity Determined
by Dynamic Methods with Direct Current Measurement in the Labra-
dor Current". M.Sc. Thesis, Dept. of Oceanography, Florida.
State University College of Arts and Sciences, (December).

Seaconsult Ltd., 1978. "Analysis of Ocean Currents, Davis Strait-
1977". Report submitted to Imperial Oil Ltd. Arct. Pet. Oper.
Assoc. (APOA) Report 138.

Simpson, J.H.; Allen, C.M.; and Morris, N.C.G., 1978. "Fronts on
the Continential Shelf". Journal of Geophysical Research, Vol.
83, No. C9 (September 20), p. 4607-4614.

Skidmore, J., 1979. "Labrador Sea Synoptic Ice Description". In:
Oil Spill Scenario for the Labrador Sea. Edited by B.R. LeDrew
and K.A. Gustajtis. Economic and Technical Review Report EPS

3-EC-79-4, Environmental Impact Control Directorate, November 1979, p. 149-168.

Smith, E.H.; Soule, F.M.; and Mosby, O., 1937. "The Marion and General Greene Expeditions to Davis Strait and Labrador Sea, 1928-1935. Scientific Results, Part 2, Physical Oceanography" U.S. Coast Guard Bulletin No. 19.

Solomon, H. and Ahlnas, K., 1978. "Eddies in the Kamchatka Current". Deep Sea Research, Vol. 25, No. 4 (April), p. 403-410.

SPRI, 1973. Illustrated Glossary of Snow and Ice. By Terrence Armstrong, Brian Roberts, and Charles Swithenbank. Printed for Scott Polar Research Institute, Cambridge. (Menston, Yorkshire: The Scholar Press Ltd.).

Squire, V.A. and Allan, A.J., 1977. "Propagation of Flexural Gravity Waves in Sea Ice". C-CORE Publication 77-2.

Stuart, J.T., 1979. "Stability and Transition: Some Comments on the Problems". In: IUTAM Laminar-Turbulent Transition Symposium, Stuttgart, Germany, Sept. 16-22, 1979, R. Eppler and H. Fasal, eds., p. 1-13.

Tang, C.L., 1980. "Observation of Wavelike Motion of the Gaspé Current". Journal of Physical Oceanography, Vol. 10, No. 6 (June), p. 853-860.

Taylor, P.J., 1977. Quantitative Methods in Geography, An Introduction to Spatial Analysis. (Boston: Houghton Mifflin Company).

Tee, K.T., 1978. "A Numerical Model of the Homogeneous Labrador Sea". Atmosphere-Ocean, 12th Annual Congress, p. 29 (Abstract only).

Teitgen, R., 1979. "Laminar-Turbulent Transition in Pipe Flow: Development and Structures of the Turbulent Slug". In IUTAM Laminar-Turbulent Transition Symposium, Stuttgart, Germany, Sept. 16-22, 1979, R. Eppler and H. Fasel, eds., p. 27-36.

Thompson, R., 1971. "Topographic Rossby Waves at a Site North of the Gulf Stream". Deep Sea Research, Vol. 18, No. 1 (January), p. 1-19.

Thorndike, A.S. and Colony, R., 1982. "Sea Ice Motion in Response to Geostrophic Winds". Journal of Geophysical Research, Vol. 87, No. C8, (July 20) p. 5845-5822.

Untersteiner, N., 1968. "Natural Desalination and Equilibrium Salinity Profile of Perennial Sea Ice". Journal of Geophysical Research, Vol. 73, No. 4 (Feb. 15), p. 1251-1257.

Vukovitch, F.M., et al., 1979. "Gulf Stream Boundary Eddies off the East Coast of Florida". Journal of Physical Oceanography, Vol. 9, No. 6 (November), p. 1214-1222.

Wadhams, P., 1973. "Attenuation of Swell by Sea Ice". Journal of Geophysical Research, Vol. 78, No. 18 (June 20), p. 3552-3563.

Wadhams, P., 1978. "Wave Decay in the Marginal Ice Zone Measured From a Submarine". Deep Sea Research, Vol. 25, No. 1 (January), p. 23-40.

Wadhams, P.; Gill, A.E.; and Linden, P.F., 1979. "Transects by Submarine of the East Greenland Polar Front". Deep Sea Research, Vol. 26, No. 12A (December), p. 1311-1327.

Wadhams, P., 1980. "Ice Characteristics in the Seasonal Sea Ice Zone". Cold Regions Science and Technology, 2, p. 37-87.

Wadhams, P., 1981. "The Ice Cover in the Greenland and Norwegian Seas". Reviews of Geophysics and Space Physics, Vol. 19, No. 3 (August), p. 345-393.

Wadhams, P. and Squire, V.A., 1983. "An Ice-Water Vortex at the Edge of the East Greenland Current". Journal of Geophysical Research, Vol. 88, No. C5 (March, 30), p. 2770-2780.

Weeks, W.F. and Lee, O.S., 1958. "Observations on the Physical Properties of Sea Ice at Hopedale, Labrador". Arctic, Vol. 11, No. 3, p. 134-155.

Weeks, W.F. and Assur, A., 1967. "The Mechanical Properties of Sea Ice". U.S. Army Cold Regions Research and Engineering Lab (CRREL), Report II-C3, Hanover, N.H.

Weeks, W.F., 1976. "Sea Ice Conditions in the Arctic". AIDJEX Bulletin, No. 34 (December), p. 173-205.

Weir, C.R., 1979. "Observations of the Labrador Current Through the Use of Satellite Tracked Buoys". In: Proceedings of Symposium on Research in the Labrador Coastal and Offshore Region, May 8-10, 1979. Memorial University of Newfoundland; p. 205.

Wheeler, J.D., 1981. "Probability Distributions for Structure Loading by Multi-year Ice Floes". In: POAC '81, Proceedings of the Sixth International Conference on Port and Ocean Engineering Under Arctic Conditions, July 27-31, Université Laval, Quebec, Canada, (Vol. II), p. 643-652.

Winsor, W. and LeDrew, B.R., 1979. "Ice Feature Characterization, Labrador Offshore". In: Oil Spill Scenario for the Labrador

Sea. Edited by B.R. LeDrew and K.A. Gustajtis. Economic and
Technical Review Report EPS 3-EC-79-4, Environmental Impact
Control Directorate, November 1979, p. 169-220.

WMO, 1970. WMO Sea Ice Nomenclature. Secretariat of the World
Meteorological Organization, Geneva, Switzerland.

Wright, B. and Berenger, B., 1980. "Ice Conditions Affecting Hydro-
carbon Production in the Labrador Sea". In: Labrador Ice
Dynamics Experiment. LIDEX Workshop Report, March 6-8, St.
John's, Nfld. (Memorial University of Newfoundland, NICOS),
p. 56-62.

Younger, M.S., 1979. A Handbook for Linear Regression. (North Scitu-
ate, Mass.+ Duxbury Press).

Zubov, N.N., 1943. Arctic Ice. Translated from Russian by U.S.
Navy Oceanographic Office and the American Meteorological
Society. Editing and Publishing by U.S. Navy Electronics Labora-
tory.

Appendix A

A Comparison of Criteria for Describing Multi-Year
Ice Occurrence During 1979

A.1 Introduction

As a supplement to the analysis described in Section 4.5,
an investigation was conducted to determine the relative power
efficiency of three criteria which can be used to describe the
amount of multi-year ice occurring in a region. The comparison
was made between the sum of floe diameters, the sum of floe sur-
face areas, and the number of floes.

Ultimately, it is the sum of floe surface areas which is
the absolute descriptor of coverage, hence amount, of multi-year
ice in terms of surface area (m^2 or km^2). However, calculation
of floe surface area is laborious and not always justifiable in
light of the information which is sought. Moreover, the amount
of multi-year ice as described by sum of surface areas or sum of
diameters is really of secondary importance in the operational
sense because such an aggregate value is not an intuitively
tangible concept. While it is conventional to describe sea ice
in terms of its proportion of total concentration (usually as a
fraction of 10) it would be more appropriate if each multi-year
floe could be treated as an individual hazard, much in the same
manner as are icebergs. Therefore, for operational purposes, it
is important to describe multi-year ice in terms of its floe
frequency which indicates the concentration of such hazards in a
region; of course, statistics describing the size frequency dis-
tribution are a valuable supplement.

For interpretation of spatial trends as they relate to environmental influences the relationship of multi-year ice coverage to its frequency must be known. The importance of evaluating both parameters in drawing conclusions can be illustrated with reference to the original case stated in Section 4.3.

If the correlation between frequency and sum of diameters is not significant, then the only conclusion must be that the absence of significant covariance is due to multi-year ice (in terms of % coverage) being approximately homogeneously distributed throughout the MIZ. Logically, therefore, variations in floe frequency represented by regions of very large numbers must be due to the dynamic environment of the MIZ which results in the disintegration of multi-year floes into smaller pieces in some regions. Possible processes accounting for this include propagating swells or an advection landward into the pack by fragments created from the destruction of old floes along the seaward margin of the MIZ.

Alternatively, a strong correlation would lead to the conclusion that as the number of floes increased, so did the fraction of coverage by multi-year ice, indicating that the variation in % coverage of multi-year ice was heterogeneous and confined to groups. Neither of the two explanations given for the uncorrelated case above would account for this phenomenon; rather, given that the principal mode of transport for multi-year ice is the Labrador Current, then the grouping can be considered a result of dynamics of flow within the current core. The con-

clusion now derived is that the grouping is due to shear deformation and elongation of originally homogeneous fields of old floes drifting southward in a current stream where velocities progressively decrease away from the centre of the current core. Once this initial conclusion has been established, further investigation would suggest the occurrence of alternating laminar and turbulent modes of flow as described in Section 8.3

Therefore, while the distribution of multi-year floe hazards can be verified simply by providing a frequency count, the underlying cause of the distribution can only be determined by looking at the variation in coverage. If variation in coverage is linearly associated with floe frequency, then only one variable (i.e. number of floes) is needed to describe both parameters. It is this hypothesis which is investigated here.

A.2 Methodology

Data used in the analysis was obtained from maps which had been drawn of the multi-year floe distributions occurring in the Petro-Canada data set. Since the maps had been drawn with the intention of performing subsequent analysis involving surface area calculations, the outlines of individual floes were reproduced with great care. The photographs were backlit, and the floes were traced onto drafting paper using Rapidograph technical drawing pens nos. 0 and 00.

A sample of photographic cells from each flight line was then chosen for analysis. Within each selected cell, the floes

were counted, their diameters measured, and their surface areas calculated. Three numbers were produced from each cell, representing the individual sums of these descriptive variables.

The relationships were investigated in two stages. In the first, non-parametric Spearman's rank correlation analysis was applied to the three main permutations of the sampled data set, specifically, sum of diameters with number of floes, sum of surface areas with number of floes, and sum of surface areas with sum of diameters.

In the second stage, linear regression was used to describe the strength of the sum of diameters as a predictor of the sum of surface areas. The purpose here was to provide gross estimates of the sum of surface areas, and not the area of an individual floe; any cells containing only one floe were therefore not included in the analysis. In order to eliminate heteroscedasticity and to make the two samples significantly normal, the data were transformed to values of $\log_{10}$. After transformation, the Kolmogorov-Smirnov goodness-of-fit test (Ebdon, 1977) was applied to both sets of data to test for significant normality. The procedure is to test the null hypothesis that the sample data has been drawn from a normally distributed population. Significance of the test is based on the K-S statistic which represents the absolute maximum difference measured between the theoretical and observed distributions.

When regression analysis was performed, the residuals statistics revealed five of the paired values to be significant outliers at more than three standard deviations from the mean; the

173

procedure used to test their significance is described more fully
in Younger (1979). After the initial regression analysis, sus-
pected outliers were deleted from the data set and the regression
was performed again. When the second regression equation was
established, the 99% confidence limits for its estimate of Y
based on an individual observation of X were calculated. If the
Y value of the suspected outlier lay outside the 99% confidence
limit of the predicted Y for that value of Y, then it was deemed
to be a statistically significant outlier and remained in exclu-
sion from the data set. The points were only deleted after it
was impossible to conclude with any confidence that they had not
occurred due to error in measurement. In total, 2 points were
deleted from the April 25 set, and 1 from each of the May 01,
May 12, and May 31 sets. The sizes of the samples used in the
non-parametric analysis techniques and in the regression are
detailed in Table 13.

A.3 Results

A.3.1 Correlation

Figure 36 shows the scattergrams of the bivariate pairs
tested in the correlation analysis. Data presented in Figures
36a, c, and e are scaled as a percentage of the maximum value
in their respective set; Figure 36 b, d, and f show the data
expressed as z-scores.

For correlation, the null hypothesis stated that for each
tested pair of variables, no significantly linear relationship
existed. The alternative hypothesis stated that each variable

pair was significantly correlated in a linear manner; the level
of significance for rejecting the null hypothesis was set at
$\alpha = 0.001$. The results of the Spearman's rank correlation are
presented in Table 14; in all cases, the alternative hypothesis
can be accepted. For sum of surface areas vs. sum of diameters,
the correlation is very high (0.9823), with at least 99.9% con-
fidence that a Type I error was not committed; the slope is also
close to 1.0, indicating a near-perfect relationship. For sum
of diameters vs. floe frequency, the correlation is also very,
high (0.9834) with at least 99.9% confidence and a slope also
close to 1.0. For the correlation between sum of surface areas
and floe frequency, the relationship is slightly less linear,
with a coefficient of 0.9376 at a minimum confidence of 99.9%
and a slope of 0.94554.

This slight decrease in correlation is also evident in the
scattergrams, with Figures 36c and 36d showing a slightly wider
scatter than is apparent in the other tested relationships.
Since the sum of surface areas is to be taken as the absolute
measure of amount, then it would seem that the use of sum of
diameters vs. frequency as a descriptor of the varying amount
produces a slightly inflated statistic since it yields a
stronger correlation coefficient. The difference between the
calculated coefficients is 0.0458, indicating that the sum of
diameters method over-estimates the strength of the relationship
slightly by 4.6%. However, in both cases the relationships are
linear and statistically significant at better than $\alpha = 0.001$.
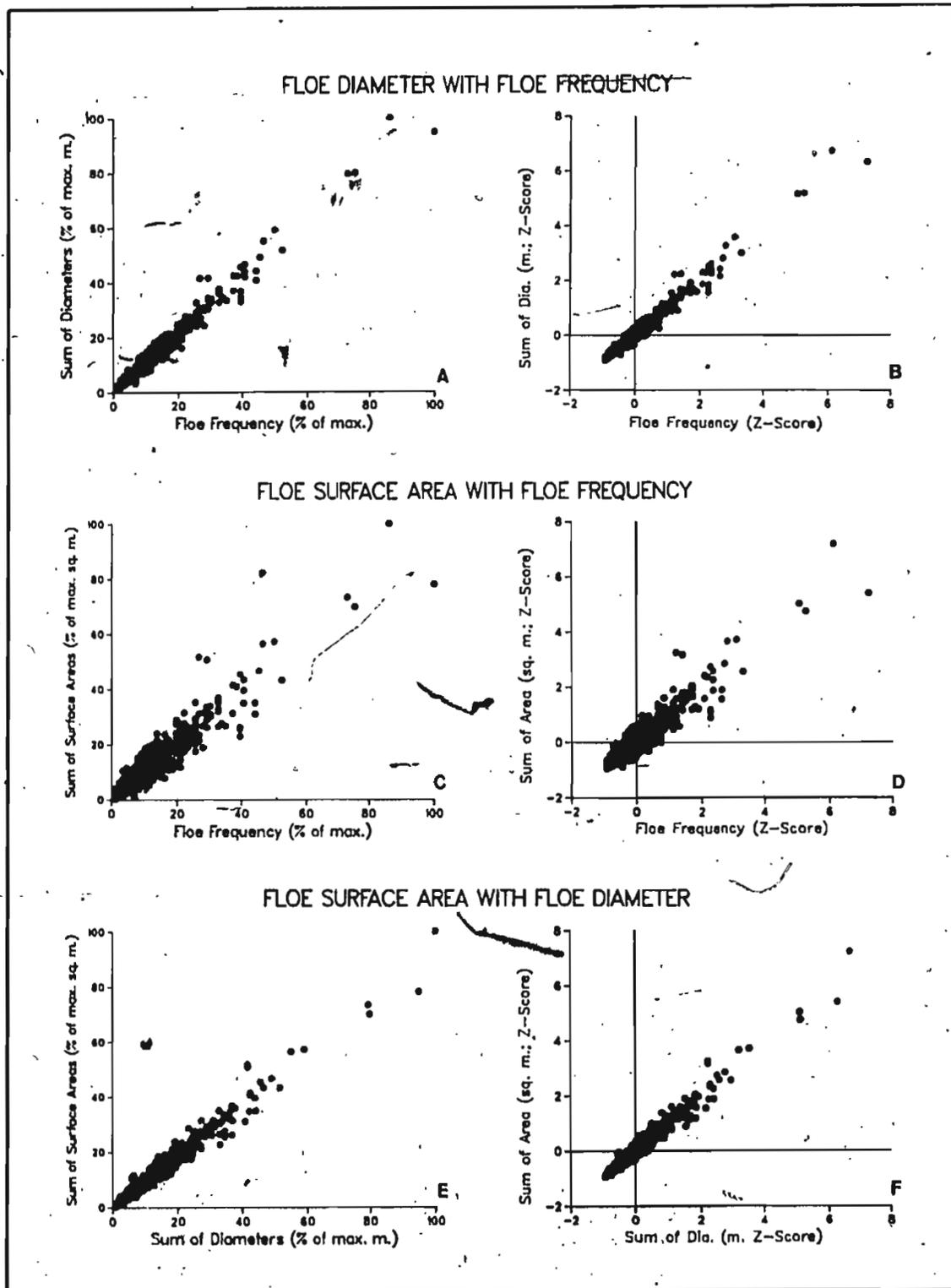
Figure 36 – Scattergrams showing relationships of sum of floe diameters with floe frequency, sum of surface areas with floe frequency, and sum of surface areas with sum of diameters.

Table 13 — Sample size for correlation and regression, used to compare sampling distributions produced from number of floes, sum of diameters, and sum of surface areas.

Data Set	For Correlation		For Regression Analysis	
	#cells	#floes	#cells	#floes
April 25	69	470	52	446
May 01	92	738	73	711
May 12	75	961	72	955
May 26	75	1046	69	1040
May 31	57	458	47	447
June 07	92	1058	88	1054
Total Set	460	4731	401	4653

Table 14 — Results for Spearman rank correlations analysis of number of floes, sum of diameters and sum of surface areas.

Variable Pair:	Sum of diameters /floe frequency	Sum of surface areas/floe frequency	Sum of surface areas/sums of diameters
Coefficient:	0.9834	0.9376	0.9823
Significance:	0.000	0.000	0.000
N. of Cases:	460	460	460
Slope:	0.98644	0.94554	0.98454

A.3.2 Regression analysis: sum of surface areas prediction as a function of sum of diameters.

Results of the K-S test for normality are summarized in Table 15. In all cases, for a rejection level of $\alpha = 0.001$, no significant difference is found between the observed and theoretical distributions, hence allowing for acceptance of the null hypothesis with the conclusion that the data are normally distributed. For the sample with the largest absolute difference between the two distributions (May 31, sum of surface areas) there was still a 15% probability of committing a Type I error in rejecting the null hypothesis.

The null hypothesis for the regression procedure stated that sum of diameters was unable to significantly predict occurrence for the sum of surface areas with confidence. The research hypothesis stated that the sum of diameters was a statistically significant predictor of the sum of surface areas per cell. The test was applied with a level of significance set at $\alpha = 0.001$ for accepting the research hypothesis. Test results are listed in Tables 16 and 17.

For the regression, significance is determined on the basis of the F-statistic. This statistic evaluates the F-ratio by comparing the variation produced in $\bar{Y}_x$ as a direct function of X, with the variation produced due to error (i.e., variance not explained by the regression equation). The computed F statistic is sufficiently significant for rejection of the null hypothesis

178

Table 15: Results of Kolmogorov-Smirnov test for normality on log$_{10}$ data.

For Sum of Surface Areas:

Date	#Cases	Absolute Difference	K-S Z	2-Tailed P
April 25	52	0.07226	0.521	0.949
May 01	73	0.07065	0.604	0.859
May 12	72	0.09709	0.824	0.506
May 26	69	0.11449	0.951	0.326
May 31	47	0.16656	1.142	0.147
June 07	88	0.05075	0.476	0.977
Total Sample	401	0.04441	0.889	0.408

For Sum of Diameters:

Date	#Cases	Absolute Difference	K-S Z	2-Tailed P
April 25	52	0.07530	0.543	0.930
May 01	73	0.06677	0.570	0.901
May 12	72	0.08713	0.739	0.645
May 26	69	0.09714	0.807	0.533
May 31	47	0.13431	0.921	0.365
June 07	88	0.06729	0.631	0.820
Total Sample	401	0.03632	0.727	0.665

Table 16: Results of analysis of variance used to test significance of sum of diameters as predictor of sum of surface areas in regression analysis.

Day	Source of Variation	D.F.	Sum of Squares	Mean Square	F.	Sig. F.
April 25	Regression	1	7.82452	7.82452	990.74	0.0000
	Error	50	0.39488	.00790		
May 01	Regression	1	7.99061	7.99061	1227.49	0.0000
	Error	71	0.46219	0.00651		
May 12	Regression	1	9.80421	9.80421	2619.60	0.0000
	Error	70	0.26198	0.00374		
May 26	Regression	1	16.61038	16.61038	2599.05	0.0000
	Error	67	0.42819	0:00639		
May 31	Regression	1	6.31954	6.31954	1493.61	0.0000
	Error	45	0.19040	0.00423		
June 07	Regression	1	8.77510	8.77510	1948.72	0.0000
	Error	86	0.38726	0.00450		
Total Sample	Regression	1	59.75488	59.75488	9973.19	0.0000
	Error	399	2.39063	0.00599		

180

Table 17: Regression statistics for sum of surface areas as predicted by sum of diameters per cell.

DATE	R^2	STD.ERR. OF ESTIMATE	CONSTANT INTERCEPT	STD.ERR. OF CONSTANT	T	SIG.T.	B SLOPE	STD.ERR. OF B	BETA	STD.ERR. OF BETA	T	SIG.T.
April 25	0.95916	0.08887	1.19052	0.08757	13.595	0.0000	1.09007	0.03463	0.97568	0.03100	31.476	0.0000
May 01	0.94532	0.08068	1.34153	0.07716	17.387	0.0000	1.03573	0.02956	0.97228	0.02775	35.035	0.0000
May 12	0.97397	0.06118	1.27413	0.05645	22.573	0.0000	1.05594	0.02063	0.98690	0.01928	51.182	0.0000
May 26	0.97487	0.07994	1.13849	0.05763	19.757	0.0000	1.08980	0.02138	0.98735	0.01937	50.981	0.0000
May 31	0.97075	0.06505	1.18742	0.07006	16.949	0.0000	1.06896	0.02766	0.98527	0.02549	38.647	0.0000
June 07	0.95773	0.06710	1.33297	0.06192	21.528	0.0000	1.02670	0.02326	0.97864	0.02217	44.144	0.0000
TOTAL	0.96153	0.07741	1.23783	0.02813	44.005	0.0000	1.06398	0.01065	0.98058	0.00982	99.866	0.0000

if the relationship between Y and X is stronger than variation due to error (Younger, 1979). Referring to the analysis of variance in Table 16, for all tested cases the calculated F statistic has a degree of significance of at least $\alpha = 0.001$. For April 25, the data set with the smallest F-statistic at 990.74, the variation due to regression is about 990.7 times greater than that due to error (Younger, 1979). Therefore, in all tested cases it is possible to reject the null hypothesis, and conclude that the relationship between X and Y is significant such that sum of diameters is a significant predictor of the sums of surface areas. The coefficient of determination (R^2), listed in Table 18 is quite high for all data sets; for the combined sample from all individual days, the R^2 is 0.96153, indicating that 96% of the variance in Y (sum of surface areas) is explained by a linear regression on X (sum of diameters). Of the individual days, May 01 has the weakest coefficient, calculated at 0.94532.

The standardized regression coefficient, Beta, is also very high for the combined sample, with a value of 0.98058. This means that a change of one standard deviation in the sampling distribution of X, produces a change of 0.98 ($\pm$ 0.0982) standard deviations in the sampling distribution of Y, a near-perfect relationship. For individual days, the minimum standardized regression coefficient was 0.97228 (May 01). The computed t-statistic for significance of Beta is listed in Table 17; in all cases it has a level of significance of at least $\alpha = 0.001$. For individual days, the least-squares fit of Beta is shown in Figure 37; for the combined total sample refer to Figure 39.
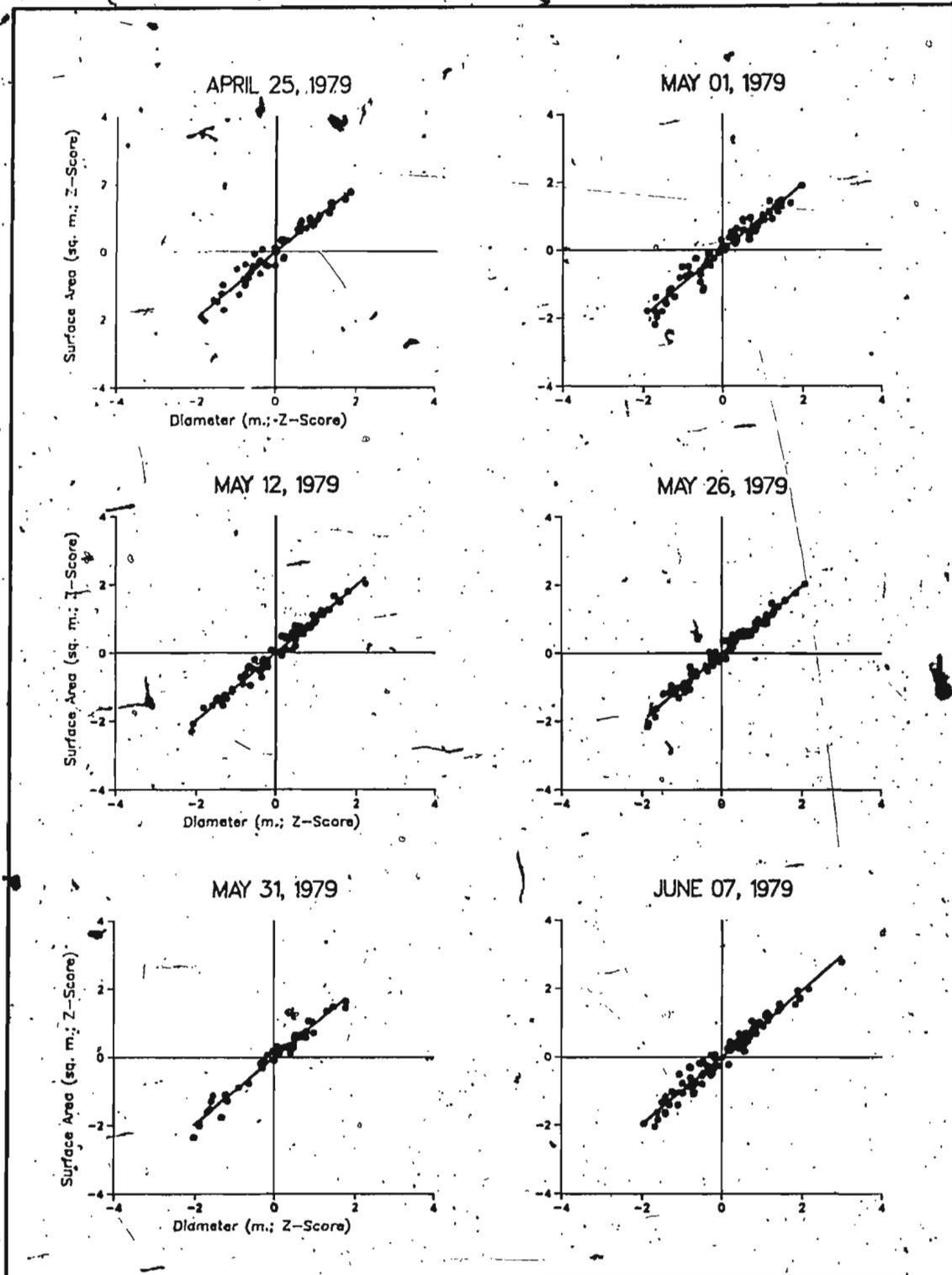
Figure 37 – Sum of multi-year floe surface areas per cell as a function of sum of diameters (based on beta coefficient from standardized data).

Based on the regression analysis, the predicted value of Y for any data set can be determined according to the following formula:

$$10^y = a + b \, (log_{10}x)$$

where: 10^y is the anti-log$_{10}$ of the product from the right side of the equation, i.e. the sum of surface areas.

a is the constant or intercept of the least squares fit.

b is the regression coefficient or slope of the least squares fit.

Since a and b have been calculated on the basis of log_{10} values, the predicting X value (sum of diameters) must also be transformed to log_{10} before entry into the equation. The actual value of Y, in terms of square metres, is found by taking the product of the right side of the equation as an exponent of 10.

The slope and intercept values, as well as their respective values of standard error are listed in Table 17 for each data set. The t-statistic and its significance for each value is also given; in all cases, both the slope and intercept are significant at a level of at least $\alpha = 0.001$. For each data set, the sum of surface areas can be estimated from the sum of diameters by inserting the relevant values of intercept (a) and slope (b) into the formula. The regression line, its residuals,

and its 95% confidence intervals for estimation of an individual value of Y based on X are plotted in Figure 38 for each day; the combined sample is shown in Figure 39.

The final conclusion drawn from the regression analysis is that, on a per cell basis, sum of diameters (m) is a strong and statistically significant predictor of the sum of surface areas (m^2) when the data are subjected to a $\log_{10}$ transformation.
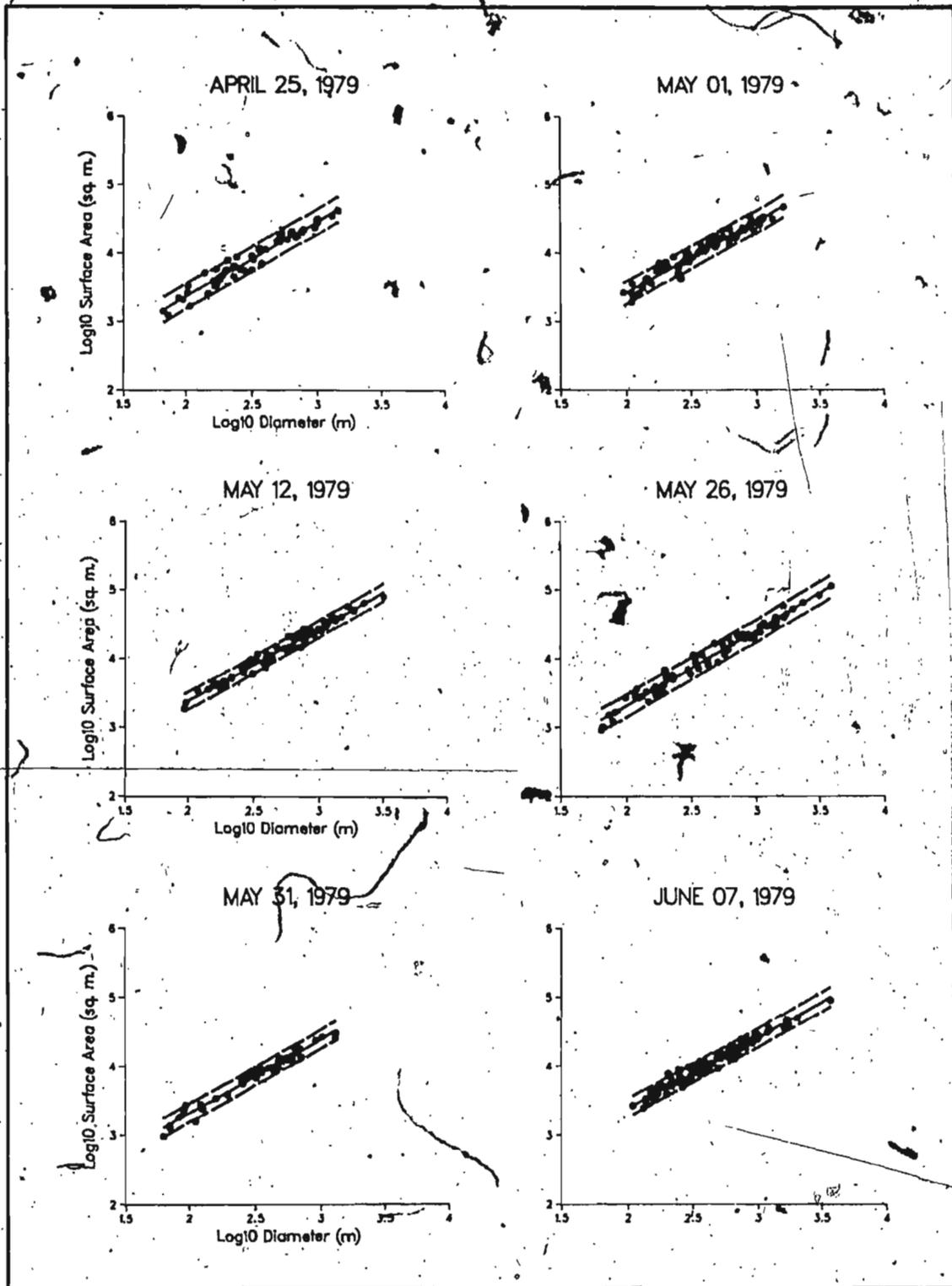
Figure 38 – Sum of multi-year floe surface areas per cell as
predicted by the sum of diameters; with 95% con-
fidence limits for an individual observation.

186

SURFACE AREA AS A FUNCTION OF FLOE DIAMETER
### From Six Overflights; April 25–June 07, 1979.
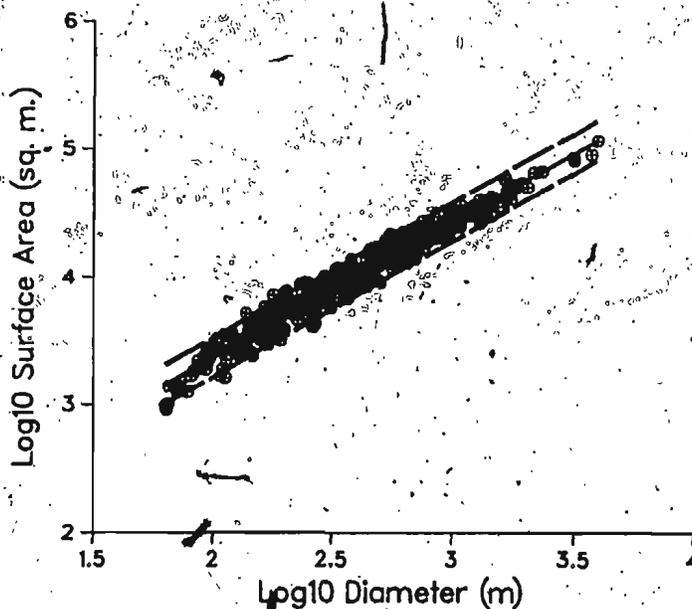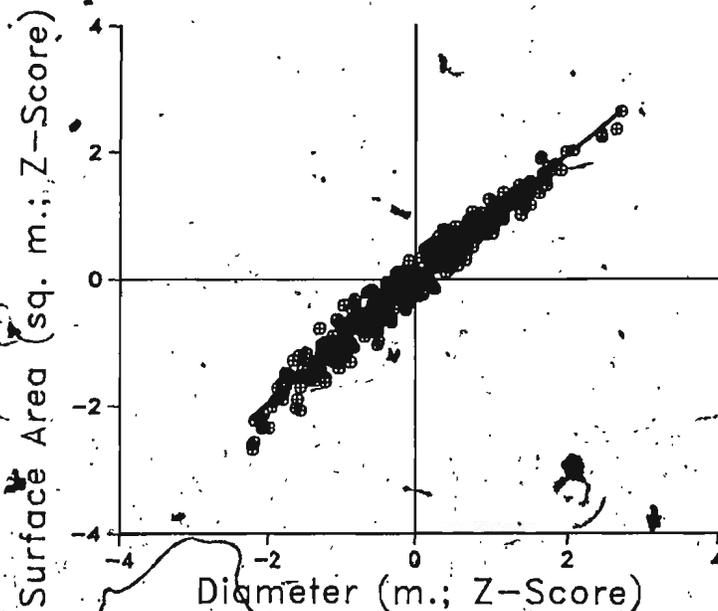
Figure 39 — Sum of multi-year floe surface areas per cell as a
function of the sum of diameters; from all values
sampled. Diagram B gives 95% confidence limits for
an individual observation.

Appendix B

Alternative Method for Testing Significance of Observed
Distributions for 1979 Multi-Year Ice

B.1 Overview and Results

Norcliffe (1977) states that, as an alternative to the one-sample chi-square test, the one-sample Kolmogorov-Smirnov test may be applied to compare an observed distribution to one which is theoretical. This test measures the maximum difference between two cumulative frequency distributions, $F_0(X)$ and $S_N(X)$, where:

$F_0(X)$ is the theoretical distribution expected under the null hypothesis.

$S_N(X)$ is an observed distribution being tested under the alternative hypothesis.

The statistic (D) is calculated as (Norcliffe, 1977):

$$D = \max \left| S_N(X) - F_0(X) \right|$$

where: D is the absolute value of the maximum difference between the two distributions.

To apply this test to the multi-year ice distributions observed during 1979, the cumulative distribution under the null hypothesis was determined by assuming that all cells along a given flight line contained an equal number of multi-year floes; the average expected number per cell is listed in Table 10 (p. 92). The cumulative expected value for any given cell was then determined by adding its expected value to the sum of the expected values for each cell which preceeded it along the line sequentially from cell no. 1. This produced the straight, dashed line shown in Figure 40. The cumulative observed distribution

188

was obtained in a similar manner by calculating the cumulative sum of observed frequencies up to and including each respective cell in the sequence; this is shown by the solid, curved line.

The null and alternative hypotheses were the same as specified on p.90; the test was two-tailed, with a rejection level set at $\alpha = 0.001$. Test results are listed in Table 18; in all cases the differences between the observed and theoretical distributions are significant at better than $\alpha = 0.001$, thus allowing for acceptance of the alternative hypothesis for all flight dates.
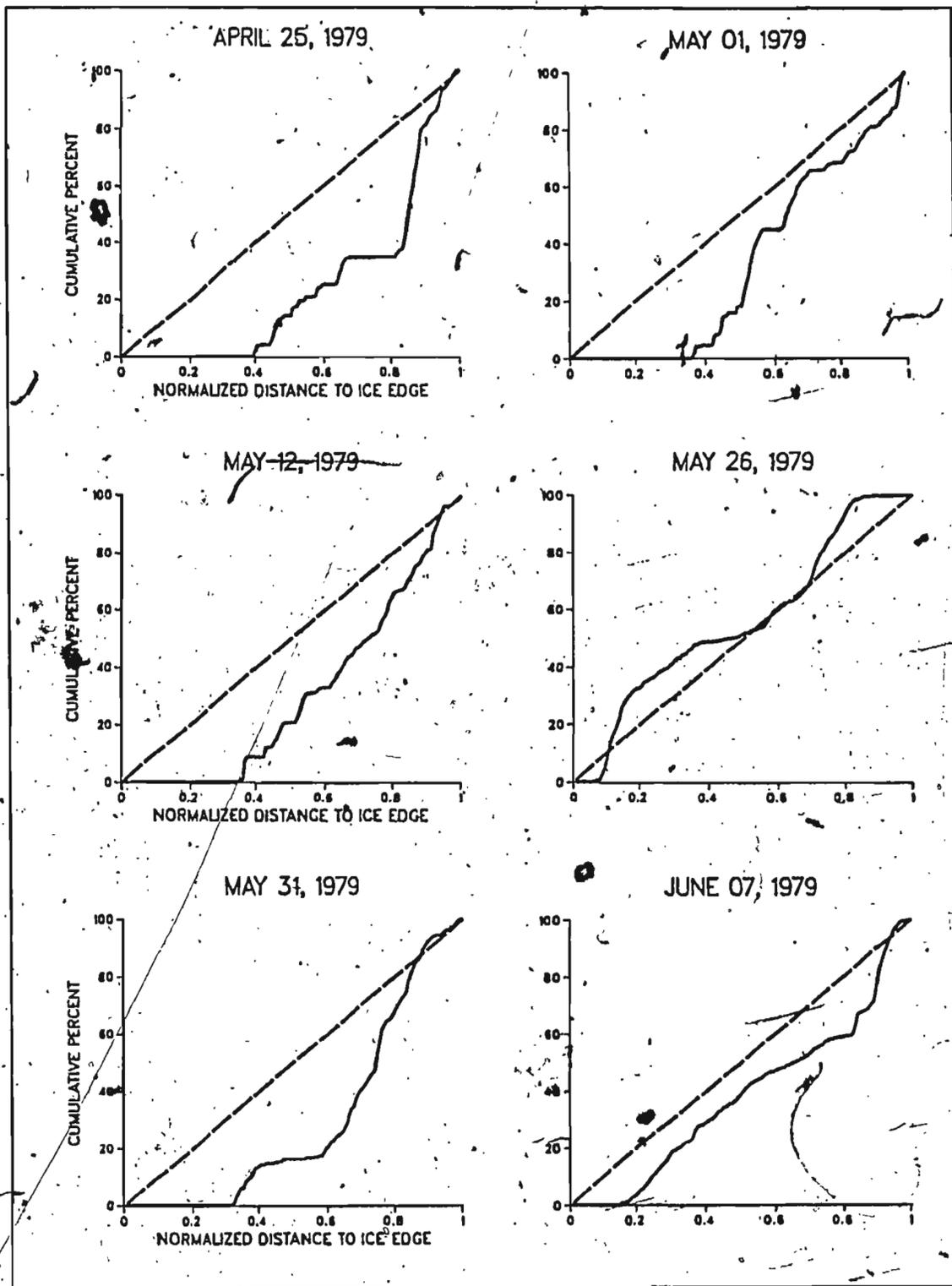
Figure 40 — Cumulative observed distribution (solid line) compared
with cumulative theoretical distribution for each flight
date during 1979.

Table 18 - Results of Kolmogorov-Smirnov one-
sample test on multi-year floe
distributions.

Most Extreme Differences

Date	Absolute	Positive	Negative	K-S Z	2-Tailed Prob.
April 25	0.7415	0.7415	-0.2585	8.055	0.000
May 01	0.6901	0.6901	-0.3099	7.591	0.000
May 12	0.6519	0.6519	-0.3481	5.794	0.000
May 26	0.6198	0.6198	-0.3802	4.821	0.000
May 31	0.6458	0.6458	-0.3542	5.480	0.000
June 07	0.6312	0.6312	-0.3689	4.929	0.000